# Nuclear magnetic resonance of $C_{60}$ and fulleride superconductors

Charles H. Pennington and Victor A. Stenger

*Department of Physics, Ohio State University, 174 West 18th Avenue, Columbus, Ohio 43210*

The alkali-doped solid materials $A_3C_{60}$ (where $A$ is an alkali metal), which are superconductors with transition temperatures among the highest known apart from the high-$T_c$ cuprates, are among the most exciting outgrowths of the discovery of the family of fullerene molecules. The structural, electronic, and superconducting properties of the alkali fullerides have been subjects of great controversy. In this article the authors review nuclear magnetic resonance (NMR) investigations of the alkali fullerides and of undoped $C_{60}$. They show that, although the NMR data certainly provide evidence for unusual static and dynamic structural properties, there is little evidence for unusual normal- and superconducting-state electronic properties, such as strong correlations in the normal state or nonphononic mechanisms of superconductivity. [S0034-6861(96)00603-4]

## CONTENTS



  

## I. INTRODUCTION

Nuclear magnetic resonance (NMR) has proven to be a remarkably versatile tool for the elucidation of key properties of superconductors (MacLaughlin, 1976), beginning in 1959 with Hebel and Slichter's (1959) striking confirmation of the "pairing" aspect of the Bardeen-Cooper-Schrieffer (BCS) theory, and followed by successive generations of NMR experiments on new families of unusual superconductors, including heavy-fermion systems (Asayama *et al.*, 1988), superfluid $^3$He (Volhardt and Wölfle, 1989), organic superconductors (Ishiguro and Yamaji, 1989), and high-$T_c$ cuprates (Slichter, 1994). This review pertains only to the most recently discovered unusual superconducting material, the alkali fullerides $A_3C_{60}$ ($A$ is an alkali metal: K, Rb, or Cs), which are doubly intriguing in that they contain the soccerball-shaped molecule $C_{60}$, or "buckminsterfullerene" (see Fig. 1) and that their transition temperatures, which reach as high as $T_c$=33 K for $RbCs_2C_{60}$, are among the very highest for superconductors thought to be described by the BCS model of phonon-mediated pairing.

Nuclear magnetic resonance and related magnetic resonance experiments, muon-spin relaxation and electron-spin resonance (ESR), have addressed each of the three most crucial (and interrelated) issues of alkali fullerides—their static and dynamic structural properties, their mechanism of superconductivity, and their normal-state electronic structure. Thus, in reviewing the applications of magnetic resonance approaches to fullerene superconductors, we also hope to provide an overview of the major issues surrounding the materials themselves. Despite our intentions, this specialized review cannot supplant several excellent more general reviews of fullerenes that have appeared (Hebard, 1992; Axe *et al.*, 1994; Dresselhaus *et al.*, 1994; Gelfand, 1994; Lieber and Chen, 1994; Lieber and Zhang, 1994; Pickett, 1994; Ramirez, 1994; Weaver and Poirier, 1994).

We begin in Sec. II with a review of the basic features and issues of fullerenes and fullerene superconductivity, emphasizing "conventional wisdom." This section might be skipped by a reader who is already current on most issues. Successive sections reveal how NMR data alternately support and challenge the conventional views.

Section III.A outlines some fundamental parameters of NMR—the resonance frequency and shifts in the resonance frequency including chemical (orbital) and Knight (spin) shifts. Also introduced are the nuclear-electron-spin hyperfine coupling terms—dipolar, and Fermi contact. Then Secs. III.B and III.C provide the tools to make *a priori* estimates of some of the basic NMR parameters, including hyperfine couplings and chemical and Knight shifts. Some of these estimates differ widely from experimental results; we give possible interpretations. In addition, Secs. III.B and III.C may be useful references for those wishing to make their own independent investigations beyond what we have presented here. The concept of spin-lattice relaxation ($1/T_1$) is introduced in Sec. III.D. Behaviors of $1/T_1$ in insulators, conventional metals, metals with strong electronic correlations, and superconductors are also discussed.

Section IV presents the use of NMR as a structural probe in fullerene materials. Topics include the beautiful and simple phenomenon of motional narrowing of the $^{13}$C line shape in solid $C_{60}$, the "fingerprinting" of different alkali intercalant combinations through alkali-metal NMR, and one- and two-dimensional NMR-based studies of the orientational dynamics of the $C_{60}$ molecule in both pure and alkali-doped $C_{60}$. The data on alkali fullerides give a clear indication that the current thinking about the structure of these materials is seriously incomplete.

Section V covers NMR as a probe of the superconducting-state properties of alkali fullerides. Knight-shift-based NMR measurements of the superconducting-state spin susceptibility are discussed, as well as spin-lattice relaxation ($T_1$) and issues surrounding it—the famous "Hebel-Slichter" coherence peak and the low-temperature Arrhenius behavior revealing the superconducting energy gap. Data are then discussed in the light of calculations based on BCS and Eliashberg theory, taking the electron-phonon coupling spectrum $\alpha^2F(\omega)$ to be strongly peaked at one frequency. The full body of data is not entirely consistent with such a crude model, leaving open the possibility that a model including more structure in $\alpha^2F(\omega)$ (perhaps two peaks) might be sufficient. Comparisons with other families of superconductors are made.

Section VI addresses the issue of whether the NMR properties, especially in the normal state, are consistent with simple "band theory" interpretations of the electronic structure, or whether some kind of "strong-correlation" interpretation is required, analogous to what is observed in high-$T_c$ superconductors. Furthermore, normal-state temperature, pressure, and alkali-dopant-dependent NMR spin-lattice relaxation data are used in conjunction with the McMillan equation to extract information about the phonon pairing mechanism, in addition to that derived from superconducting-state NMR data.

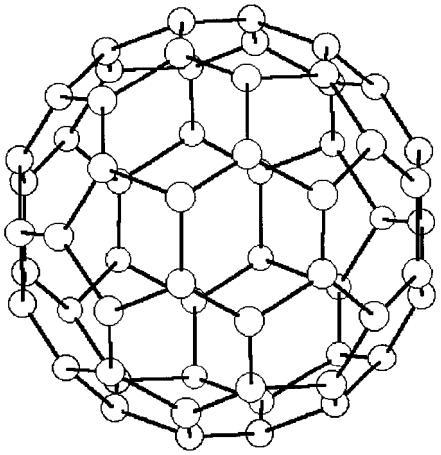

FIG. 1. The fullerene $C_{60}$.

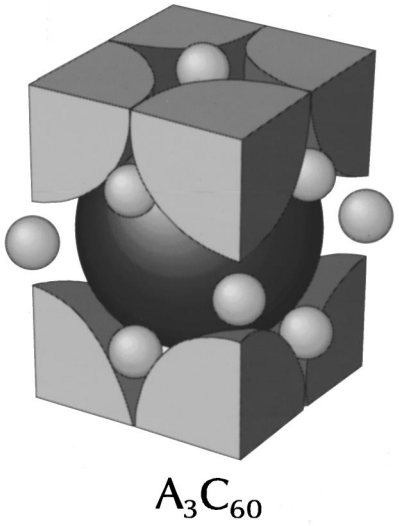


FIG. 2. Unit cell of $A_3C_{60}$ (Murphy *et al.*, 1992). The small spheres represent alkali ions and the large spheres are the $C_{60}$ molecules. In a given unit cell there are two ions with tetrahedral coordination and one ion with octahedral coordination.

This is followed by a summary and concluding remarks in Sec. VII.

## II. BASIC FEATURES OF FULLERENES AND FULLERENE SUPERCONDUCTIVITY

We first survey the relevant structural and electronic features of fullerenes and alkali-fulleride materials and the phenomenology and theory of fullerene superconductivity, building a starting picture for comparison with the results of magnetic resonance experiments.

### A. Structure

The well-known "soccerball" structure of the $C_{60}$ molecule (Kroto *et al.*, 1985) is shown in Fig. 1. In pure $C_{60}$ solid the molecules are centered on the points of an fcc lattice with lattice constant $a$=14.17 Å (Heiney *et al.*, 1991). That structure is preserved when the solid is alkali doped to form $A_3C_{60}$ (Stephens *et al.*, 1991); the alkali-metal atoms insert themselves into interstitial sites, between the $C_{60}$ molecules (Fig. 2). (Throughout this review we largely omit discussion of Na-containing $C_{60}$ materials, which behave differently from the other alkali-doped materials in important ways. See, for example, Yildirim *et al.*, 1995).

For each formula unit $A_3C_{60}$ in the fcc structure one alkali atom occupies a large interstitial site of octahedral coordination, located at the center of six $C_{60}$ molecules at the points of an octahedron. The two remaining alkali atoms in the formula unit $A_3C_{60}$ occupy smaller tetrahedral coordination sites (Stephens *et al.*, 1991).

If one thinks of the $C_{60}$ molecules as hard spheres that are touching their nearest neighbors, then one can define a $C_{60}$ hard-sphere molecular radius $R_{C_{60}}$ equal to $a/(2\sqrt{2})$. For tetrahedrally coordinated alkali atoms at positions $(1/4,1/4,1/4)a$ measured from a $C_{60}$ at the origin, one can estimate a "radius" $R_{\rm tet}$ for the tetrahedral site of $[\sqrt{3}/4-1/(2\sqrt{2})]a$, which gives $R_{\rm tet}\approx 1.1$ Å. (Analogous reasoning gives an octahedral site radius $R_{\rm oct}=[1/2-1/(2\sqrt{2})]a\approx 2.1$ Å.) The ionic radii of the alkali ions are larger than the nominal radius of the tetrahedral interstitial site. The ionic radii are 1.33, 1.48, and 1.67 Å for K, Rb, and Cs, respectively (Mahan, 1975). Thus the tetrahedral ions exist in very cramped quarters, and their radius is probably the primary factor controlling the lattice constant (Ziebarth *et al.*, 1995). The fcc lattice constant $a$ for $A_3C_{60}$ increases from ~14.2 Å ($K_3C_{60}$) to 14.5 Å ($RbCs_2C_{60}$) as one increases the ionic radii of the alkali dopant in the series from K to Rb to Cs (Fleming *et al.*, 1991).

In addition, it is believed that the presence of the alkali ions places an important constraint upon the orientations the $C_{60}$ molecules—namely, that each $C_{60}$ should be oriented such that a hexagonal face is pointed along each of the crystal ⟨111⟩ directions, so that the alkali ion can "bed down" into the center of a carbon hexagon (Stephens *et al.*, 1991). Figure 3 shows that for each $C_{60}$ molecule there are two inequivalent orientations which can accomplish this feat. Both possibilities are thought to exist with equal populations at low temperature. This residual low-temperature disorder is known as "merohedral disorder." Gelfand and Lu (1992) have shown that the presence of this disorder greatly influences electronic structure, washing away the sharp features found in the electronic density of states as a function of energy and shortening the electronic mean free path to a distance of the order of the intermolecular spacing. More recently Teslic *et al.* (1995) have found evidence for short-range orientational correlations.

Several important lengths characterizing $C_{60}$ and $A_3C_{60}$ compounds, including some discussed above and some that are deferred to Sec. II.B, are summarized in Table I.

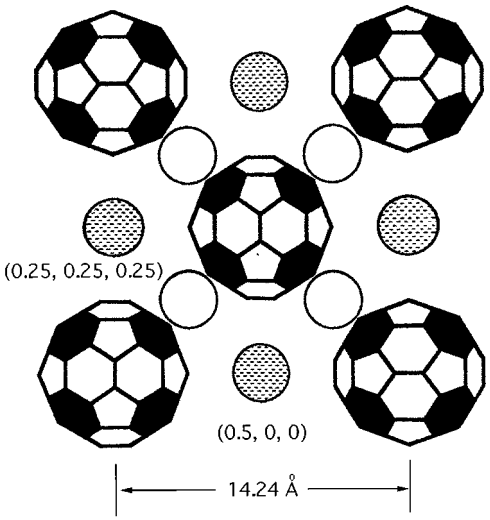


FIG. 3. The structure of $A_3C_{60}$ (Stephens *et al.*, 1991). Open and hatched spheres represent alkali ions at the tetrahedral and octahedral sites, respectively. The presence of the ions at the interstitial sites produces merohedral disorder among the $C_{60}$ molecules: the orientation of each $C_{60}$ is constrained such that the face of a hexagonal carbon ring (shaded) must point towards an alkali ion (i.e., along the crystal ⟨111⟩ directions). There are only two inequivalent $C_{60}$ orientations that can accomplish this, each shown in the figure, and each is thought to exist with equal populations at low temperature. Several NMR experiments, however, challenge this simple model (see Sec. IV).

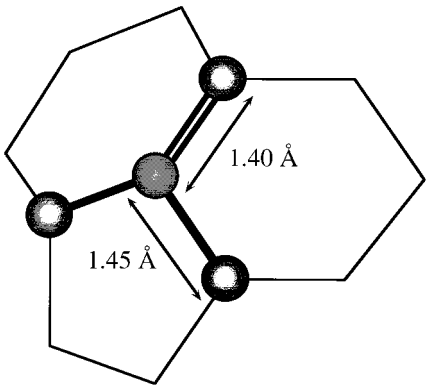


FIG. 4. Schematic drawing of a section of a $C_{60}$ molecule emphasizing the carbon-carbon chemical bonding. Each carbon atom is a member of two hexagons and one pentagon and is bonded to three carbon neighbors. Two of these bonds (the "5-6 bonds") form the pentagonal faces and provide a borderline between a pentagon and a hexagon. The length of a 5-6 bond is ~1.45 Å, (Yannoni, Bernier, *et al.*, 1991). The third bond connects two pentagons and borders two hexagons (the "6-6 bonds"). The length of a 6-6 bond [~1.40 Å (Yannoni, Bernier, *et al.*, 1991)] is shorter than that of a 5-6 bond and may be considered to be formally a double bond, although in fact the "5-6" and "6-6" bonds do not have greatly different bonding strengths.

### B. Electronic structure

#### 1. Molecular electronic structure

Just as in benzene and graphite, the atomic orbitals of interest in $C_{60}$ are primarily the $p_z$ orbitals, where $z$ is perpendicular to the molecular plane for benzene and perpendicular to the (local) surface of the buckyball sphere in that case. One significant difference between fullerene and graphite is caused by the finite curvature of the $C_{60}$ molecule. For graphite the appropriate set of atomic orbitals are $p_z$ and $3sp^2$. In the case of $C_{60}$ the curvature is expected to lead to an admixture (estimated as ~9%) of $s$ into the $p_z$ orbital (Haddon, 1988); (however, see Sec. III.B.2a).

Each carbon in the $C_{60}$ molecule is a member of two hexagons and one pentagon, and thus is bonded to three C neighbors. Figure 4 gives a schematic drawing of the buckyball emphasizing the chemical bonding. Two of these bonds ("5-6 bonds") form the pentagonal faces and provide a borderline between a pentagon and a hexagon, while one connects two pentagons and borders two hexagons ("6-6 bonds"). The "5-6" bonds are somewhat longer (~1.45 vs 1.40 Å; Yannoni, Bernier, *et al.* 1991) than the "6-6" bonds, and hence the "6-6" bonds are formally considered to be double bonds and the 5-6 single. In reality the hopping amplitudes for these two types of bonds differ by only ~10% (Gelfand, 1994, p. 104; for a more precise approach see Satpathy *et al.*, 1992, p. 1779). Put another way, the difference in bond lengths is small on the overall scale of carbon-carbon bond lengths (single bond ~1.54 Å; double ~1.33 Å; triple ~1.20 Å), and they are both similar to that of benzene, 1.39 Å.

Molecular orbitals form due to the overlap ($\pi$ bonding) between neighboring atomic $p_z$ orbitals, and the icosahedral symmetry of the molecule specifies certain degeneracies. Figure 5 (left panel) gives an energy-level diagram specifying each of the $60p_z$ derived orbitals, their degeneracies, and their occupancies for the case of neutral $C_{60}$. Of primary interest are the "HOMO" (highest occupied molecular orbital) and "LUMO" (lowest unoccupied molecular orbital). The HOMO is of $h_u$ symmetry, and the LUMO $t_{1u}$. In this notation "$h$" and "$t$" specify degeneracies of 5 and 3, respectively, and the subscripts "$u$" and "$g$" specify odd or even parity.

A sketch of a representative $t_{1u}$ orbital is given in Fig. 6. The importance of this figure for our purposes is that the sign of the wave function changes rather rapidly with position within the molecule. This quick variation should reduce the overlap with the atomic wave functions of neighboring alkali atoms, which will tend to reduce the hyperfine couplings to the alkali nuclei.

The total range of energy for the $C_{60}$ $p_z$-derived levels is ~15 eV (Satpathy, 1986), taking $t$=2.7 eV for the Hückel parameter for hopping between neighboring atomic sites.

#### 2. Electronic structure in the solid

The molecular electronic structure provides a starting point for thinking about the electronic structure of the

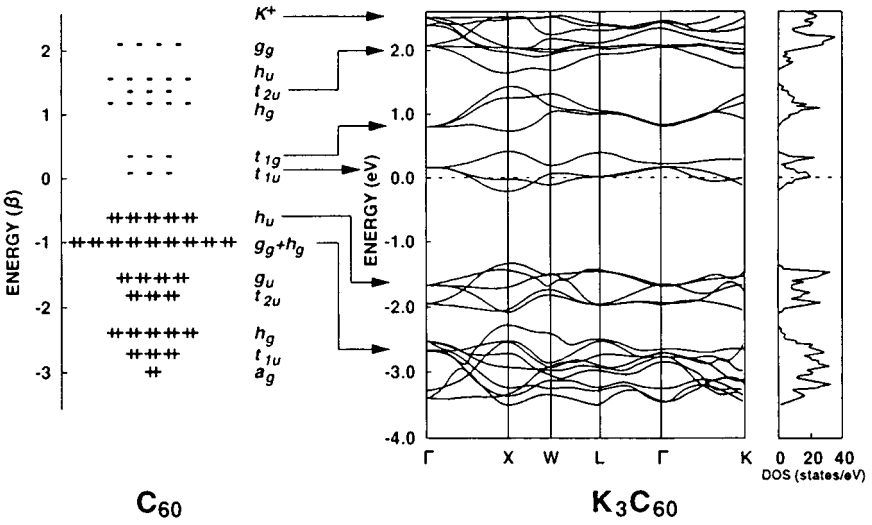


FIG. 5. Electronic structure of $C_{60}$. (Left) Hückel theory calculation of the molecular energy spectrum of neutral $C_{60}$. Each of the 60 $p_z$ derived levels is shown with its respective degeneracies and occupancies. Of interest are the HOMO (highest occupied molecular orbital), which has $h_u$ symmetry, and the LUMO (lowest unoccupied molecular orbital), which posseses $t_{1u}$ symmetry. Doping with an alkali atoms leads to occupation of the $t_{1u}$ level. Right: Band structure and density of states using the LDA formalism (Haddon *et al.*, 1986; Hebard, 1992).

solid (Saito and Oshiyama, 1991; Haddon, 1992): In undoped $C_{60}$ the $h_u$-derived band is filled and $t_{1u}$ empty, and hence $C_{60}$ is an insulator. In $A_3C_{60}$, however, the alkali metal is expected to donate its electron to the $t_{1u}$-derived conduction band. Hence $A_3C_{60}$ is expected to be a metal, with a half-filled $t_{1u}$ band.

In the solid, molecular orbitals on neighboring molecular sites mix to form bands, also shown in Fig. 5 (right panel). The $t_{1u}$-derived band has a calculated width of ~0.5 eV for $K_3C_{60}$ Satpathy *et al.*, 1992; Gelfand, 1994), much less than the 15-eV total energy range for the molecular energy levels.

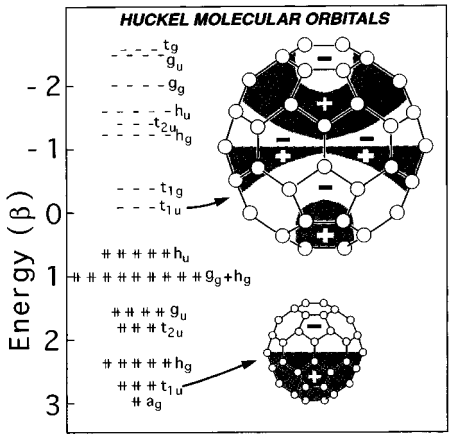


FIG. 6. A representative $t_{1u}$ orbital (Gelfand, 1994). The sign of the wave function is indicated by the dark or light shading. This quick variation should reduce the overlap with the atomic wave functions of neighboring alkali atoms, which will tend to reduce the hyperfine couplings to the alkali nuclei.

The narrow 0.5-eV bandwidth can be understood qualitatively in terms of the relative values of the intramolecular and intermolecular nearest carbon-carbon distances. Within the molecule C-C bond lengths are ~1.4 Å. The closest approach between carbon atoms on adjacent molecules, however, is larger. That distance between carbons can be estimated (crudely) as the distance of closest approach of the buckyball spheres, $d_{\text{C-C}} \approx (a/\sqrt{2} - 2R)$ (Satpathy *et al.*, 1992), where $a$ is the lattice spacing and $R$ is the radius of the buckyball sphere (~3.55 Å; Allen, 1995). In fact, the intermolecular nearest C-C distance may exceed this estimate by ~0.1 Å (Ziebart *et al.*, 1995). This estimate gives $d_{\text{C-C}} \sim 2.94$ Å for $a$=14.2 Å ($K_3C_{60}$)—much greater than the intercarbon spacing on the molecule of ~1.4 Å. In fact, for the compound $Cs_2RbC_{60}$, the distance $d_{\text{C-C}}$ (~3.15 Å) approaches the interlayer spacing in graphite (3.35 Å).

Table II, adapted from the review article of Gelfand (1994), summarizes the results of local-density-approximation calculations of the electronic density of states at the Fermi level for $K_3C_{60}$ and $Rb_3C_{60}$.

### 3. "Experimentalist's" picture of electronic structure

In order to gain insight into the electronic energy scales, we consider the radial falloff of a carbon $2p$ wave function. The normalized radial wave function $R(r)$ for a hydrogenlike atom of effective nuclear charge $Z_{\text{eff}}$ is given by

$$R(r) = \frac{1}{2\sqrt{6}} \left( \frac{Z_{\text{eff}}}{a_0} \right)^{3/2} \sigma \exp(-\sigma/2); \quad \sigma = Z_{\text{eff}}(r/a_0). \tag{1}$$

TABLE I. Selected lengths (given in Å) that characterize the $C_{60}$ molecule, the undoped $C_{60}$ solid, the interstitial sites available for alkali dopants, and the alkali dopants themselves. *$C_{60}$ molecular radii:* Molecular radii are characterized in two ways: first according to the positions of the atomic nuclei (as defined by Allen *et al.*, 1995), then according to a ''hard-sphere'' model for an fcc lattice of $C_{60}$ molecules with lattice spacing 14.2 Å. *Intercarbon spacings:* Intercarbon spacings for the $C_{60}$ molecule are given for the ''6-6'' (bordering two carbon hexagons) and ''5-6'' (bordering a carbon pentagon and a carbon hexagon) bonds. These may be compared with the given values for C-C single, double, and triple bonds, and with the bond length for benzene. *Intermolecular C-C spacing:* The approximate ''closest approach'' between carbons on *adjacent* $C_{60}$ molecules for the fcc structure is given and is seen to be close to the *interlayer* spacing for graphite—suggesting that $C_{60}$ should indeed be thought of as a molecular solid. *Lattice constants (at room temperature):* Room-temperature fcc lattice constants are given for $C_{60}$ and several alkali-doped $C_{60}$ compounds. *Interstitial site ''cage'' radii:* Using the ''hard-sphere'' model of the $C_{60}$ molecule, estimates are given for the radius of the interstitial cavities in which alkali intercalants reside. These lengths may usefully be compared with the alkali ionic radii. *Intercalant ionic radii:* Ionic radii for the alkali intercalants are given. These values are based on the ''hard-sphere'' approach applied to non-$C_{60}$ materials—for example, the alkali halides.

| Quantity | Length or distance in Å | Reference |
|---|---|---|
| *$C_{60}$ molecular radii:* | | |
| $C_{60}$ sphere radius (defined by positions of atomic nuclei) | 3.55 | Allen *et al.* 1995 |
| $C_{60}$ hard-shell radius (Taking lattice spacing $a$=14.2 Å) | 5.02 | |
| *Intercarbon spacings:* | | |
| C-C bond length: (''6-6 bonds; undoped $C_{60}$) | 1.40±0.015 | Yannoni, Bernier, *et al.*, 1991 |
| C-C bond length: (''5-6 bonds; undoped $C_{60}$) | 1.45±0.015 | Yannoni, Bernier, *et al.*, 1991 |
| Bond length in benzene | 1.39 | Mahan, 1975 |
| Typical C-C single bond length | 1.54 | |
| Typical C-C double bond length | 1.33 | |
| Typical C-C triple bond length | 1.20 | |
| *Intermolecular C-C spacing* | | |
| Distance of closest approach between carbons on nearest-neighbor molecules | 3.1 | Ziebarth *et al.*, 1995 |
| *Interlayer spacing for graphite* | 3.35 | |
| *Lattice constants (at room temperature):* | | |
| $C_{60}$ | 14.16 | Tanigaki *et al.*, 1992 |
| $K_3C_{60}$ | 14.24 | Tanigaki *et al.*, 1992 |
| $Rb_3C_{60}$ | 14.38 | Tanigaki *et al.*, 1992 |
| $RbCs_2C_{60}$ | 14.56 | Tanigaki *et al.*, 1992 |
| *Interstitial site ''cage'' radii (taking $a$≈14.2 Å)* | | |
| Octahedral site | 2.1 | |
| Tetrahedral site | 1.1 | |
| Intercalant ionic radii | | |
| $K^+$ | 1.33 | Mahan, 1975 |
| $Rb^+$ | 1.48 | Mahan, 1975 |
| $Cs^+$ | 1.67 | Mahan, 1975 |

TABLE II. Summary of local-density-approximation calculations of electronic densities of states for fullerene superconductors. Adapted from the review article of Gelfand (1994). Results of various local-density-approximation calculations for the density of states at the Fermi level for $K_3C_{60}$, and the ratio of the density of states of $Rb_3C_{60}$ to that of $K_3C_{60}$. The lattice parameters for $K_3C_{60}$ and $Rb_3C_{60}$ are taken to be 14.24 and 14.44 Å, respectively.

| Density of states ($K_3C_{60}$) | Ratio: Density of states $Rb_3C_{60}$ to $K_3C_{60}$ | Reference |
|---|---|---|
| 6.6 | 1.26 | Erwin and Pickett, 1992 |
| 8.5 | 1.18 | Huang *et al.*, 1992 |
| 8.6 | 1.21 | Satpathy *et al.*, 1992 |
| 9.0 | 1.14 | Novikov *et al.*, 1992 |
| 9.8 | 1.27 | Martins and Troullier, 1992 |
| 12.5 | 1.25 | Oshiyama *et al.*, 1992 |

For the neutral carbon atom, Eq. (1) may be used as a phenomenological approximation if $Z_{\text{eff}}$ is taken to be 3.14 (where the reduction relative to the nuclear charge of 6 results from screening by the two core electons and partial screening by the other valence electrons) (Clementi and Raimondi, 1963; Tycko *et al.*, 1993).

We suppose that the overlap, or hopping integral, between two carbon atoms, should scale very crudely with the quantity $R^2(r=d/2)$, where $d/2$ is half the distance between the atoms. Inserting $d$=1.4 Å for the intramolecular and 3 Å for the intermolecular C-C distance, we "predict" that the intramolecular energy scale is on the order of 30 times that of the conduction bandwidths. This is the correct order of magnitude, if we consider estimates given above of ~15 and 0.5 eV for the full energy range of the $2p_z$ orbital-derived molecular levels and the conduction bandwidth of ~0.5 eV. Figure 7 illustrates the "overlap" of the C radial wave functions from these distances. Taking this approach one step further, we crudely estimate the ratio of the density of states for $Rb_3C_{60}$ (using 14.44 Å for the lattice constant) to that of $K_3C_{60}$ (using 14.24 Å), and find a value of 1.4. This value is somewhat different from local-density-approximation calculations, which range from 1.14 to 1.27 (Gelfand, 1994).

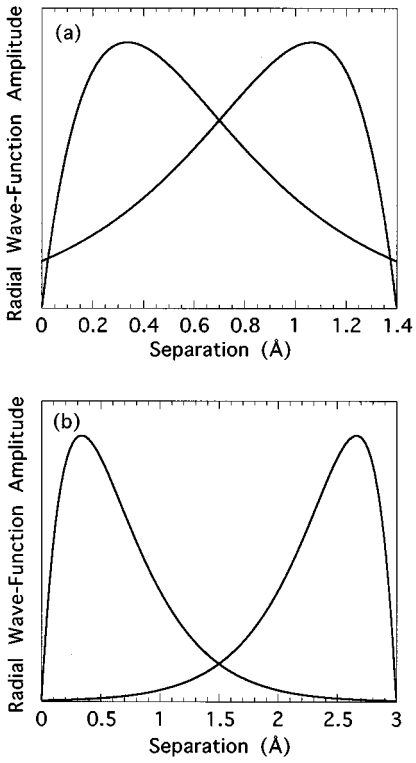


FIG. 7. $2p$ radial wave functions for carbon atoms centered at the origin and at distances 1.4 Å (a, top panel), representing an intramolecular nearest-neighbor C-C distance, and 3 Å (b, bottom panel), the approximate smallest distance between two carbon atoms on adjacent molecules. The electronic bandwidth should scale approximately as the product of these wave functions evaluated at the midpoint. The product is some 30 times larger for the intramolecular C-C spacing, which explains crudely why the range of molecular energy levels (only those composed primarily of $2p_z$ orbitals) is ~15 eV, some 30 times larger than the conduction bandwidth ~0.5 eV in the solid (though the exact agreement of these numbers is coincidental).

### C. Superconductivity

Currently the better part of the physics community suspects the conventional Bardeen-Cooper-Schrieffer phonon pairing mechanism as the source of superconductivity in alkali fullerides. The BCS mechanism is generalized in Eliashberg theory, which takes into account the full frequency-dependent electron-phonon coupling spectrum and so-called "strong-coupling" effects (McMillan and Rowell, 1969; Scalapino, 1969; Carbotte, 1990). The appeal of the conventional mechanism is simply that, from what has been measured thus far, it appears plausible—despite some unusual properties of fullerene materials, one can construct a set of parameters within the BCS framework which matches most of the experimental data. The future may bring results that further spot-weld the edifice together or, perhaps, evidence that causes a substantial rethinking. Given the suspicion, however, we examine briefly the features and parameters of a BCS interpretation, including the phonon modes that could be the agents of electron pairing, the McMillan equation, and the observed dependence of $T_c$ on lattice spacing $a$.

#### 1. Phonon modes

Figure 8 gives a schematic representation of the phonon density of states. A novel feature of the phonon spectrum is that the various intuitively understood modes are well separated in frequency. Modes involving carbon atoms vibrating relative to one another within the $C_{60}$ molecule (intramolecular modes) appear at the high-frequency range of ~200–2000 $cm^{-1}$. This range may be usefully subdivided into low-frequency (~200–800 $cm^{-1}$) modes involving radial vibrations, and high-

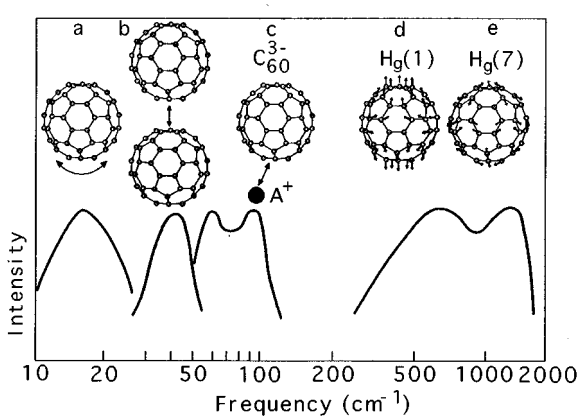


FIG. 8. Schematic representation of the phonon density of states in the $A_3C_{60}$ compounds (Hebard, 1992). The motions involved in each distinct mode are illustrated above the frequency band. At low energies (~10–20 $cm^{-1}$) the compounds exhibit librational modes involving rigid reorientations of individual $C_{60}$ molecules (and this mode is illustrated above the 10–20 $cm^{-1}$ peak in the figure). Next in increasing energy are the intermolecular modes (~20–50 $cm^{-1}$), where $C_{60}$ molecules move relative to adjacent $C_{60}$ molecules. At somewhat higher frequencies (~50–100 $cm^{-1}$) are the optic modes. The predominant modes at high energies are the intramolecular phonon modes, which can be subdivided into two groups: those having radial displacements (~200–800 $cm^{-1}$) and those having tangential displacements (~1000–1500 $cm^{-1}$). These five distinct modes can be considered as candidates for the dominant electron pairing agent. Because they occur at distinct bands of frequency, it seems likely that the pairing agent may be specified through experimental results.

frequency (~1000–1500 $cm^{-1}$) modes involving vibrations tangential to the surface of the molecular sphere. Tangential modes have higher frequency than do radial modes because they involve a variation in the C-C bond length. The modes involving rigid reorientations of the entire molecule (vibrational modes) are, as expected, at a much lower energy, of ~10–20 $cm^{-1}$.

Modes involving vibrations in which the distance between adjacent molecules varies (intermolecular) appear at 20–50 $cm^{-1}$, and optic modes, involving vibrations of the alkali-metal atoms relative to the (heavier) $C_{60}$ molecule (optic modes) occur at somewhat higher frequencies of 50–100 $cm^{-1}$.

The separation of the characteristic frequencies given for the modes in Fig. 8 will be important, because if one can determine only the frequency of the phonons involved in pairing, then the modes of vibration are also specified.

Table III lists the phonon modes, and the quantity $T_c/\omega$ for each, with $T_c$ taken as 30 K ($T_c$ for $Rb_3C_{60}$ is 29 K).

TABLE III. Listing of characteristic $A_3C_{60}$ phonon modes and their approximate frequencies. Also given is the ratio $T_c/\omega$ for each mode, where $T_c$ is taken as 30 K, the approximate value for $Rb_3C_{60}$ (29 K) and $Rb_2CsC_{60}$ (31 K). If one of these phonon modes were to play a predominant role in electron pairing, then $T_c/\omega$ would be a parameter characterizing the degree of strong coupling.

| Phonon mode: Frequency: ($cm^{-1}$) | $T_c/\omega$ |
|---|---|
| Molecular reorientations 20 $cm^{-1}$ | 1.0 |
| Intermolecular vibrations 40 $cm^{-1}$ | 0.5 |
| Optical ($C_{60}$-alkali vibrations) 100 $cm^{-1}$ | 0.2 |
| Intramolecular: radial (500 $cm^{-1}$) | 0.04 |
| Intramolecular: tangential (1400 $cm^{-1}$) | 0.015 |

### 2. $T_c$ and lattice-constant dependence

Figure 9 shows transition temperatures for alkali fullerides as a function of lattice constant $a$, with both alkali intercalant (e.g., $K_3C_{60}$, $Rb_2CsC_{60}$, etc.) and applied pressure as implicit variables. It is clear that $T_c$ for fcc structured $A_3C_{60}$ compounds is at least almost a universal function of the lattice parameter. [This statement does not hold for the Na-containing $C_{60}$ materials (Yildirim *et al.*, 1995)]. This can be easily understood within the BCS framework. The crudest form of BCS theory, neglecting electron-electron Coulomb repulsion, gives the expression for $T_c$ (Tinkham, 1980)

$$k_B T_c = 1.13\hbar\omega_{\rm ph} \exp(-1/\lambda_{\rm ph}), \tag{2}$$

where $\omega_{\rm ph}$ is the Debye frequency and $\lambda_{\rm ph}=N(\varepsilon_F)V$ is the product of the density of states at the Fermi energy $N(\varepsilon_F)$; $V$ is the electron-phonon coupling matrix element. As the lattice parameter increases, the overlap of

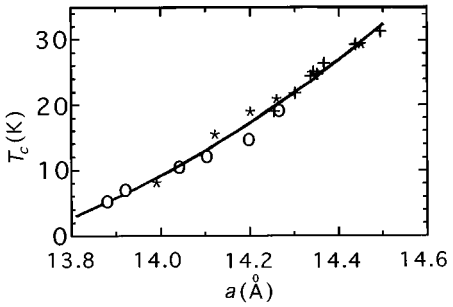


FIG. 9. Transition temperature $T_c$ for alkali fullerides as a function of lattice constant $a$, with both alkali intercalant and applied pressure as implicit variables (Zhou *et al.*, 1992). The open circles indicate $K_3C_{60}$, the asterisks symbolize $Rb_3C_{60}$, and the plus signs denote a member of the $A_{3-x}A_xC_{60}$ ($A$=K, Rb, or Cs) family at 300 K and 1 bar. It is clear that $T_c$ for fcc structured $A_3C_{60}$ compounds is at least almost a universal function of the lattice parameter.

the molecular wave functions decreases, driving $N(\varepsilon_F)$ and $T_c$ up, according to Eq. (2).

Equation (2) is only valid in the weak-coupling limit ($\lambda \ll 1$) and with electron-electron Coulomb repulsion neglected. The McMillan equation (McMillan, 1968) provides a more versatile formula for $T_c$:

$$k_B T_c = \frac{\hbar \omega_{\rm ph}}{1.2} \exp\left[\frac{-1.04(1+\lambda_{\rm ph})}{\lambda_{\rm ph} - \mu^*(1+0.62\lambda_{\rm ph})}\right] \quad (3)$$

where $\mu^*$ parametrizes the effects of electron-electron Coulomb repulsion (Sec. II.D.2). Isotope effect experiments relate $\mu^*$ and $\lambda_{\rm ph}$ for a known value of $\omega_{\rm ph}$ (Ramirez *et al.*, 1992a), and thus Eq. (3) may be used to extract $\lambda_{\rm ph}$ and $\mu^*$ for a known $\omega_{\rm ph}$.

Ramirez *et al.* (1992b) used measurements of the specific-heat jump at $T_c$ to set an upper limit on $\lambda_{\rm ph}$, and hence an upper limit on $\omega_{\rm ph}$. They found $\lambda_{\rm ph}$ must be less than one, $\mu^* \sim 0.1$–$0.2$, and $\omega_{\rm ph} \sim 1400\ {\rm cm}^{-1}$. Although $\lambda_{\rm ph}$ is certainly not close to zero in this scenario, we might call it "weak coupling" in a relative sense, since the phonon frequencies involved are large, and $T_c/\omega_{\rm ph}$ is small (0.015).

This "weak-coupling" interpretation is probably favored by a plurality of investigators at present, as it is consistent with infrared reflectivity (Degiorgi *et al.*, 1992) and, to some extent, NMR and muon-spin relaxation (see Sec. V). Other experiments, however, including scanning tunneling microscope $I$-$V$ curves (Zhang *et al.*, 1991) and NMR (the small size of the Hebel-Slichter coherence peak; see Sec. V) suggest the importance of lower-frequency phonons.

A full understanding of fullerene superconductivity within the BCS framework and based upon Eliashberg theory (for a review see Carbotte, 1990) must await tunneling data that probe the full phonon coupling spectrum and from which all of the unknowns of Eq. (3) may be obtained. The extraordinary success of this approach in conventional superconductors is reviewed by McMillan and Rowell (1969), Scalapino (1969), and Carbotte (1990).

### D. Objections to this conventional view

The brief synopsis of the parameters of superconductivity given above reflects the conventional view that (1) the normal state of alkali fullerides is reasonably well described by band theory, and that (2) superconductivity is phonon mediated and can be described in terms of BCS theory. Currently this view is widely but not universally held.

#### 1. Strong correlations?

From an *a priori* point of view, one is skeptical that calculations based on band theory would reproduce the important physics. Band-theory calculations yield bandwidths for the $t_{1u}$ band of $W \sim 0.5$ eV, while the on-molecule Coulomb repulsion $U$ can either be estimated as $e^2/\varepsilon R$ ($R$=molecular radius=3.55 Å), yielding $\sim 1$ eV for $\varepsilon = 4$ (Varma *et al.*, 1991), or be measured using Auger spectroscopy for solid $C_{60}$ as 1.6 eV (Lof *et al.*, 1992). Finding $U$ to be larger than $W$, Lof *et al.* (1992) suggest that the stoichiometric compound $K_3C_{60}$ is in fact a magnetic insulator and that conductivity and superconductivity result only from a slight off-stoichiometry, $K_{3-\varepsilon}C_{60}$, as in the $La_{2-x}Sr_xCuO_4$ system.

Controversy surrounding the issue of correlations has been stimulated by photoemission results, which find an occupied bandwidth of $\sim 1.2$ eV (Benning *et al.*, 1993; see also the review by Pickett, 1994), about four times larger than expected from the local-density approximation.

Although the details of the effects of correlations certainly may not be predicted in advance, they would be expected to reveal themselves in some way through the NMR data. The case of high-$T_c$ superconductors provides a precedent—the effects of spin fluctuations on the NMR properties in those systems is reviewed by Slichter (1994). In Secs. III and VI addressing normal-state NMR data we shall pay close attention to any evidence suggesting deviations from the local-density approximation.

#### 2. $\mu^*$ and validity of the Migdal-Eliashberg theory?

Related to the issue of correlations is the issue of the parameter $\mu^*$, appearing in Eq. (3), and parametrizing the effects of electron-electron Coulomb repulsion. $\mu^*$ is related to the dimensionless Coulomb repulsion parameter $\mu$, equal to $UN(\varepsilon_F)$. Here $N(\varepsilon_F)$ is the density of states at the Fermi energy, approximately related to the electronic bandwidth $W$ by $N \sim 4/W$, where $W \simeq 10.5$ eV (Gelfand, 1994) and $U$ is the molecular Coulomb repulsion, estimated above as $\sim 1$ eV. Then $\mu \simeq (8\ \text{states/eV}\cdot C_{60})\ x\ (1\ \text{eV}) \simeq 8$.

The relevant parameter in superconductivity is $\mu^*$, a "renormalized" $\mu$, reflecting the different effective frequencies of $\mu$ and $\lambda_{\rm ph}$ (Morel and Anderson, 1962):

$$\mu^* = \frac{\mu}{1 + \mu \ln(\Omega_{\rm cutoff}/\omega_{\rm ph})} \quad (4)$$

Here $\Omega_{\rm cutoff}$ is the frequency above which screening of the Coulomb interaction is not effective, usually taken to be the smaller of the electronic bandwidth or the plasma frequency (Varma *et al.*, 1991).

$\mu^*$ works against phonon pairing [see Eq. (3)]. In order to maintain realistic values of $\lambda_{\rm ph}$ one needs to find $\mu^* \ll 1$, in fact typically between 0 and 0.2. We see from Eq. (4) that, given that $\mu$ is large, we need to make the logarithm $\ln(\Omega_{\rm cutoff}/\omega_{\rm ph})$ in the denominator of Eq. (4) large. To illustrate a typical scenario, for Al we take $\Omega_{\rm cutoff} = \varepsilon_F = 11.7$ eV and $\omega_{\rm ph} = \omega_{\rm Debye} = 0.034$ eV (Ashcroft and Mermin, 1976) and find 5.84 for the logarithm. Hence regardless of the size of $\mu$, $\mu^*$ will be less than 0.17.

For alkali fullerides, however, one's first guess for $\Omega_{\rm cutoff}$ and $\omega_{\rm ph}$ would be $\sim 0.6$ eV (the $t_{1u}$ bandwidth) and 0.17 eV (typical intramolecular phonon frequency)—clearly not a recipe for obtaining a small $\mu^*$ (Chakravarty *et al.*, 1992). Those who favor intramo-

lecular phonon coupling (e.g., Varma *et al.*, 1991; Schluter *et al.*, 1992) argue that the relevant $\Omega_{\text{cutoff}}$ should be taken as the full energy range for the carbon $p_z$ orbitals (~15 eV); doing so easily yields a reasonable $\mu^*$. It is perhaps an even more serious problem that, since the electronic bandwidth is not much greater than the intramolecular phonon frequencies, electron-phonon scattering cannot be thought of as occurring only close to the Fermi energy, and thus the approximations used in Eliashberg theory may not be valid. We refer the reader to Pickett (1994) for more insightful commentary on these matters.

#### 3. Non-BCS mechanisms?

Finally, non-BCS mechanisms have been proposed (Chakravarty *et al.*, 1991; Friedberg *et al.*, 1992). Chakrvarty, Gelfand, and Kivelson (1991) propose an all-electronic pairing mechanism. The scale is set by the ratio of the Coulomb interaction $U$ (~5–10 eV) between two electrons on the same C atom to the hopping amplitude $t$ (~2–3 eV) between nearest intramolecular C neighbors. As expected, for small $U/t$ (more specifically, to first order in $U/t$), the effective electron-electron interaction is repulsive. However, for larger $U/t$ (second order), the virtual involvement of the full range of $p_z$-derived molecular orbitals results in an attractive electron-electron interaction which could lead to superconductivity.

Again, Pickett (1994) and Gelfand (1994) have each given more full and insightful reviews of this controversy.

### E. Summary

Certainly some fraction of those who initially began to do research on alkali-fulleride superconductivity have since moved on, subscribing to the view outlined above that $C_{60}$ superconductors are simply BCS superconductors with high $T_c$'s due to an optimum combination of parameters. In fact a wide range of data, including much of the NMR, can be explained using such a model. Nevertheless there are considerations, also outlined above, which raise doubt. The high frequencies of the intramolecular phonons, as compared to the electronic bandwidth, may result in new physics. Indeed there is even controversy regarding the normal-state electronic structure—one can argue reasonably that electron-electron correlations should play a big role, as they certainly do in the high-$T_c$-related compound $La_2CuO_4$, which is predicted by band theory to be a metal, but which is in fact an antiferromagnetic insulator. With these issues in mind it certainly seems appropriate to ask to what extent we can understand the body of experimental data, including especially the relatively new NMR data, with our current models.

## III. FUNDAMENTALS OF NMR, PARAMETERS OF FULLERENE NMR, AND SOME SURPRISES

This concludes our brief outline of the basic features of fullerenes and fullerene superconductivity. We now turn to the fundamentals of NMR—resonance frequencies and shifts and spin-lattice relaxation—and to estimates of relevant shifts and hyperfine parameters in fullerenes. This section should serve as a guide for those attempting to connect experimental results with the relevant issues in greater detail than we have presented. Thus this section, especially Secs. III.B and III.C, might be skipped on a first reading and/or by the casual reader. In Sec. III.A we discuss NMR frequency shifts, including chemical (orbital) and Knight (spin) shifts. The fundamental hyperfine coupling mechanisms (the Fermi contact interaction and the electron-nuclear dipole-dipole interaction) which result in the Knight shift in metals are defined. In Secs. III.B and III.C we provide a detailed analysis of the expected chemical and Knight shifts for the $^{13}C$ nucleus and for the alkali-metal nuclei $^{39}K$, $^{87}Rb$, and $^{133}Cs$. For all of the nuclei the experimental values of the shifts are found to be unexpectedly small. In fact, the observed Rb Knight shift appears to be almost two orders of magnitude smaller than one would predict from state-of-the-art calculations based on the local-density approximation. In Sec. III.D we review spin-lattice relaxation rates in metals and superconductors.

### A. The nuclear-spin hamiltonian

First we discuss mechanisms leading to NMR frequency shifts, the chemical and Knight shifts, and for the latter the associated hyperfine coupling mechanisms. Much of what follows is well known in the NMR community and is covered thoroughly in textbooks by Abragam (1961) and Slichter (1990).

#### 1. Resonance frequencies and shifts

The effective nuclear-spin Zeeman Hamiltonian $\mathcal{H}$, appropriate for calculating energy levels and NMR frequencies, is given by

$$\mathcal{H} = -\gamma_n \hbar \vec{H}_0 \cdot (\overleftrightarrow{1} + \overleftrightarrow{K}_s - \overleftrightarrow{\sigma}) \cdot \vec{I} + \mathcal{H}_Q \tag{5}$$

where $\vec{H}_0$ is the vector applied magnetic field, $\gamma_n$ is the nuclear gyromagnetic ratio, $\vec{I}$ is the nuclear-spin vector, and $\mathcal{H}_Q$ is the Hamiltonian describing the interaction of the nuclear electric quadrupole moment with the local electric-field gradient. In most of our considerations we shall neglect $\mathcal{H}_Q$. Values of the gyromagnetic ratio $\gamma_n$, nuclear spin $I$, and natural abundances are given for the nuclear species of interest in Table IV.

The tensors $\vec{K}_s$ and $\vec{\sigma}$ are called the Knight-shift and chemical-shift tensors, respectively. Both give the fractional shifts of the positions of the magnetic resonance frequencies, relative to the frequency in a reference compound containing the same nucleus.

The Knight-shift tensor $\vec{K}_s$ is present only in metallic samples and results from (1) the polarization of the conduction electron spins by the applied magnetic field (the

TABLE IV. Gyromagnetic ratio, spin, and natural abundance for the nuclei of interest. $^{13}C$ has a small natural abundance, but nevertheless due to the large number of carbons per $C_{60}$ molecule and per gram of material it is quite feasible to observe natural abundance $^{13}C$ NMR. The naturally abundant isotope $^{12}C$ has no nuclear moment. Approximate resonance frequencies for each nucleus can be obtained by multiplying the gyromagnetic ratio by the applied field. Typical fields are ~10 tesla, giving frequencies of order 100 MHz.

| Nucleus | Gyromagnetic ratio (MHz/tesla) | Spin | Natural abundance (%) |
|---|---|---|---|
| $^{13}C$ | 10.705 | 1/2 | 1.108 |
| $^{39}K$ | 1.987 | 3/2 | 93.08 |
| $^{85}Rb$ | 4.111 | 5/2 | 72.8 |
| $^{87}Rb$ | 13.932 | 3/2 | 27.2 |
| $^{133}Cs$ | 5.585 | 7/2 | 100 |

Pauli susceptibility), and (2) the hyperfine coupling of the nuclear spin to this electron-spin polarization. $\vec{K}_s$ can be written as

$$\vec{K}^s = \vec{A}\chi^s \tag{6}$$

where $\vec{A}$ is the hyperfine coupling tensor and $\chi^s$ is the Pauli susceptibility. [In Eq. (6) we have taken $\chi^s$ to be isotropic; in general $\chi^s$ must also be written as a tensor.]

The chemical-shift tensor $\vec{\sigma}$ results from orbital magnetism, both diamagnetic shielding and Van Vleck paramagnetic, and it is the shift most familiar to chemists who use NMR to characterize solutions of organic molecules. In some cases the chemical shift is also referred to as the "orbital" shift.

For fields along the $z$ principal axis of the total shift tensor (assuming that the axes of $\vec{K}_s$ and $\vec{\sigma}$ coincide), the NMR frequency is given by

$$\omega = \gamma H_0(1 + K_{zz} - \sigma_{zz}). \tag{7}$$

What is measured experimentally is the *difference* in resonance frequency between the sample of interest and that of a reference compound also containing the nuclear species being studied. For $^{13}C$ the reference compound is tetramethylsilane (TMS). Insulators are usually chosen as the reference compound, since they have zero Knight shift. They do, however, have chemical shifts relative to a hypothetical bare nucleus. Thus measured shifts relative to a reference compound represent the sum of the Knight shift and the chemical shift relative to the reference compound. It is often not straightforward to deduce the separate contributions of the Knight- and chemical-shift terms.

Experimentally obtained shifts for $C_{60}$ and $C_{60}$ compounds at a few representative temperatures are given in Table V. Discussion of the shifts is then given in Secs. III.B and III.C.

### 2. Fundamental hyperfine coupling mechanisms and associated shifts

Implicit in the term $\vec{K}_s$, the Knight-shift tensor, appearing in Eq. (5) are two fundamental Hamiltonian

TABLE V. NMR shifts for several $C_{60}$ compounds in order of increasing lattice constant, for several nuclear species and locations within the unit cell, and for the following temperatures: room temperature, just above $T_c$ (in italics), and near zero (in boldface). $^{87}Rb$ and $^{133}Cs$ line positions are given for three positions within the unit cell: the site of octahedral coordination ("$O$") and the two sites of tetrahedral coordination, $T$ and $T'$. The presence of *two* tetrahedral NMR lines is unexpected; only one tetrahedral peak is expected in the assumed fcc lattice structure. The extra peak, first reported by Walstedt *et al.* (1993), is discussed in Sec. IV.B.2.d. The "center of mass" of the $T$ and $T'$ line-shape peaks for $^{87}Rb$ and $^{133}Cs$ line shapes are also given in the column labeled "CM, $T$, $T'$." The line positions are discussed thoroughly in Secs. III.A, B, and C and in IV.

| | $^{13}C$ | $^{87}Rb$ | | | | $^{133}Cs$ | | | | $^{39}K$ | | |
|---|---|---|---|---|---|---|---|---|---|---|---|---|
| | | $O$ | $T$ | $T'$ | CM ($T$,$T'$) | $O$ | $T$ | $T'$ | CM | $O$ | $T$ | CM |
| | 187[a] | | | | | | | | | 56 | 116 | 110 |
| $K_3C_{60}$ | 195[b] | | | | | | | | | | | |
| | **162**[b] | | | | | | | | | | | |
| $K_2RbC_{60}$ | 188 | 65 | | | | | | | | | 116 | 116 |
| | | –30 | | | | | | | | | | |
| | | **–4** | | | | | | | | | | |
| $KRb_2C_{60}$ | 184 | 65 | 192 | | 192 | | | | | | 123 | 123 |
| | 182[a] | 68 | 192 | 281 | 206 | | | | | | | |
| $Rb_3C_{60}$ | 192[b] | | | | | | | | | | | |
| | **151**[b] | | | | | | | | | | | |
| | 182[a] | | 193 | 312 | 211 | 30 | | | | | | |
| $Rb_2CsC_{60}$ | 186[a] | | | | 78 | –90 | | | | | | |
| | **147**[a] | | | | **–117** | **9** | | | | | | |
| $RbCs_2C_{60}$ | 177 | | 223 | 320 | 228 | 19 | 265 | 397 | 285 | | | |

[a]Stenger *et al.* (1995)
[b]Tycko *et al.* (1992)

terms describing nuclear-electron spin-spin hyperfine coupling (Abragam, 1961; Slichter, 1990). These same terms are also among the factors that determine the spin-lattice relaxation rate $1/T_1$ (Sec. III.D). We shall write these expressions in terms of a nuclear spin $\vec{I}$ and an electron spin $\vec{S}$. Of course, for many-electron systems $\vec{S}$ should be replaced by the spin-density operator, as follows:

$$\vec{S}(\vec{r}) \rightarrow \sum_{i=\text{all electrons}} \vec{S}_i \delta(\vec{r}-\vec{r}_i).$$

We shall discuss two hyperfine terms and their resulting Knight shifts—the Fermi contact term and nuclear-electron dipole-dipole term:

#### a. The Fermi contact term

The *Fermi contact* hyperfine coupling term is given by

$$\mathcal{H}_{\text{contact}} = \frac{8\pi}{3} \gamma_e \gamma_n \hbar^2 \vec{I} \cdot \vec{S} \delta(\vec{r}) \tag{8}$$

where $\vec{r}$ is the position vector of the electron, and the nucleus is taken to be at the origin. For metals with spin susceptibility $\chi^s$, this term leads to a Knight shift given by

$$K^s = \frac{8\pi}{3} \langle |\psi(0)|^2 \rangle_{E_F} \chi^s \tag{9}$$

where $\langle |\psi(0)|^2 \rangle_{E_F}$ is the average over the Fermi surface of the squared magnitude of the Bloch wave functions evaluated at the site of the nucleus. Note that non-*s* electrons will have no contact interaction, since they vanish at the site of the nucleus.

We comment briefly on normalization in Eq. (9) (and other expressions for shift). If $\chi^s$ is taken to be the dimensionless susceptibility, then $\langle |\psi(0)|^2 \rangle_{E_F}$ should be normalized to a volume of 1 $\text{cm}^3$. Alternately, $\chi^s$ for "per atom" can be used in conjunction with a $\langle |\psi(0)|^2 \rangle_{E_F}$ normalized to one atomic volume (the volume of the Wigner-Seitz cell).

#### b. Nuclear-electron dipole-dipole coupling

Non-*s* electron spins couple to the nucleus through the magnetic dipole-dipole interaction

$$\mathcal{H}_{\text{dip-dip}} = \frac{\gamma_e \gamma_n \hbar^2}{r^3} \left[ 3 \frac{(\vec{I}\cdot\vec{r})(\vec{S}\cdot\vec{r})}{r^2} - \vec{I}\cdot\vec{S} \right]. \tag{10}$$

Upon integrating over the electron coordinates for a $2p_z$, orbital with $z$ defined as the "parallel ($\|$)" direction, one obtains (Slichter, 1990; pp. 516–524)

$$\mathcal{H}_{\text{dip}} = (\tfrac{2}{5}) \gamma_e \gamma_n \hbar^2 \left\langle \frac{1}{r^3} \right\rangle (2 I_\| S_\| - I_{\perp 1} S_{\perp 1} - I_{\perp 2} S_{\perp 2}), \tag{11}$$

giving an anisotropic Knight-shift tensor:

$$K_\| = \frac{4}{5} \left\langle \frac{1}{r^3} \right\rangle \chi^s; \quad K_\perp = -\frac{2}{5} \left\langle \frac{1}{r^3} \right\rangle \chi^s. \tag{12}$$

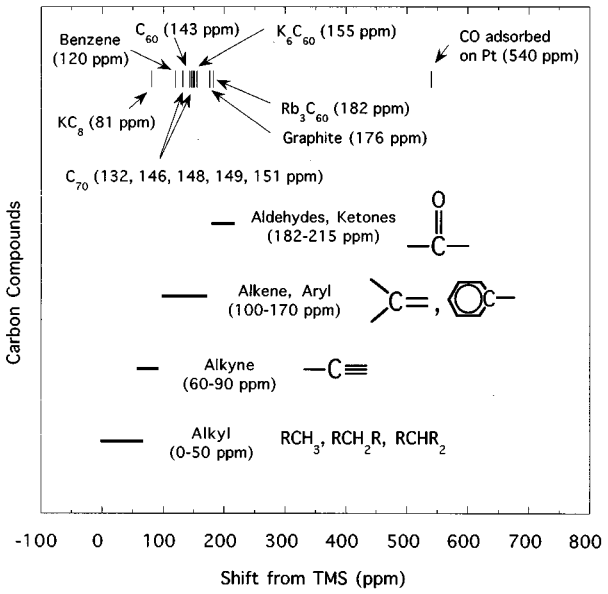


FIG. 10. $^{13}C$ NMR shifts at room temperature for a range of carbon compounds. The shifts are measured in parts per million (ppm) from tetramethylsilane (TMS). Graphite and alkali-intercalated graphite $C_8K$ resonate at 176 and 81 ppm, respectively (Mizutani *et al.*, 1981). Solid $C_{60}$ is at 143 ppm, in the range of aromatic compounds, and the superconducting alkali-fulleride compound $Rb_3C_{60}$ is at 182 ppm. The inequivalent carbon sites of $C_{70}$ in a mixed $C_{60}/C_{70}$ powder (resolved by magic-angle spinning methods) are at 132, 146, 148, 149, and 151 ppm (Tycko, Dabbagh, Fleming, *et al.*, 1991), also in the aromatic range. Insulating $K_6C_{60}$ is at 155 ppm (Tycko, Haddon, *et al.*, 1991). Finally, the $^{13}C$ resonance of carbon monoxide adsorbed on a platinum surface is at 540 ppm (Shore, 1986), a "world record" shift for $^{13}C$. Also shown for comparison are ranges of shifts for $^{13}C$ nuclei in various types of organic compound (Solomons, 1990).

Both Fermi contact Knight shifts and those associated with dipole-dipole coupling are important for alkali $C_{60}$ compounds. We shall discuss each in greater detail for the $^{13}C$ and alkali-metal ($^{39}K$, $^{87}Rb$, and $^{133}Cs$) nuclei, respectively, in Secs. III.B and III.C.

### B. $^{13}C$ shifts and hyperfine couplings

Now we turn to the specifics of the chemical and Knight shifts and the hyperfine couplings of the $^{13}C$ nucleus in $C_{60}$ compounds. (For convenience, we note that $^{13}C$ has a natural abundance of 1.108%, and a gyromagnetic ratio of $2\pi \times 10.705$ MHz/tesla.) Of course we shall make an effort to understand the shifts from theory, but just as often the shifts can be used phenomenologically, as tools of characterization and classification. NMR shifts for a wide range of $^{13}C$ compounds are given in Fig. 10. (In fact, this is a plot of the isotropic part of the shift $\bar{\sigma}$, defined as the average of the three principal components of the total shift tensor.) $C_{60}$ appears at 143 parts per million (ppm) to higher frequency relative to tetramethyl silane, well within the range for

aromatics. $K_3C_{60}$ then appears at 187 ppm or 44 ppm higher. Taking a very crude approach, we might guess that $C_{60}$ and $K_3C_{60}$ have the same chemical shift, and thus the extra 44 ppm represents the Knight shift of the metallic $K_3C_{60}$ compound. In that case, we must regard the 44-ppm $^{13}C$ Knight shift as being very small—especially if we compare it to the Knight shift of 540 ppm that Shore (1986) obtains for $^{13}C$ on supported Pt catalysts, where the carbon orbitals are strongly mixed with the Pt conduction band. As we shall see, it is not surprising that the $^{13}C$ shift should be much smaller than 540 ppm. Nevertheless, the apparent $^{13}C$ Knight shift is substantially smaller than one would expect.

#### 1. $^{13}C$ chemical shifts

Of course we must treat the chemical and Knight-shift contributions separately. We first consider the shift of $C_{60}$, which must be entirely a chemical-shift, since $C_{60}$ is an insulator.

##### *a. Chemical shifts in $C_{60}$ (insulating)*

As mentioned above, the 143-ppm shift of $C_{60}$ relative to tetramethyl silane lies in the range of aromatic molecules. In fact, the full chemical-shift tensor for $C_{60}$, $-(\sigma_{xx},\sigma_{yy},\sigma_{zz})=(220,186,25)$ ppm (Yannoni, Johnson, *et al.*, 1991), is similar to that of oriented benzene, $\sim(190,190,10)$ ppm (Mehring, 1983; Veeman, 1984), which confirms the aromatic character of the $C_{60}$ molecule. Although this observation may not seem surprising, there has been controversy. Haddon *et al.* (1991) and Ruoff *et al.* (1991) measured unexpectedly small diamagnetic susceptibilities; the former find $\chi_g=-0.35\times10^{-6}$ cm$^3$/gram, comparable to diamond ($-0.49\times10^{-6}$ cm$^3$/gram), and much smaller than graphite (orientation averaged: $-7.3\times10^{-6}$ cm$^3$/gram); (DiSalvo *et al.*, 1979). Haddon *et al.* initially interpreted their result to imply small ring currents—that excited-state "Van Vleck" paramagnetic contributions quench the diamagnetic contributions. They attribute an "ambiguous" aromatic character to the fullerenes.

Subsequently, though, Pasquarello, Schluter, and Haddon (1992) use the London approximation to find that (1) Ring currents are of the same approximate magnitude as those in benzene (approximately $7\times10^{-9}$ amps/tesla, as estimated by the authors from the result of Pasquarello *et al.*); (2) Ring currents are paramagnetic on the pentagons ("5-6" bonds) and diamagnetic but much smaller on the "6-6" bonds; and (3) While the pentagon currents are paramagnetic, diamagnetic currents, which flow all around the $C_{60}$, result in a very small total susceptibility.

##### *b. An additional orbital shift in metals?*

In addition to the aromaticlike chemical shifts in insulating $C_{60}$, one might inquire about the possibility of an additional orbital or chemical shift in the metallic compounds, which is associated with partially filled molecular orbitals (see, for example, Noer and Knight, 1964). From a molecular point of view, we say that the magnetic field, through its interaction with the electron orbital angular momentum, mixes the three molecular $t_{1u}$ states, thereby unquenching the angular momentum. The orbital magnetism then interacts with the nuclear spin. This effect is widely known as the "Van Vleck" contribution to the susceptibility. This picture carries over easily to a description of electrons in a conduction band—the field then mixes unfilled Bloch states into the filled states. The mechanism involves electron energy levels ranging throughout the band—not just those within $k_BT$ of the Fermi energy—and thus, like the other orbital shift mechanisms, we expect it to be unaffected by the superconducting transition.

We can use second-order perturbation theory (Slichter, 1990) for an order-of-magnitude estimate for this extra shift (here denoted $K^L$):

$$K^L \approx \frac{\mu_B^2 |L_i|^2}{W}\left\langle \frac{1}{r^3}\right\rangle .$$

Here $\mu_B$ is the Bohr magneton, $|L_i|^2$ is a matrix element for the angular momentum operator (between two quenched molecular $t_{1u}$ states), and $W$ is an energy denominator. $W$ should be of the order of the electronic bandwidth, 0.5 eV. For $\langle 1/r^3\rangle$ we take $\frac{1}{60}$ of the atomic value (ESR measurements give $\langle a_0^3/r^3\rangle=1.7$; Weil *et al.*, 1994). The factor of $\frac{1}{60}$ is used because the molecular wave functions are distributed over 60 carbon atoms, and thus at each atom the wave function's probability density is reduced to (on average) 1/60th of the atomic value. Setting $|L_i|^2$ to unity, we estimate a shift of $\sim$25 ppm. In some sense this value is small—we shall show that the Knight shifts should be about an order of magnitude higher than this number—but it turns out experimentally that the total shift is not so large, and a 25-ppm additional orbital shift may be a significant fraction of the total.

#### 2. Hyperfine and Knight-shift coupling tensors

The $^{13}C$ hyperfine coupling to the electron spin density in $A_3C_{60}$ is a complex affair. We shall see that the $^{13}C$ Knight shift for $K_3C_{60}$ estimated above as $\sim$44 ppm is surprisingly small and has important implications regarding the *s*-electron component of the electronic density of states at the Fermi level. For the hyperfine coupling tensor $\overleftrightarrow{A}$ (Sec. III.A), it is convenient to treat separately the isotropic part, which is equal to the average of the three principal components of the tensor, and the remaining traceless anisotropic part, resulting from nuclear-electron dipole-dipole coupling [Eq. (10)]. In Secs. III.B.2.a.i, ii, and iii we shall estimate the isotropic hyperfine coupling terms and use them, together with measured spin susceptibilities, to make an *a priori* estimate of the isotropic part of the Knight shift. Then in Sec. III.B.2.b we shall estimate the anisotropic part of the hyperfine coupling and Knight-shift tensors and compare our estimate with experimental data.

*a. Isotropic part of the Knight shift*

The Fermi contact interaction [Eq. (8)], in which the nuclear spin interacts with unpaired electron-spin density in $s$ orbitals at the position of the nucleus, is the source of all isotropic parts of the spin-hyperfine interaction. The unpaired spin density, however, is produced through several mechanisms, involving both on-atomic-site unpaired electrons and unpaired electrons on neighboring atomic sites.

Karplus and Fraenkel (1961) have developed a successful theory that can be used to predict these isotropic couplings for a $^{13}C$ nucleus to unpaired electrons in both the on-site $2p_z$ orbitals and in $2p_z$ orbitals of nearest-neighbor carbons, to which the carbon is $\pi$ bonded. They find a nuclear-electron-spin Hamiltonian can be written as follows:

$$\mathcal{H}=\vec{I}\cdot\left[\left(A_{\rm iso}+\sum_{j=1}^{3}B'\right)\vec{S}_0-\sum_{j=1}^{3}B\vec{S}_j\right] \tag{13}$$

where $\vec{I}$ is the $^{13}C$ nuclear spin, $\vec{S}_0$ is the on-site electron spin in the $2p_z$ orbital, and $\vec{S}_i$ are the spins in $2p_z$ orbitals on neighboring carbon atoms. The first summation runs over the three $sp^2$ orbitals on the atom containing the $^{13}C$, and the second summation runs over the three nearest-neighbor carbons. The terms $A_{\rm iso}$, $B$, and $B'$ are now defined briefly, then discussed in the following subsections:

(1) $A_{\rm iso}$: Direct Fermi contact + core polarization

(a) Direct Fermi contact coupling of the $^{13}C$ spin with any $2s$ spin density that is admixed into the $2p_z$ wave function of the on-site electron spin. In $C_{60}$ the $2s$ admixture would result from nonplanarity of the molecule.

(b) Core polarization: Coupling of the $^{13}C$ spin to the on-site $2p_z$ electron spin through the latter's polarization of the (filled) on-site $1s$ core electrons ("core polarization").

(2) $B'$: Spin polarization of the $\sigma$ bonds
Coupling of the $^{13}C$ spin to the on-site $2p_z$ electron through its polarization of the (filled) on-site $sp_2$ orbitals that make up the $\sigma$ bonds ("$2s$ spin polarization")

(3) $B$-spin polarization of $\sigma$ bonds by a neighbor ("transferred hyperfine coupling")
Coupling of the $^{13}C$ spin to the electron-spin densities in $2p_z$ orbitals on neighboring carbons through their polarization of the on-site $2s$ orbitals that make up the $\sigma$ bonds ("transferred" $2s$ spin polarization).

(i) *$B$ and $B'$: The spin-polarization terms.* We first treat the terms $B$ and $B'$, which concern the spin polarization of $\sigma$ bonds by the $2p_z$ electron. Figure 11 shows two carbon atoms, labeled atom 1 and 2, connected by a filled $\sigma$ bond. Atom 1 contains the $^{13}C$ nucleus under consideration. In the top panel atom 1 has an unpaired up spin in its $2p_z$ orbital.

The $B'$ term arises as follows: because of the exclusion principle and Coulomb energy, the down-spin orbital in the $\sigma$ bond is preferentially pushed away from atom 1, relative to the up-spin orbital, leaving behind a net up-spin density at the site of the nucleus. This can be understood by noting that the spatial part of the wave function for two spins having opposite directions is symmetric under exchange of the spatial coordinates of these two electrons, so that Coulomb repulsion for opposite spins can be large. In contrast, the spatial part of the wave function for two up spins is antisymmetric, and thus Coulomb repulsion is reduced (Landau and Lifshitz, 1977). Thus, even though the $\sigma$ bond is filled with an up and down spin, there is a net up-spin density that

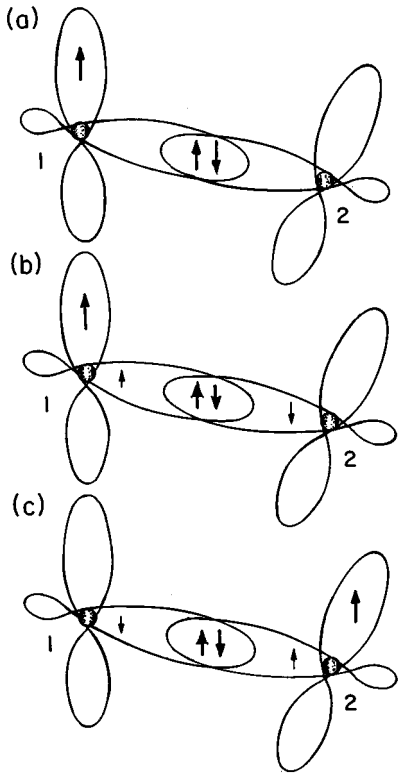


FIG. 11. Schematic diagram depicting the spin-polarization contributions to the isotropic part of the $^{13}C$ Knight shift in $A_3C_{60}$. (a) Two carbon atoms (1 and 2) connected by a filled $\sigma$ bond. Atom 1 contains the $^{13}C$ nucleus under consideration and has an unpaired up spin in its $2p_z$ orbital. Panel (b) illustrates how the spin density for the on-site $2p_z$ orbital results in a spin polarization of the atomic $2s$ orbitals and hence an on-site, "spin-polarization" hyperfine coupling term. Because of the exclusion principle and Coulomb energy, the down-spin orbital in the $\sigma$ bond is preferentially pushed away from atom 1, relative to the up-spin orbital, leaving behind a net *up*-spin density at the site of the nucleus. This is depicted schematically by the small up arrow next to atom 1. This net up-spin density, which resides in atom 1's $sp_2$ orbital, interacts with the $^{13}C$ nucleus on atom 1 through the Fermi contact mechanism. Panel (c) illustrates the transferred hyperfine coupling mechanism. The up electron spin is now in the $2p_z$ orbital of atom 2. Now the down-spin density is preferentially repelled from atom 2, generating a net down-spin density on atom 1 (small down arrow). This "transferred hyperfine coupling" from 2 to 1 can interact with the $^{13}C$ on atom 1. Note that it has a sign that is opposite to that of the on-site interaction.

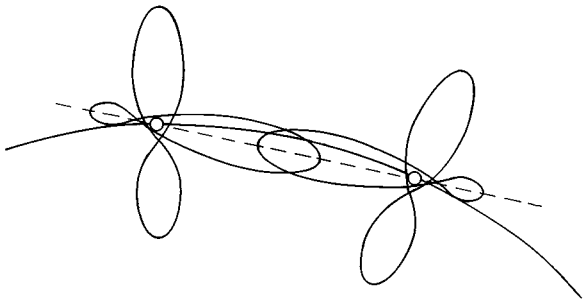

FIG. 12. Illustration of the expected carbon-carbon bonding scheme in $C_{60}$. Two near-neighbor carbon atoms are pictured lying on the surface of the buckyball sphere. Neglecting the curvature of the molecule, we assign an $sp_2$ bonding scheme. Each carbon has a $2p_z$ orbital oriented radially with respect to the molecular sphere, and these two orbitals participate in forming a $\pi$ bond between the two carbons. Also shown are $\sigma$ bonds (well below the Fermi energy) between the carbons, formed from the $sp_2$ atomic orbitals oriented tangentially to the buckyball sphere. This zeroth-approximation picture is modified by effects of curvature, as discussed in the text.

resides in atom 1's $sp^2$ orbital. This spin density interacts with the $^{13}C$ nucleus through the Fermi contact mechanism. This is depicted schematically in panel (b) by the small "up" arrow next to atom 1.

The $B$ term ("transferred hyperfine coupling") is closely related. Panel (c) in Fig. 11 shows an up electron spin in the $2p_z$ orbital of atom 2. The down-spin density is repelled from atom 2 and toward atom 1, which holds the $^{13}C$ nucleus. Now there is a net down-spin density on atom 1, which interacts with the $^{13}C$ on atom 1. The fact that the spin density is down on atom 1 in this instance accounts for the sign in front of this term in Eq. (13).

It is found (Karplus and Fraenkel, 1961) that if each carbon is equivalent in Fig. 11, then $B=B'\simeq 1.6\times10^{-12}$ eV.

(ii) *$A_{iso}$: Direct Fermi contact and core-polarization term.* The term $A_{\rm iso}$ is the coupling of the $^{13}C$ nuclear spin to the on-site electron, and it contains the effects of both items 1(a) and 1(b) above.

Term 1(b), the core polarization of the $1s$ electrons, is known to be approximately $-1.50\times10^{-7}$ eV (Karplus and Fraenkel, 1961), which is negative and comparable to $B$ and $B'$.

In the absence of curvature of the buckyball molecule, term 1(a) (the direct Fermi contact term resulting from admixture of $2s$ into the $2p_z$) would make no contribution, and we would be left with *only* the core-polarization contribution, giving $A_{\rm iso}=-1.50\times10^{-7}$ eV. The presence of curvature, however, changes this conclusion dramatically and should result in a large, positive value for $A_{\rm iso}$.

Thus in Fig. 12 is shown a carbon atom, containing a $^{13}C$ nucleus, which is double bonded to its near neighbor, which lies 11.6° below the horizontal (Haddon, 1988). To zeroth approximation, two types of bond are present—the sigma bond made up of adjoining $sp_2$ orbitals, and the $\pi$ bond, made up of overlapping $p_z$ orbitals. But in fact, due to the curvature of the $C_{60}$ molecule, the $sp_2$ orbitals, which ordinarily lie within the $xy$ plane (defined by the $p_z$ orbital), must tilt somewhat to match with the neighboring carbon. Most important for our hyperfine considerations, there must also be a small $s$ admixture in the $p_z$ orbital, so that it may retain its orthogonality. (Here we assume "orbital following.") Deviations from orbital following are considered in the ESR literature (Schrader and Karplus, 1964.)

Karplus (1959) has given the wave functions applicable in this situation in terms of the angle $\theta$ made with the horizontal (11.6° for $C_{60}$). Denoting the modified wave functions $p_z'$ and $\sigma_i'$, and writing in terms of the orbitals $s$, $p_z$, and $p\sigma_i$ (where $i$=1,2,3 and $p\sigma_i$ is a $p$ orbital that would point along the axis of one of the three carbon-carbon bonds in the structure with no curvature), we have

$$|2p_z'\rangle=(1-2\tan^2\theta)^{1/2}|2p_z\rangle-\sqrt{2}\tan\theta|2s\rangle,$$
$$2sp_2'^{i}\rangle=(\tfrac{2}{3}\sec^2\theta)^{1/2}|2p\sigma^i\rangle+(\tfrac{1}{3}-\tfrac{2}{3}\tan^2\theta)^{1/2}|2s\rangle. \quad (14)$$

Note that $p_z$ and $sp_2$ are obtained for $\theta$=0 as expected. From Eq. (14) we estimate for the $p_z'$ orbital an $s$-orbital weighting equal to 9.2% of the $p_z$ weighting, in agreement with Haddon (1988). Haddon observes that the angle $\theta$=11.6° is in some sense large—the corresponding angle for pure $sp_2$ is 0, while for $sp_3$ it is 19.4°, and thus we are more than halfway toward reaching $sp_3$. Yet the $s$ weighting of 9.2% is much smaller than the analogous weighting in $sp_3$ (33%). The degree of rehybridzation, then, is rather insensitive to $\theta$ for small $\theta$ values.

Karplus and Fraenkel calculate that, with this wave function, the admixture of the $2s$ wave function into the $p_z$ orbital results in an additional direct Fermi contact contribution to $A_{\rm iso}$ equal (in eV) to $138\times10^{-7}\times2\tan^2\theta$, giving the following estimate for $A_{\rm iso}$:

$$A_{\rm iso}=[-1.5+138\times(2\tan^2\theta)]\times10^{-7}\ \text{eV}. \quad (15)$$

(In addition, they find a modest change in $B$ and $B'$.) The predictions of Karplus and Fraenkel of the hyperfine couplings as a function of the angle $\theta$ given above have been tested experimentally using the election-spin resonance of hydrocarbon radicals, e.g., Fessenden, 1967.

(iii) *A priori estimate of the Knight shift in $Rb_3C_{60}$.* The terms estimated in the last section enable us to estimate the isotropic part of the Knight shift for $^{13}C$ in $Rb_3C_{60}$. First we note that the effects of the $B$ and $B'$ hyperfine contributions cancel each other, since $B\sim B'$. (Their effects upon spin-lattice relaxation ($1/T_1$) would *not* cancel if the electron-spin density were free to vary from atom to atom within the molecule.)

We estimate $A_{\rm iso}$ from Eq. (15) and find $A_{\rm iso}=10.1\times10^{-7}$ eV. Note that this value is large and positive, as compared to the previous estimate, $A_{\rm iso}=-1.5\times10^{-7}$ eV, which was obtained assuming no molecular curvature and no $2s$ admixture into the $2p_z$ orbital. Using the revised value of $A_{\rm iso}$ and the spin sus-

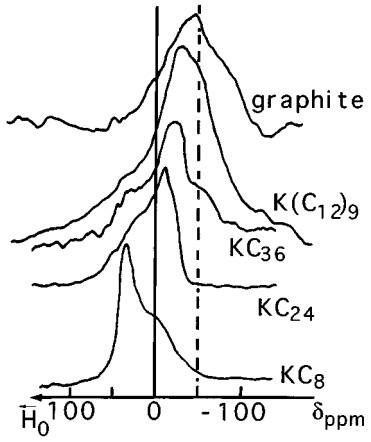


FIG. 13. $^{13}C$ NMR spectra of graphite and the graphite intercalation compounds $K(C_{12})_9$, $KC_{36}$, $KC_{24}$, and $KC_8$ (Cornad *et al.*, 1980). The right-hand direction is the direction of increasing frequency for a fixed field. Note that the most highly doped compound, $KC_8$, is shifted to *lower* frequency relative to undoped graphite. The shift is to lower frequency because of the negative "1*s* core-polarization" hyperfine coupling term, whereby unpaired spin density in the $2p_z$ orbitals distorts the radial wave function of the 1*s* core electrons, resulting in unequal up and down 1*s* electron-spin densities at the site of the nucleus. In the $C_{60}$ compounds the curvature of the molecule is expected, in the simplest picture, to admix the 2*s* wave function into the $2p_z$, resulting in a larger, positive hyperfine coupling term. (This discussion neglects important effects of transferred hyperfine coupling described in the text.).

ceptibility measured by Ramirez, Rosseinsky, *et al.* (1992) of $\sim 1.3\times10^{-3}$ cm$^3$/molecule $C_{60}$ ($3.6\times10^{-29}$ cm$^3$/carbon atom), we obtain the following estimate for the $^{13}C$ isotropic shift $K_s$:

$$K_s=\left(\frac{A_{\rm iso}}{\gamma_e\gamma_n\hbar^2}\right)\chi^s\approx 440 \text{ ppm}. \tag{16}$$

This differs substantially from the earlier experiment-based estimate of 44 ppm. The small experimentally measured shift brings to mind the photoemission data, which indicate an electronic bandwidth several times wider than is predicted by band theory; yet, the interpretation of that data is unclear at present. [See discussion in Pickett 1994; p. 305–310.] We suspect a more prosaic mechanism—that the admixture of an *s* wave function into the atomic orbitals making up the Bloch wave functions near the Fermi energy is several times smaller than is predicted above, based on the theory of orbital following. We present in the next section an independent experimental result that supports the conclusion.

[Parenthetically, we note that the machinery of this section can be used with reasonable success on historical data. For example, the center of mass of the $^{13}C$ line for graphite intercalation compound $KC_8$ is shifted to lower frequency relative to graphite by $\sim$60 ppm (Conard *et al.*, 1980); our number, 60 ppm, is taken from their published line shapes (Fig. 13) and differs somewhat from that given in their Table 1 (90 ppm) because we have used the center of mass of the line shape, while it appears that they took the peak. Using the spin susceptibility of this compound of $1.8\times10^{-29}$ cm$^3$/carbon atom (obtained from specific-heat data; Dresselhaus and Dresselhaus, 1981; p. 273) and a hyperfine coupling of $-2.4\times10^{-19}$ erg, we estimate a Knight shift to lower frequency of 30 ppm, which we believe is reasonable given some uncertainty in extracting the spin susceptibility.]

(iv) *A reevaluation of the hyperfine coupling and the s character of the "$p_z$" orbitals.* The measured $^{13}C$ shift in $Rb_3C_{60}$ is much less than expected. What, then, is the source of this discrepancy? Either the measured susceptibility is in error (several times too large) or the hyperfine coupling is much smaller than anticipated. The former possibility seems unlikely, since susceptibility values obtained through ESR (Wong *et al.*, 1992; Jannosy *et al.*, 1993) agree with the static measurements.

A more likely possibility is that the fraction of *s*-orbital character is less than anticipated. Hawkins *et al.* (1991a,b) have used NMR to probe this issue. Their method involved the use of $^{13}C$ 2D NMR spectroscopy to measure the indirect nuclear coupling $J_{12}$ (Abragam, 1961; Slichter, 1990) between nearest-neighbor carbon atoms, carbon 1 and carbon 2. "Indirect" nuclear coupling is an electron-mediated coupling between nuclear spins $\vec{I}_1$ and $\vec{I}_2$ of the form $J_{12}\vec{I}_1\cdot\vec{I}_2$, well known in analytical chemistry as the source of "multiplets" in the high-resolution NMR spectra of organic molecules (Morrison and Boyd, 1973). Indirect nuclear coupling does not result in measurable splittings in an unadulterated $C_{60}$ molecule in solution, because in that situation all $^{13}C$ nuclei are chemically equivalent. (It is well known in the NMR community that indirect nuclear coupling is not effective between chemically equivalent spins. The problem is treated thoroughly by Abragam, 1961, pp. 480–495.) Hawkins *et al.* remedy the situation by bonding a new structural unit to the molecule, forming $C_{60}(OsO_4)$ (4-*tert*-butylpyridine)$_2$. Then carbon atoms are inequivalent according to their positions in the molecule relative to the osmyl unit.

An empirically well-established relationship exists between the indirect coupling between two carbon atoms $J_{12}$ and the *s* character (%*s*) of the atomic orbitals forming the bond, namely (Weigert and Roberts, 1972; Wehrli and Wirthlin, 1976),

$$J_{12}=7.3\,\frac{(\%s)^2}{100}-17[\text{Hz}]. \tag{17}$$

Utilizing this relationship, Hawkins *et al.* extract the *s* character for the "5-6" bonds (31.5%) and for the "6-6" bonds (34%). Taking $2\times31.5+34=97$, they deduce the 3% *s* character "left over" for the $p_z$ orbital—about one-third the expected amount.

Using this result in conjunction with Eqs. (15) and (16), we reestimate $A_{\rm iso}=+2.4\times10^{-7}$ eV and a Knight shift of $\sim$100 ppm, more than a factor of four smaller than estimated previously, and in better agreement with the apparent experimental value. The apparently small *s* character of the $C_{60}$ molecule may indicate that the $\sigma$ bonds involved are effectively "bent," as in Fig. 14.

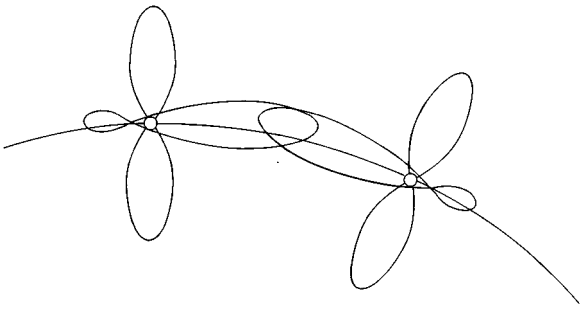

FIG. 14. Schematic diagram depicting the possibility of "bent" $\sigma$ bonding between carbon atoms on a buckyball, which could explain the anomalously small isotropic Knight shift of $^{13}C$. One expects that the curvature of the $C_{60}$ molecule would mix $2s$ into the $2p_z$ atomic orbitals (where $z$ points radially with respect to the $C_{60}$ sphere). In the "bent" bonding picture, however, the $sp_2$ orbitals on neighboring C's that make up the $\sigma$ bonding orbital remain nearly perpendicular to their respective $2p_z$ orbitals, resulting in a smaller $2s$ admixture.

### b. Anisotropic part

The anisotropic part of the Knight shift should be a simpler affair. The only anisotropic hyperfine coupling is the nuclear-electron magnetic dipole-dipole coupling [Eq. (10)].

Figure 15 gives a schematic view of a carbon atom on the surface of a buckyball sphere, with the atomic $p_{z'}$ orbital protruding radially, along the $z'$ direction at an angle of $\theta$ with respect to the magnetic field, which points along $z$ (vertically) in the figure. One expects that, approximately, the $z'$ axis will be a principle axis for the hyperfine tensors—we shall call $z'$ the $\|$ axis. The $x'$ and $y'$ directions perpendicular to $z'$ should be approximately equivalent. Thus we refer here to the $\|$ and $\perp$ axes.

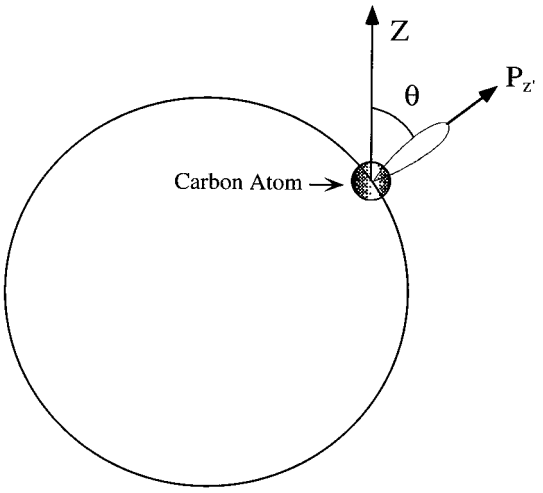


FIG. 15. Coordinate system for discussion of anisotropic Knight shift. The atomic $P_{z'}$ orbital points radially along the $z'$ direction at an angle $\theta$ with respect to the applied magnetic field ($z$ direction).

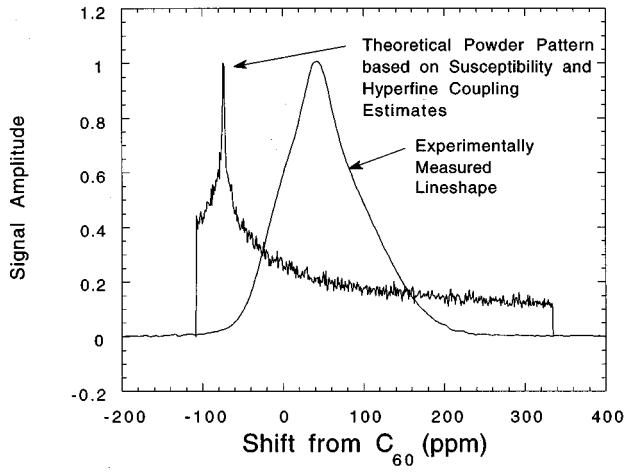


FIG. 16. The experimentally measured $^{13}C$ NMR line shape of $Rb_2CsC_{60}$ at 80 K (Pennington *et al.*, 1995), together with a theoretical prediction. The theoretical powder pattern shape results from a shift tensor, which is obtained as follows: to obtain the Knight-shift contribution, an *a priori* estimate of the dipolar hyperfine coupling of the $^{13}C$ nuclear spin to the electron spin in a $2p_z$ orbital is used in conjunction with the measured spin susceptibility of Ramirez, Rosseinsky, *et al.* (1992). The chemical shift-tensor contribution is taken to be the shift tensor of the undoped $C_{60}$ solid; this contribution tends to cancel partially the Knight-shift contribution. The theoretical pattern is clearly too broad to fit experiment. This issue is resolved in Sec. IV.A.

Taking Eq. (10) and integrating over the electron spatial coordinates for a $2p_z$ orbital, we find that the effective nuclear-electron spin Hamiltonian $H_{\rm dip}$ becomes (Slichter, 1990)

$$\mathcal{H}_{\rm dip}=\tfrac{2}{5}\gamma_e\gamma_n\hbar^2\left\langle\frac{1}{r^3}\right\rangle(2I_{\|}S_{\|}-I_{\perp 1}S_{\perp 1}-I_{\perp 2}S_{\perp 2}). \quad (18)$$

Electron-spin resonance splittings (Weil *et al.*, 1994) in carbon radicals yield a value of $4.7\times10^{-7}$ eV for the parameter $\frac{2}{5}\gamma_e\gamma_n\hbar^2\langle 1/r^3\rangle$. Again utilizing Ramirez' spin susceptibility, we estimate the principal axes of the anisotropic part of the shift tensor as

$$K_{z'z'}\sim 400 \text{ ppm}; \quad K_{x'x'}=K_{y'y'}\sim -200 \text{ ppm}.$$

In order to compare this with experiment we must also include an estimate for the chemical shift. The anisotropic part of the chemical shift, however, tends to cancel the anisotropic Knight shift.

For the chemical shift, we use the measured anisotropic part of the $C_{60}$ chemical shift (77, 43, –118) ppm, plus the measured isotropic shift of 50 ppm of $Rb_2CsC_{60}$ at 80 K relative to $C_{60}$, and add (–200, –200, 400) to obtain a total shift tensor (–73, –107, 332). Figure 16 shows the measured 80-K $^{13}C$ line shape of $Rb_2CsC_{60}$, along with a calculated powder pattern predicted using this estimated shift tensor. It can be seen that the experimental data are much narrower than the theoretical prediction. We return to this issue in Sec. VI.

### C. Alkali-metal nuclei ($^{87}$Rb, $^{133}$Cs, and $^{39}$K): Shifts and hyperfine couplings

We now give a parallel treatment of the shift and hyperfine coupling parameters of the alkali-metal nuclei. Again, we must consider separately the chemical and Knight shifts. Remarkably, we find that the experimentally measured alkali-metal Knight shifts are almost two orders of magnitude smaller than one would estimate from band theory.

#### 1. Alkali-metal chemical shifts

There are three chemical-shift contributions to consider: the core-electron contribution, the contribution from $C_{60}$ ring currents, and a mechanism associated with overlap of the Rb atomic orbitals with the $C_{60}$ molecular orbitals.

##### *a. Core–electron contributions to alkali chemical shifts*

The first term is the diamagnetic shielding of the core electrons of the $A^+$ ion. Since this is purely an atomic property, the trick is to use the free ion as the reference (R. Walstedt, private communication). All additional shifts are associated with the environment of the atom and its influence.

In practice, most NMR laboratories are not equipped to make measurements on the $A^+$ ion. Fortunately, the shift of the free ion relative to dilute aqueous solutions is known from atomic-beam and optical pumping experiments (Lindman and Forsen, 1978). (The relative shifts of the free atom and the free ion are expected to be small on theoretical grounds. We neglect that difference here.)

The effective (screened) gyromagnetic ratios for the *free* ion/atom alkali nuclei are (in MHz per tesla) 16.54640 for $^7$Li; 11.26143 for $^{23}$Na; 1.986538 for $^{39}$K; 13.92812 for $^{87}$Rb; 5.582408 for $^{133}$Cs (Hayne *et al.*, 1968; White *et al.*, 1968; Beckmann *et al.*, 1974; Lindman and Forsen, 1978). The shifts of dilute aqueous solutions of the alkali ions relative to the corresponding free ions are paramagnetic and equal to 11.0 ppm for $^7$Li; 60.5 ppm for $^{23}$Na; 105.1 ppm for $^{39}$K; 211.6 ppm for $^{87}$Rb; and 344.0 ppm for $^{133}$Cs.

If we choose the free ion as the reference, the core contributions to the chemical shift are zero. Taking this convention, the total $^{87}$Rb shifts in $Rb_3C_{60}$ are equal to (Table V) 68 ppm for the octohedral site, 192 ppm for the tetrahedral site ($T$), and 281 ppm for the "extra" tetrahedral site (see Sec. IV.B.2.d).

##### *b. Alkali chemical shifts from ring currents on the $C_{60}$ ion*

The field-induced ring currents on the $C_{60}$ ion, discussed in Sec. III.B.1, produce magnetic fields near the surface of the buckyball sphere and may shift the alkali NMR lines away from the position of the free $A^+$ ion. Pasquarello *et al.* (1992) calculate the field shift that would be seen by a hypothetical probe nucleus as a function of radial distance away from the center of the buckyball molecule. The extra field peaks near the surface of the molecule at ~12 ppm (orientationally averaged) in the plane of a pentagon and ~–5 ppm in a hexagon. These contributions are negligible.

##### *c. Other alkali chemical-shift mechanisms*

Finding little orbital shift in the above crude model in which the Rb nucleus acts as a noninvasive magnetic-field probe, we now speculate about whether the interaction of the Rb atom with the $C_{60}$ molecule should result in a substantial chemical shift.

It seems counterintuitive that a closed-shell ion would have a paramagnetic chemical shift, yet, experimentally, chemical shifts of alkali-halide solids and solutions can vary by tens or hundreds of ppm, depending upon solvent, concentration, and counterion (Bloembergen and Sorokin, 1958; Deverell, 1968; Lindman and Forsen, 1978; Akitt, 1987). For example, $^{87}$Rb in a dilute aqueous RbCl solution has a shift of ~211 ppm (to higher frequency) relative to the free $Rb^+$ ion. The mechanism is thought to be as follows:

To a zeroth approximation we neglect the overlap between atomic wave functions on neighboring counterions in an ionic crystal. Then the one-electron eigenstates for an ion in a magnetic field would be the $s$ states ($l$=0) and the three $p$ states ($l$=1; $m$=1,0,–1). The $s$ state has no orbital angular momentum, and the three $p$ states are each filled, giving zero for the total magnetic moment regardless of the applied field.

In fact, the idealized atomic wave functions on neighboring ions are not orthogonal, but overlap each other somewhat, and thus they are not appropriate choices as elements of a Slater determinant for a many-electron wave function. In order to orthogonalize them, one must take the atomic wave function and mix in a small component of the wave function for the neighboring atom. The use of such orthogonalized atomic wave functions in the Slater determinant does lead to a chemical shift. This mechanism was first proposed to explain the shifts in alkali halides by Kondo and Yamashita (1959). Ikenberry and Das (1965a, 1965b, 1966) subsequently carried out explicit calculations on alkali halides. (The mechanism is also thought to be operative in producing the shifts in alkali halide solutions.) The expression for $\sigma$ is

$$\sigma = -\tfrac{16}{3} Z \left\langle \frac{1}{r^3} \right\rangle \left\langle \frac{1}{\Delta E} \right\rangle \times \left( \sum \text{(squared overlap integrals)} \right), \tag{19}$$

where $\langle 1/r^3 \rangle$ is for the highest occupied $p$ atomic orbitals, $\langle 1/\Delta E \rangle$ is a weighted average excited-state energy, $Z$ is the number of near neighbors, and the summation over "squared overlap integrals" is dominated by the overlaps between atomic orbitals on adjacent atoms which are oriented parallel to the bond axis ($\sigma$ bonds).

The difficulty in this expression is that there is no simple estimate for $\langle 1/\Delta E \rangle$; unlike the Knight shift, the chemical shift does not just involve states near the Fermi energy.

TABLE VI. Hyperfine splittings and hyperfine coupling parameters for alkali-metal atoms. (Here we have converted measured hyperfine splitting frequencies by dividing by $\gamma_n \gamma_e \hbar/2\pi$.)

| Isotope atom | Hyperfine splitting (MHz) | $\frac{8\pi}{3}\langle\lvert\Psi(0)\rvert^2\rangle$ |
|---|---|---|
| $^{7}$Li: | 803 | $2.61\times10^{25}$/cm$^3$ |
| $^{23}$Na: | 1772 | $8.47\times10^{25}$/cm$^3$ |
| $^{39}$K: | 462 | $12.5\times10^{25}$/cm$^3$ |
| $^{87}$Rb: | 6835 | $26.4\times10^{25}$/cm$^3$ |
| $^{133}$Cs: | 9193 | $88.6\times10^{25}$/cm$^3$ |

It is tempting to argue that the overlap integrals in the above expression should be small, due to the rapid changes in sign of the $C_{60}$ molecular orbitals near $E_F$ (Fig. 6); however, it is not clear that those molecular orbitals are the dominant terms.

Thus, overall, it is not clear to the authors whether one should expect for the alkali-metal atom nuclei a substantial (tens or hundreds of ppm) extra chemical shift.

### 2. Alkali-metal nuclei: Knight shifts

Despite uncertainties concerning the chemical shift outlined above, we can conclude that chemical shifts are substantially smaller than 1000 ppm, perhaps at most a few hundred ppm. Now we discuss the Knight shift. We find that theoretical estimates are about two orders of magnitude larger than what would be estimated from experiment.

#### *a. The Fermi contact shift*

The Fermi contact contribution to the Knight shift is the best known and best understood (Knight, 1956). It is also usually dominant in situations where partially filled *s* orbitals are present. It has not yet been fully realized in the literature that the Knight shifts for the alkali nuclei in $C_{60}$ compounds are not just small, but actually much smaller than is reasonably expected.

The contact hyperfine term [Eq. (8)], leads to a shift given by $K^s$:

$$K^s = \frac{8\pi}{3}\langle\lvert\Psi(0)\rvert^2\rangle\chi^s. \tag{20}$$

Here $\langle\lvert\Psi(0)\rvert^2\rangle$ is the probability density of the Bloch wave function evaluated at the site of the nucleus, averaged over the Fermi surface (Slichter, 1990).

The coefficient of $\chi^s$ may be compared to measured hyperfine splittings for the free atom, which are given in Table VI (normalized to one atom; Radzig and Smirnov, 1985).

Satpathy *et al.* (1992, pp. 1789–1790) use the local-density approximation to estimate the admixture of the tetrahedral and octohedral Rb 5*s* wave function into the $t_{1u}$ molecular orbital. Their fractional admixtures range from $\sim10^{-3}$ for octahedral Rb to $\sim2\times10^{-2}$ (total) for the two tetrahedral Rb; these estimates depend somewhat upon buckyball orientation, but they should serve our purposes as an order-of-magnitude estimate.

In order to estimate the Knight shifts for Rb from Eq. (20), we consider a primitive unit cell of the $Rb_3C_{60}$ structure containing one $C_{60}$ and three Rb. One $t_{1u}$ orbital should then have $\sim1\%$ weighting of each tetrahedral Rb 5*s* orbital, so that $(8\pi/3)\langle\lvert\Psi(0)\rvert^2\rangle$ is equal to $10^{-2}\times26.4\times10^{25}$/cm$^3$ (see Table VI). Taking the susceptibility of Ramirez, Rosseinsky, *et al.* (1992a) of $2.2\times10^{-27}$/cm$^3$/$C_{60}$, we estimate a Knight shift of 5800 ppm, comparable to the shift in Rb metal (6530 ppm; Knight, 1956). The actual measured shifts are perhaps a few hundred ppm.

The estimate given, and the conclusion that the Rb shift for $Rb_3C_{60}$ should be approximately equal to that of Rb metal, may seem counterintuitive if one thinks of Rb in $Rb_3C_{60}$ as being almost fully ionized. The key to understanding the estimate is as follows. The size of wave function at the Rb site (in $Rb_3C_{60}$) which we use is in some sense small, since $(8\pi/3)\langle\lvert\Psi(0)\rvert^2\rangle$ is only 1% of the atomic value. In reality, though, it is not so small, because it is normalized to the volume of a $Rb_3C_{60}$ primitive unit cell. The analogous quantity for Rb metal, normalized to an equal volume [one cell containing one $C_{60}$ and three Rb ions can be assigned a volume of 746 Å$^3$, which would contain $\sim8.5$ Rb atoms in Rb metal (density 1.53 g/cm$^3$)], is also reduced, to about $\sim1/8.5$ times the atomic value. Furthermore, the volume susceptibility (for 1 cm$^3$) of $Rb_3C_{60}$ ($2.9\times10^{-6}$) is about 3.6 times that of Rb metal ($0.8\times10^{-6}$; Ashcroft and Mermin, 1976; p. 664). Finally, the experimental Rb-metal shift is about 2.8 times smaller than one would estimate in this manner—a significant discrepancy, but not an order of magnitude. The factors $8.5\times3.6\times2.8$ make up for the factor of 100 lost from the 1% 5*s* weighting in $Rb_3C_{60}$ and fully "explain" why our estimate gives a shift similar to that in Rb metal.

Thus the small size of the Knight shifts in $Rb_3C_{60}$ is quite surprising. Given this fact, however, we must consider core-polarization terms, which one would have expected would be significantly smaller than the Fermi contact term.

#### *b. Core polarization*

Core-polarization hyperfine couplings result from exchange polarization of the core electrons by unpaired valence (or conduction) electrons (Watson and Freeman, 1961). We have already discussed core-polarization effects for $^{13}$C. For that nucleus the core polarization effects are well known. The reason for this is that carbon radicals, with the electron in the $2p_z$ orbital, are well known and heavily studied with ESR.

For the case of the alkali-metal atoms, however, the situation is more unusual. In an alkali-metal solid, the Fermi contact Knight shift is heavily dominant, and there is no need to consider core polarization. For the opposite limit of alkali halide salts, there are no conduction electrons and no spin paramagnetism.

There are, of course, other situations in which the alkali-metal ion appears in a metallic sample, notably graphite intercalation compounds. NMR work on the al-

kali nuclei has been performed on these materials (e.g., Carver, 1970), yet core polarization was not known to be encountered. We shall see experimentally that core polarization probably plays a role in the shifts and relaxation rates for the alkali-metal nuclei, but we find it beyond our means to make *a priori* estimates.

### D. Spin-lattice relaxation ($1/T_1$)

In addition to the Knight shift, the spin-lattice relaxation rate ($1/T_1$) may also be used to extract information about the electronic structure of metals and superconductors. $1/T_1$ is the rate at which nuclear-spin magnetization $M$ returns to equilibrium after being disturbed from its Curie-law-determined value $M_0$. The initial disturbance is typically produced through an rf pulse, for example, a "180° pulse," which inverts the magnetization from $M_0$ to $-M_0$. Following the disturbance the magnetization is monitored as a function of the time $\tau$ following the initial pulse.

The quantity $M(\tau)$-$M_0$ represents the deviation from thermal equilibrium, and in the simplest case this quantity relaxes to zero with an exponential time dependence:

$$[M(\tau)-M_0]\propto e^{-\tau/T_1} \tag{21}$$

where $T_1$ is called the "spin-lattice relaxation time."

Very generally, with the applied magnetic field along the $z$ direction, relaxation requires that the nuclear-spin experience some kind of fluctuating magnetic field with a component perpendicular to $z$, and with a fluctuation spectrum that is nonzero at the NMR resonance frequency.

In an undoped $C_{60}$ solid we shall find that relaxation results from molecular reorientational motion and chemical-shift anisotropy (Sec. IV.B.1.b). For alkali-doped metal samples, however, the relaxation results from the Korringa mechanism, which we now discuss briefly.

#### 1. $1/T_1$ in metals

In a metal, nuclear-spin lattice relaxation is usually dominated by the nuclear-electron hyperfine interaction, which can simultaneously flip the nuclear spin from level $m$ to $m'$ and scatter a conduction electron from a filled Bloch state $\vec{k},s$ (where $s$ is the electron-spin state) to an empty state $\vec{k}',s'$. On the electronic energy scale, the scattering is almost elastic, because the Zeeman splittings (~100 MHz) are typically less than $10^{-6}$ eV.

For the case of noninteracting conduction electrons, this mechanism is easily treated using Fermi's "golden rule" (see, for example, Slichter, 1990; 151–157), which gives

$$\frac{1}{T_1}=\int_0^\infty |\langle i|V_{e-n}|f\rangle|^2\rho^2(\varepsilon)f(\varepsilon)[1-f(\varepsilon)]d\varepsilon \tag{22}$$

where $f(\varepsilon)$ is the Fermi-Dirac distribution function (the statistical probability that a one-electron state with energy $\varepsilon$ is occupied), $\rho$ is the electronic density of states, and $|\langle i|V_{e-n}|f\rangle|^2$ is an averaged effective matrix element for the electron-nuclear hyperfine scattering.

The factors $\rho(\varepsilon)f(\varepsilon)$ and $\rho(\varepsilon)[1-f(\varepsilon)]$ in Eq. (22) have simple interpretations—the former is the density of occupied electron states and the latter the density of unoccupied states. Clearly both are required for scattering. Both terms appear in the integral with the same argument $\varepsilon$ because we have neglected the nuclear Zeeman splitting. The function $f(\varepsilon)[1-f(\varepsilon)]$ will have a width of approximately $k_BT$, and thus $1/T_1$ will be proportional to temperature. This behavior $1/T_1\propto T$ is known as "Korringa" behavior (Korringa, 1950).

We give two concrete examples:

If the Fermi contact interaction [Eq. (8)] is dominant, as is usually the case if there is appreciable $s$ character in the Bloch wave functions at the Fermi surface, then the relaxation rate (for the case of noninteracting electrons) is given by

$$1/T_1T=\tfrac{64}{9}\ \pi^3\hbar^3\gamma_e^2\gamma_n^2[\langle|\psi(0)|^2\rangle_{E_F}]^2\rho^2(E_F), \tag{23}$$

where $\gamma_n,\gamma_e$ are the nuclear and electron gyromagnetic ratios, and $\langle|\psi(0)|^2\rangle_{E_f}$ is the average over the Fermi surface of the squared magnitude of the Bloch wave functions evaluated at the site of the nucleus. For this simple case the quantities $T_1T$ and the Knight shift $K^s$ (Sec. III.A.2.a) are related by

$$T_1T(K^s)^2=\left(\frac{\hbar}{4\pi k_B}\right)\frac{\gamma_e^2}{\gamma_n^2}\,\beta, \tag{24}$$

which is the so-called "Korringa relation." The parameter $\beta$ is equal to one for noninteracting electrons and can be used as phenomenological parameter to characterize the importance of electron-electron interactions (more precisely, the extent of spin correlations). We cite a few examples: for the series of simple metals Li, Na, Rb, Cu, and Al, $\beta$ is given, respectively, by 1.7; 1.5; 1.3; 1.3; 1.2 (see Slichter, 1990; page 157). But $\beta$=0.07 for planar $^{63}$Cu in the high-$T_c$ superconductor $YBa_2Cu_3O_7$, where strong antiferromagnetic fluctuations exist (Millis *et al.*, 1990; p. 172).

Antropov *et al.* (1983) have suggested that the *dipolar* hyperfine interaction (Sec. III.A.2.b) between the $^{13}$C nucleus and the electron in the $2p_{z'}$ C orbital dominates spin-lattice relaxation in alkali fullerides. (Here the prime is used to denote that the $z'$ axis of the carbon orbital may not coincide with the $z$ direction of the applied field.) In that case the relaxation rate is expected to be anisotropic (dependent upon the angle between $z$ and $z'$), with an average over the solid angle $\Omega$ given by

$$\langle(T_1T)^{-1}\rangle_\Omega=\left(\frac{\pi}{2}\right)k_B\hbar^3\gamma_e^2\gamma_n^2\left[\frac{4}{5}\left\langle\frac{1}{r^3}\right\rangle\rho(\varepsilon_F)\right]^2, \tag{25}$$

or, in a convenient form for $^{13}$C by

$$\langle(T_1T)^{-1}\rangle_\Omega=\left(\frac{\gamma_n}{^{13}\gamma}\right)^2(0.063)\times\left[\frac{4}{5}\left\langle\frac{a_0^3}{r^3}\right\rangle\rho(\varepsilon_F)\right]^2\ \text{(eV)}^2\,\text{s}^{-1}\,\text{K}^{-1}, \tag{26}$$

where $a_0$ is the Bohr radius, $\gamma_n$ is the nuclear gyromagnetic ratio, and $^{13}\gamma$ is the $^{13}C$ gyromagnetic ratio, equal to $2\pi\times10.705$ MHz/tesla. By using this relaxation rate with the expression for the anisotropic Knight shift [Eq. (12) in Sec. III.A.2.b] and the spin susceptibility for noninteracting electrons, $\chi^s=[(1/2)\gamma_e^2\hbar^2\rho(E_F)]$, we can find a Korringa relation for the dipolar hyperfine interaction:

$$\langle(T_1T)^{-1}\rangle_\Omega=\left(\frac{4\pi k_B}{\hbar}\right)\frac{\gamma_n^2}{\gamma_e^2}\langle K^2\rangle_\Omega\beta^{-1}. \tag{27}$$

This expression is identical to the usual Korringa relation for the contact mechanism [Eq. (24)] except that the squared shift and $(T_1T)^{-1}$ expressions are powder averages. Again we include the phenomenological parameter $\beta$.

### 2. Relation to $\chi''(q,\omega)$

Although there have not been any detailed analyses of alkali fullerides using the dynamic spin susceptibility in the literature, it is sometimes helpful to use a general expression developed by Moriya (1963) for the spin-lattice relaxation:

$$\frac{1}{T_1}=\frac{4k_BT}{\hbar}\sum_{\substack{\vec{q},\\ \alpha=xx,yy}}\left(\frac{A_\alpha(\vec{q})}{\gamma_e\hbar}\right)^2\frac{\chi''(\vec{q},\omega)}{\hbar\omega}. \tag{28}$$

Here $\chi''(\vec{q},\omega)$ is the dynamic spin susceptibility at spin wave vector $\vec{q}$ and NMR frequency $\omega$. We are intentionally vague about the set of $\vec{q}$ vectors that span the space—this issue is discussed below. Here we have taken the applied field to be along the $z$ axes. The hyperfine couplings $A_\alpha(\vec{q})/\gamma_e\hbar$ for $\alpha=xx,yy$ have units of magnetic field, and indeed represent magnetic fields produced by the nucleus precessing in the $xy$ plane and experienced by the electron-spin system. Since $\chi''$ is the imaginary, absorptive, part of the electron-spin susceptibility, one can see intuitively that Eq. (28) gives a measure of the rate of transfer of energy from the nuclear-spin system to the electron system. A derivation of this relation is given in the appendix of Pennington and Slichter (1990).

Equation (28) is much more general than the Korringa analysis for noninteracting electrons. It becomes particularly important to think in these terms when spin correlations are important—in those instances $\chi(\vec{q},\omega)$ may be peaked somewhere in $\vec{q}$ space, for example at a wave vector corresponding to antiferromagnetism.

For some well-defined cases Moriya has given expressions for $\chi''$ which may be applied (Moriya, 1956a, 1956b, 1977; Ueda and Moriya, 1975). In many cases, however, $\chi''$ is treated phenomenologically.

Hyperfine couplings $A_\alpha(\vec{q})$ are written explicitly as functions of $\vec{q}$ for two reasons. One might expect that the nucleus would only be coupled to the on-site electron spin (a delta function of position) and that the hyperfine coupling would be $\vec{q}$ independent. In fact, however, nuclei may also have important transferred hyperfine coupling to one or more neighbors (Mila and Rice, 1989). In the case of $^{17}O$ in $YBa_2Cu_3O_7$, the nucleus is situated between two spin-carrying atoms and is equally coupled to each. In that case $A_\alpha(\vec{q}=\pi)$ is equal to zero, and that particular nucleus is not sensitive to antiferromagnetic fluctuations, which has important consequences for its relaxation. This phenomenon could also exist for alkali ions in $A_3C_{60}$, if strong antiferromagnetic correlations between neighboring molecules were present. Additionally, $^{13}C$ in the $C_{60}$ molecule is expected to have transferred hyperfine coupling to its carbon neighbors (Sec. III.D.2.a), and this would have important consequences if there were antiferromagnetic correlations within the molecule.

Regarding this latter point, it is important to note that the alkali fulleride lattice has a very nontrivial basis—namely, the entire $C_{60}$ molecule and neighboring alkali ions. Equation (28) was initially derived in terms of the spatial spin susceptibility $\chi(\vec{r},\vec{r}',\omega)$, which gives the magnetization induced at a position $\vec{r}'$ by a magnetic field which is a delta function located at position $\vec{r}$ (Slichter, 1994). It is quite possible that fluctuations in the direction and magnitude of the spin density within a single $C_{60}$ molecule play an important role. In that event one must use a space of $\vec{q}$ vectors that is adequate to span the spatial variation to the needed resolution. As long as the crystal structure is periodic, the full set of reciprocal-lattice vectors can span the space; however, it may not be acceptable to use just the first Brillouin zone, which is the usual procedure.

For examples of the application of Eq. (28) see Millis *et al.* (1990) and Slichter (1994).

### 3. Spin-lattice relaxation in the superconducting state

Spin-lattice relaxation ceases to obey the Korringa law $1/T_1\propto T$ in the superconducting state. Hebel and Slichter (1959; see also Schrieffer, 1988, Chap. 3) first used the BCS theory to calculate the ratio $R_s/R_n$, of the superconducting-state relaxation rate $R_s=(1/T_1)_s$ to that of the normal state, $R_n=1/T_1\propto T$. Their predictions include an initial upturn in $R_s/R_n$ as $T$ is reduced below $T_c$, followed by a steep falloff at low temperature, where $R_s\propto\exp(-\Delta/k_BT)$ and $\Delta$ is the superconducting energy gap at low temperature. The initial upturn is now referred to as the "Hebel-Slichter (HS) coherence peak."

The Hebel-Slichter peak arises from two sources. First, as $T$ is lowered below $T_c$ a gap opens up, and states that were formerly in the gap now "pile up" at the gap edge, giving the BCS form for the density of states

$$N_{\rm BCS}=0 \quad \text{for } E<\Delta(T),$$
$$(N_{\rm norm})\frac{E}{(E^2-\Delta^2)^{1/2}} \quad \text{for } E>\Delta(T), \tag{29}$$

where $N_{\rm norm}$ is the normal-state density of states at the Fermi surface. Equation (29) for $T/T_c=0$ and 0.964, as well as the temperature dependence of the gap parameter $\Delta(T)$, is illustrated in Fig. 17. $1/T_1$ involves an integral over the square of the density of states over a range of energy $\sim k_BT$; that integral increases as the states pile up.

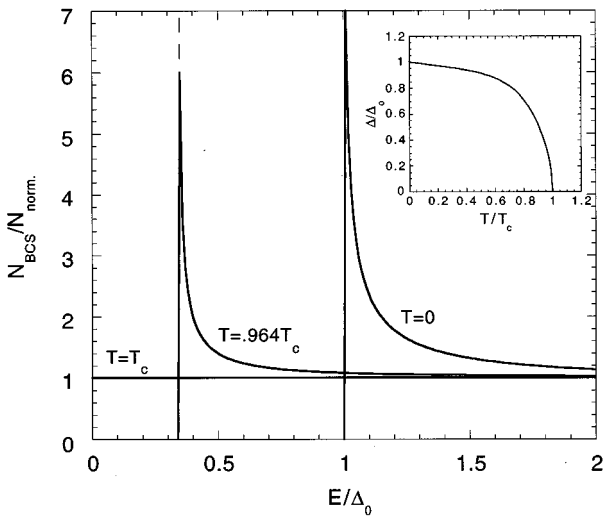


FIG. 17. Plot of the normalized BCS density of states $N_{\rm BCS}/N_{\rm norm}$ given by Eq. (29). The inset shows the temperature dependence of the gap parameter $\Delta(T)$ in the weak-coupling limit of the BCS theory.

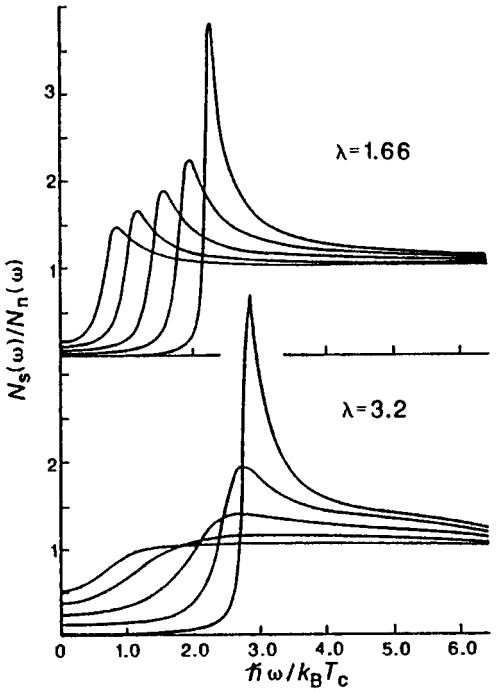


FIG. 18. Eliashberg calculation [using the $\alpha^2F(\omega)$ spectrum of $Pb_{0.9}Bi_{0.1}$] of the normalized density of states $N_s(\omega)/N_n(\omega)$ as a function of energy for five temperatures: $T/T_c$=0.964, 0.928, 0.856, 0.748, and 0.568 (Allen and Rainer, 1991). The peak in $N_s(\omega)/N_n(\omega)$ shifts to the left and broadens with increasing temperature.

The second, more subtle source of the HS peak is the coherence factor, which is intimately tied to the electron pairing feature of the BCS model (see Schrieffer, 1988, Chap. 3). The coherence factor modifies the effective matrix element $|\langle i|V_{e-n}|f\rangle|^2$ appearing in Eq. (22) as follows:

$$|\langle i|V_{e-n}|f\rangle|^2 \rightarrow C_+(E_i,E_f,T)|\langle i|V_{e-n}|f\rangle|^2,$$

where

$$C_\pm(E_i,E_f,T)=\tfrac{1}{2}[1\pm\Delta^2(T)/E_fE_i]. \tag{30}$$

The BCS theory predicts that the plus sign is taken for NMR experiments, and the minus sign for, for example, ultrasonic attenuation. Observations of the sharply contrasting behaviors of $1/T_1$ (Hebel and Slichter, 1959; Redfield, 1959; Redfield and Anderson, 1959) and ultrasonic attenuation (Morse and Bohm, 1957) proved to be crucial experimental confirmations of the "pairing" aspect of the BCS theory (Cooper, 1973).

Both the effects of the coherence factor and the "pileup" of the density of states appear together in the expression for the ratio $R_s/R_n$:

$$R_s/R_n=\frac{2}{k_BT}\int_\Delta^\infty dE_i f(E_i)[1-f(E_i)]\left(1+\frac{\Delta^2}{E_iE_f}\right)\times\left[\frac{E_i}{(E_i^2-\Delta^2)^{1/2}}\right]\left[\frac{E_f}{(E_f^2-\Delta^2)^{1/2}}\right] \tag{31}$$

where $E_f=E_i+\hbar\omega_{\rm nuc}$ and $\omega_{\rm nuc}$ is the NMR frequency.

Equation (31) has a logarithmic singularity for the limit that the NMR Zeeman energy $\hbar\omega_{\rm nuc}$ approaches zero, and indeed that limit is almost appropriate, since Zeeman energies are typically only of order of a few mK. Inevitably other factors smear the pileup and render the Hebel-Slichter peak finite. However, the presence of at least some peaking is often considered to be a quite robust prediction of the BCS theory.

Known mechanisms of Hebel-Slichter peak suppression include anisotropy in the energy gap, inhomogeneity (within the sample) of the gap, and lifetime broadening of the energy gap due to thermal phonons (strong coupling). For a thorough review of each of these, see MacLaughlin (1976). The mechanism of lifetime broadening was first treated in an approximate way by Fibich (1965). More recently accurate analyses based on Eliashberg theory (Akis *et al.*, 1991a; Akis *et al.*, 1991b; Allen and Rainer, 1991) have shown that extreme conditions of strong coupling can completely eliminate the Hebel-Slichter peak and even lead to steep falloffs in $R_s/R_n$ as $T$ is lowered below $T_c$.

Figure 18 (Allen and Rainer, 1991) shows the (real part of the) density of states for two strong-coupling scenarios. Allen and Rainer find that the density of states shown in the lower panel of the figure, labeled "λ=3.2," eliminates all vestiges of the Hebel-Slichter peak. Approximately this degree of strong coupling would be expected for alkali fullerides if the optical phonons (100 $cm^{-1}$) were responsible for pairing. These strong-coupling ideas are discussed more thoroughly in the context of fullerenes in Sec. V. (In addition, suppression mechanisms associated with the applied field are discussed.)

## IV. NMR AS A STRUCTURAL PROBE

Having outlined the necessary but detailed topics of hyperfine couplings and shifts, we turn to NMR investigations of structural properties of $C_{60}$ and $C_{60}$ superconductors. We first discuss the (primarily) static structural properties as probed by NMR line-shape measurements. These studies were among the first to confirm the beautiful symmetry of the molecule and its rapid reorientational behavior in the solid. Line-shape measurements have also proven valuable in studies of doped superconductors—line-shape measurements elegantly prove, for example, that the superconductor $A_3C_{60}$ is a "line compound." Other studies address electronic structure. Then dynamical properties, obtained primarily through measurements of relaxation, both transverse ($T_2$) and longitudinal ($T_1$), and through more exotic techniques including two-dimensional NMR, are discussed. Here NMR has also proven enormously valuable in revealing unusual molecular reorientational behaviors.

### A. Line shapes and (mostly) static properties

#### 1. Pure $C_{60}$ in solution

The beauty of the $C_{60}$ molecule is of course remarkable. Although the molecule contains 60 carbon atoms, each is completely equivalent, a feat unmatched by any other molecule. Certainly the benzene molecule has a romantic history—Kekule claimed to have deduced its structure in a hallucinatory trance in which he saw a snake curling around to bite its own tail (Morrison and Boyd, 1973). The charm of the benzene molecule is its symmetry, and the equivalence of so many atoms. Now we have $C_{60}$, a three-dimensional analog with ten times as many atoms.

Materials with unusual properties rarely fail to betray themselves through their unusual NMR features, and $C_{60}$ is no exception. Figure 19(a) shows the extremely simple NMR spectrum of $C_{60}$ in solution (Taylor *et al.*, 1990). There is only one peak, at 143 ppm relative to tetramethyl silane (TMS—the standard reference molecule for $^{13}C$ NMR). The presence of only one peak confirms that in the solution environment each carbon atom in the $C_{60}$ molecule is equivalent. The line shape for $C_{70}$ in solution is given in Fig. 19(c). $C_{70}$ has five inequivalent carbon sites, out of 70 total carbon atoms. Though still a relatively simple line shape for 70 atoms in a molecule, the added complexity of the $C_{70}$ molecule relative to $C_{60}$ emerges in a richer NMR spectrum. Finally, Fig. 19(d) shows the more usual state of affairs—a line shape for the molecule 17$\alpha$-ethynyl-3-17$\beta$-estradiol in solution (pictured in the figure), which contains 20 carbon atoms.

#### 2. Pure $C_{60}$ solid

We now consider NMR structural implications for $C_{60}$ as a solid, as opposed to $C_{60}$ molecules in solution. Typically solid-state NMR line shapes are much broader than liquid-state line shapes, because in the liquid broad features are "motionally narrowed" by rapid molecular diffusion. Pure solid $C_{60}$, however, is an exception.

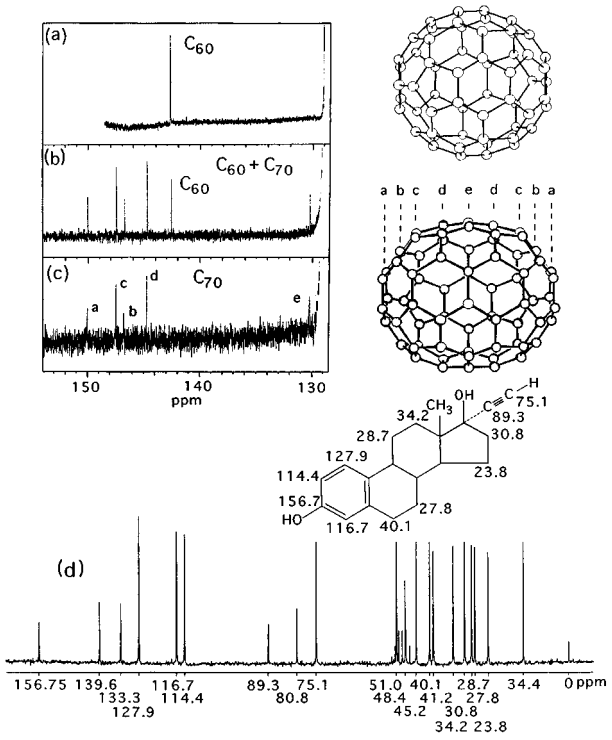


FIG. 19. NMR spectra of $C_{60}$ (a), $C_{60}$+$C_{70}$ (b), and $C_{70}$ (c) in solution (Taylor *et al.*, 1990). For $C_{60}$ there is only one peak, at 143 ppm relative to tetramethyl silane (tetramethyl silane is the standard reference molecule for $^{13}C$ NMR). The presence of only one peak confirms that in the solution environment each carbon atom in the $C_{60}$ molecule is equivalent. The line shape for $C_{70}$ in solution shows 5 inequivalent carbon sites, out of 70 total carbon atoms. Though still a relatively simple line shape for a 70-carbon molecule, the added complexity of the $C_{70}$ molecule relative to $C_{60}$ emerges in a richer NMR spectrum. Also shown for comparison (d) is the line shape for a molecule containing 20 carbon atoms, 17$\alpha$-ethynyl-3-17$\beta$-estradiol, in solution (Breitmaier and Bauer, 1984). This latter molecule yields a spectrum with a richness and complexity more typical of molecules containing tens of carbon atoms.

##### *a. Chemical-shift anisotropy and powder patterns*

The low-temperature NMR line shape for the $C_{60}$ solid is, as expected, quite different from that of $C_{60}$ in solution. Figure 20 (bottom panel) shows the line shape at 77 K (figure from Yannoni, Johnson, *et al.*, 1991; see also Tycko, Haddon, *et al.*, 1991 and Tycko, Dabbagh, *et al.*, 1991). Here the $C_{60}$ molecule's orientation is static on the NMR time scale. The symmetry of the molecule and the equivalence of all $C_{60}$ carbon atoms is now broken by two factors: first, the presence of the crystal lattice, and second, the applied magnetic field. The crystal lattice differentiates carbons according to their position within the molecule and with respect to neighboring molecules. It is clear, for example, that some carbons on the molecule lie much closer to neighboring molecules

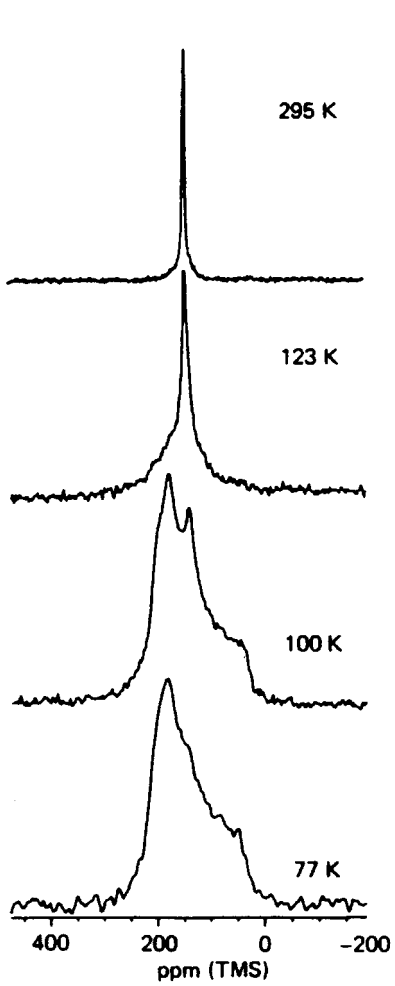


FIG. 20. $^{13}C$ NMR spectra of solid $C_{60}$ obtained at ambient temperatures of 123, 100, and 77 K (Yannoni, Bernier, *et al.*, 1991). The $^{13}C$ NMR spectrum of $C_{60}$ is expected to be a broad "powder pattern" resonance (width greater than ≈200 ppm) reflecting the chemical-shift anisotropy of the $^{13}C$ nuclei averaged over the crystallite orientations. The "motionally narrowed" NMR line at 295 K (143 ppm from tetramethyl silane) proves that $C_{60}$ molecules are rotating rapidly with respect to the NMR time scale, which is defined by the inverse of the spectral spread (≈$10^{-4}$ s). As the temperature is reduced, the powder pattern is recovered as the molecular motion decreases. At 77 K there is little evidence of the narrow line at 143 ppm, and a fit to this line shape yields an asymmetric chemical-shift tensor with components of 220, 186, and 25 ppm.

than do others. For our present discussion we shall neglect this difference. In addition, the magnetic field differentiates carbons—carbons may be distinguished, for example, by the angle that the magnetic field makes with each carbon's $2p_z$ valence orbital (which points radially with respect to the spherical molecule).

As discussed in Sec. III.A.1, the NMR frequency shift for $^{13}C$ can be expressed as a shift tensor with principal components $\sigma_{xx}$, $\sigma_{yy}$, and $\sigma_{zz}$. Taking all carbon atoms to be equivalent in the absence of a magnetic field, we may assign a shift tensor that has the same principal components but different principal axes for each atom. For a shift tensor ($\sigma_{xx}\mathbf{ii}+\sigma_{yy}\mathbf{jj}+\sigma_{zz}\mathbf{kk}$), the NMR frequency $\omega$ for a magnetic field $H_0$ making polar angles $\theta$ and $\varphi$ with respect to the atom's principal coordinate system is given by (Slichter, 1990, pp. 127–131)

$$\omega=\gamma_n H_0\left[1-\bar{\sigma}-\frac{\sigma_{\text{long}}}{2}(3\cos^2\theta-1)-\frac{\sigma_{\text{trans}}}{2}(\sin^2\theta\cos\phi)\right] \quad (32)$$

where $\gamma_n$ is the nuclear gyromagnetic ratio, $\bar{\sigma}$ is the average of the three principal shift-tensor components (the "isotropic part" of the shift tensor), and $\sigma_{\text{long}}$ (the "longitudinal part") and $\sigma_{\text{trans}}$ (the "transverse part") are given by

$$\sigma_{\text{long}}=\tfrac{1}{3}(2\sigma_{zz}-\sigma_{xx}-\sigma_{yy}); \quad \sigma_{\text{trans}}=\sigma_{xx}-\sigma_{yy}. \quad (33)$$

Of course, if we apply a magnetic field to a powder sample of $C_{60}$, the magnetic field will take on all possible orientations with respect to these principal axes, with an equal probability for any element of solid angle $d\Omega=\sin\theta d\theta d\phi$. As a result, the NMR line shape will have a broad spectrum of frequencies, known as a "powder pattern" (Slichter, 1990, pp. 605–616), ranging from $\gamma_n H_0(1-\sigma_{zz})$ to $\gamma_n H_0(1-\sigma_{xx})$, with a peak (singularity) at $\gamma_n H_0(1-\sigma_{yy})$. (By convention we choose the principal axes so that $\sigma_{zz}>\sigma_{yy}>\sigma_{xx}$.)

Such a pattern is observed in the 77-K line-shape data in Fig. 20 (Yannoni, Johnson, *et al.*, 1991). The shift-tensor components (220, 186, 25 ppm) provide a good fit.

### *b. Motional narrowing*

Remarkably, at higher temperatures the line is observed to narrow, until at room temperature the linewidth and position (143 ppm) are similar to that found in the solution sample.

The observed narrowing of the line shape is called "motional narrowing" (see, for example, Slichter, 1990, pp. 592–597) and is quite well known. Let us suppose that, in the absence of motion in a solid, a nucleus may experience two different environments, each giving a different resonance frequency $\omega_1$ and $\omega_2$. Motional narrowing will occur if the environment of the nucleus jumps rapidly, in a correlation time $\tau_c$, between these two situations, such that the jumping rate $1/\tau_c$ is fast compared to the difference frequency $\Delta\omega=(\omega_1-\omega_2)$:

$$\frac{1}{\tau_c}\gg\Delta\omega.$$

This description can be generalized to describe a range of environments and frequencies, rather than just two possibilities. In that case $\Delta\omega$ characterizes the spread in frequencies, and $\tau_c$ characterizes the time required to sample the full range.

The frequency spread is ~200 ppm, giving $\Delta\omega\sim^{13}\gamma H_0(200\text{ ppm})\sim1.2\times10^4\text{ s}^{-1}$ at the applied field of 1.4 tesla, hence $\tau_c\ll100$ $\mu$s. For the case of $C_{60}$, $\tau_c$ is a

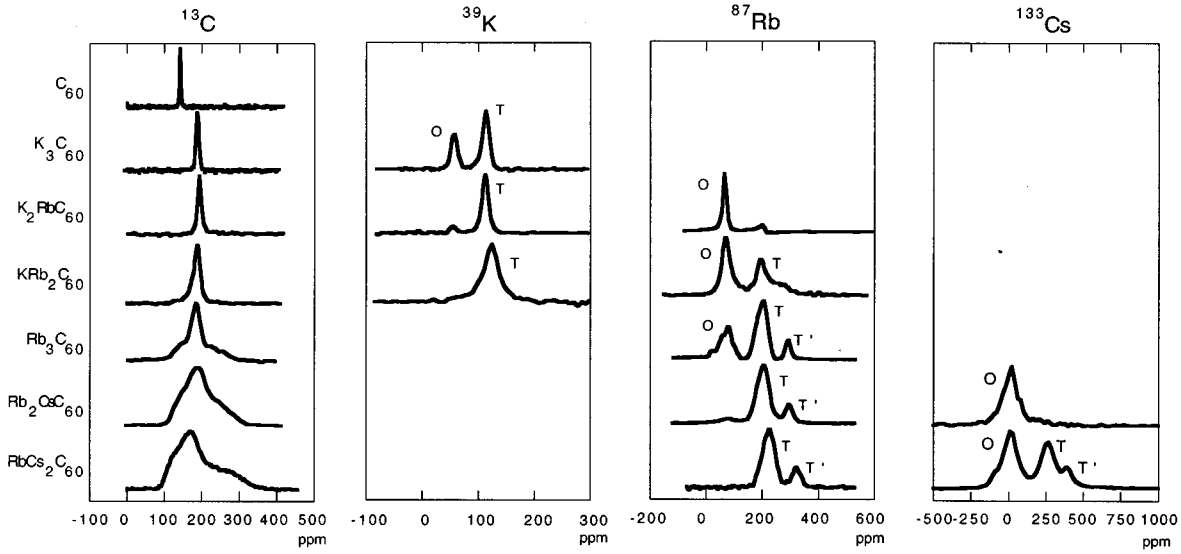


FIG. 21. Room-temperature $^{13}C$, $^{39}K$, $^{87}Rb$, and $^{133}Cs$ NMR spectra for indicated $A_3C_{60}$ compounds (data from Stenger *et al.*, unpublished). Reference compounds are tetramethyl silane (for $^{13}C$) and the free alkali $A^+$ ion for the alkali-metal nuclei. The spectra are arranged in order of increasing lattice constant from top to bottom. Peaks in the alkali line shapes are labeled as "$O$," "$T$," and "$T'$," where "$O$" is for alkali atoms in sites of octahedral coordination and "$T$" for tetrahedral. The "$T'$" is an extra, unexpected peak first reported by Walstedt *et al.* (1993). We cite five features of interest, also discussed in the text. (1) The $^{13}C$ line shape becomes progressively narrower with decreasing alkali intercalant ionic radius. This reflects "motional narrowing;" the smaller alkali ions permit less hindered reorientation of the $C_{60}$ molecule, and thus further motional narrowing of the $^{13}C$ chemical-shift anisotropy powder pattern. (2) It is observed that the larger alkali ion in a given compound will select the larger, octahedrally coordinated ($O$) interstitial site. For example, for the compound $Rb_2CsC_{60}$, a $^{133}Cs$ $O$ peak is observed, but no $T$ or $T'$ peak. Conversely, the smaller $^{87}Rb$ ion displays $T$ and $T'$ peaks, but no O peaks, indicating that the Cs fully occupies each of the octahedral sites (one for every $C_{60}$ molecule), and Rb occupies the tetrahedral sites. (3) There are trends in line position with increasing dopant radius. For example, the $T$ and $T'$ line positions shift to higher frequency with increasing dopant size, perhaps reflecting the increasing density of states (and spin susceptibility) with reduced molecular wave-function overlap. (4) The $T$ and $T'$ peaks for $^{87}Rb$ in $Rb_2KC_{60}$ are nearly merged into one peak; for the same sample the $^{13}C$ is almost fully motionally narrowed. The merging of $T$ and $T'$ reflect a rapidly changing environment of the tetrahedral Rb, alternating between environments corresponding to $T$ and $T'$. At temperatures higher than room temperature, the $T$ and $T'$ peaks collapse to form one peak. (5) $^{133}Cs$ NMR in $Cs_2RbC_{60}$ also displays a $T$, $T'$ splitting.

"reorientational" correlation time, the time required for the molecular orientation to change by a substantial angle (of the order of 45°). In fact we shall see (Sec. IV.B.1.b) that $\tau_c$ is actually of the order of 9 picoseconds at room temperature.

Although motional narrowing is ubiquitous in the NMR literature, the authors feel that the phenomenon in solid $C_{60}$ is particularly elegant and beautiful.

### 3. Line shapes in alkali-doped samples

In adding alkali dopants one takes the already beautiful array of information contained in $^{13}C$ $C_{60}$ line shapes and multiplies it manyfold. Figure 21 provides an overview of $^{13}C$ and alkali-metal room-temperature NMR line shapes for $C_{60}$ and a series of six successive $A_3C_{60}$ compounds, presented from the top of the figure to the bottom in order of increasing lattice constant (which correlates strongly with the ionic radii of the dopant ions).

#### *a. $^{13}C$ line shapes*

The $^{13}C$ line shapes show a very clear trend with increasing alkali dopant size. First, as discussed in Secs. IV.A.2 and III.B.1, the line shape of undoped $C_{60}$ is motionally narrowed and appears at a frequency 143 ppm higher than that of tetramethyl silane. [More precise $^{13}C$ NMR measurements of $C_{60}$ in solution yield a value of 143.68 ppm (Taylor *et al.*, 1990)].

The line shape of $K_3C_{60}$ is also motionally narrowed and centered at 187 ppm, which is 44 ppm higher than $C_{60}$. The added shift represents the sum of any isotropic Knight-shift contribution [which might be expected to contribute a large shift of ~440 ppm (Sec. III.B.2)] and any additional chemical shift relative to undoped $C_{60}$ (Sec. III.B.1). The shift is quite small and could conceivably be nearly all chemical shift—in fact, Tycko *et al.* (1992) report shifts of 37 ppm (relative to $C_{60}$) in *insulating* $Rb_4C_{60}$.

The centers of mass of the line shapes of remaining alkali-doped samples tends to decrease slightly as one increases the size of the alkali dopant combinations—

the shifts relative to $C_{60}$ start at 187 ppm for $K_3C_{60}$ and run to 177 ppm for $Cs_2RbC_{60}$. We note that LDA calculations (Satpathy *et al.*, 1992) yield a 44% increase in the density of states as one increases the lattice constant by 0.3 Å—the approximate range for the samples given [Satpathy *et al.* find that the density of states scales as $\exp(a/\sqrt{2}L)$ with $L$=0.58 Å]. Thus both the direction and the very small magnitude of this trend with increasing alkali-dopant size is quite puzzling.

$^{13}C$ room-temperature line shapes also broaden substantially with increasing dopant size. While the $K_3C_{60}$ line shape is largely motionally narrowed (full width at half maximum ~12 ppm), the line shape for $RbCs_2C_{60}$ spans a total width of approximately 70 ppm.

These trends in linewidth with increasing dopant size are clear indications of several things. First, at room temperature, the $C_{60}$ molecule is reorienting with correlation times of $\sim 10^{-4}$ s (Sec. IV.A.2)—the time is much faster than this for the smaller alkali samples ($K_3C_{60}$) and rather slower for the larger alkali ion samples ($RbCs_2C_{60}$). Second, the alkali ions serve to hinder $C_{60}$ reorientation, and this hindrance is more pronounced for the larger alkali ions. This observation is not unexpected—we note that the $Cs^+$ ion, with nominal radius 1.67 Å, is packed extremely tightly into the ~1.1 angstrom tetrahedral interstitial sites (Sec. II.A).

#### *b. Alkali-metal line shapes. Structural insights*

The line shapes of the alkali-metal dopant nuclei ($^{87}Rb$, $^{133}Cs$, and $^{39}K$ in Fig. 21) also tell very clear and amusing stories. [In Fig. 21 alkali-metal line positions are given relative to the free ion (Sec. III.C.1.a).] It is easiest to begin with the $^{39}K$ NMR, which is plotted for three samples—$K_3C_{60}$, $K_2RbC_{60}$, and $KRb_2C_{60}$. The $K_3C_{60}$ line shape has two peaks as expected, labeled "$T$" and "$O$," for K atoms in the "tetrahedral" and "octahedral" interstitial sites, respectively (Sec. II.A). The peaks are observed in intensity ratios of approximately 2 to 1, also as expected.

As is the case for all the alkali line shapes, we find very small shifts for $^{39}K$—the $K_3C_{60}$ octahedral ($O$) and tetrahedral ($T$) peaks are located at 56 and 114 ppm, and should perhaps be one or two orders of magnitude larger (Sec. III.C.2.a).

There is a very simple interpretation of the difference between the line shapes of $K_3C_{60}$ and $K_2RbC_{60}$. In $K_2RbC_{60}$ the octahedral ($O$) peak is missing, which is as expected. The octahedral interstitial site is larger than the tetrahedral (Sec. II.A), and the $Rb^+$ ion is larger than the $K^+$. Hence when one makes $K_2RbC_{60}$, the larger Rb ions burrow into the spacious octahedral sites, forcing the K ions to reside in the cramped tetrahedral quarters. This type of phenomenon was first reported by Maniwa *et al.* (1992) in the $^{133}Cs$ NMR line shapes of $Cs_2RbC_{60}$ and $CsRb_2C_{60}$.

The $^{87}Rb$ and $^{133}Cs$ NMR line shapes tell similar stories. For example, in $K_2RbC_{60}$ we observe only a single $^{87}Rb$ NMR peak, which comes from octahedral Rb, but in $KRb_2C_{60}$ an additional tetrahedral peak is observed. Since there is only one octahedral site per $C_{60}$ molecule, half the Rb ions are forced to reside in the tetrahedral sites.

The simplicity of this picture is spoiled, however, by the observation that, for samples in which the $Rb^+$ ions occupy tetrahedral sites, the tetrahedral NMR line shape is split into two peaks, labeled $T$ and $T'$ in Fig. 21. (The $T$ and $T'$ peaks are most clearly resolved in line shapes for $Rb_3C_{60}$, $Rb_2CsC_{60}$, and $RbCs_2C_{60}$ samples.) This splitting, first observed for $^{87}Rb$ by Walstedt *et al.* (1993), is quite unexpected. Its implications will be discussed in Sec. IV.B.3. (Figure 21 demonstrates that the $T,T'$ splitting is also resolved for $^{133}Cs$ in $RbCs_2C_{60}$.)

Finally, we comment on trends in the shifts of the alkali NMR peaks.

As noted above and in Sec. III.C.2.a, the shifts are in general much smaller than expected. In addition, though, the octahedral shifts are smaller than the tetrahedral, and in fact very close to zero for $^{87}Rb$ and $^{133}Cs$. This is consistent with LDA estimates (Satpathy *et al.*, 1992) that the admixture of the tetrahedral Rb 5$s$ orbital into $t_{1u}$ is ~20 times the admixture of octahedral Rb; however, this observation must be treated exceedingly cautiously, as we shall see below (IV.A.3.c) that the octahedral ions appear to have negative Knight shifts.

Second, in the series K...Rb...Cs we observe that the shifts for the $T$ site follow an increasing trend. The shift ranges for the three alkali nuclei are $^{39}K$, 116–123 ppm; $^{87}Rb$, 192–228 ppm; $^{133}Cs$, 285 ppm. Assuming zero chemical shift, we may divide by the atomic hyperfine coupling factor (Sec. III.C.2.a) of $(8\pi/3)\langle|\Psi(0)|^2\rangle$. Then the ratios of these shifts (for $^{39}K$ to $^{87}Rb$ to $^{133}Cs$) are 1 to 0.71 to 0.31. The trend, then, is apparently decreasing after the atomic hyperfine coupling is taken into account. The direction of this trend is quite surprising—this corrected shift should be a monotonically increasing function of (1) the spin susceptibility, (2) the matrix element connecting the respective $s$ wave functions into the molecular $t_{1u}$ orbital, and (3) the reciprocal of the energy difference between the Fermi energy $\varepsilon_F$ and the energy of the respective $s$ orbital. All of these factors except for the third would predict that the trend observed should be reversed. The third factor does predict the direction of the trend correctly; however, we note that the ionization energies of K and Cs differ by only ~0.4 eV (Mahan, 1975, p. 595), while the respective $s$ levels should be several eV above $\varepsilon_F$ (Satpathy *et al.*, 1992). Thus the direction of this trend is surprising.

Finally, a third trend is found if we look at the shift of a given nucleus for increasing lattice constant. Most prominently, in the series $KRb_2C_{60}$, $Rb_3C_{60}$, $Rb_2CsC_{60}$, $Cs_2RbC_{60}$ the position of the $T$ line increases from 192 ppm to 228 ppm (18%). LDA estimates give a 35% difference in density of states over this range. Of course, the measured shifts might also include chemical shifts (Sec. III.C.1), and in addition the spin susceptibility that enters the expression for the Knight shift could be "Stoner enhanced" (White, 1983) according to the relation $\chi^s=\chi_0^s/(1-\alpha\chi_0^s)$; here $\chi_0^s$ is the susceptibility in

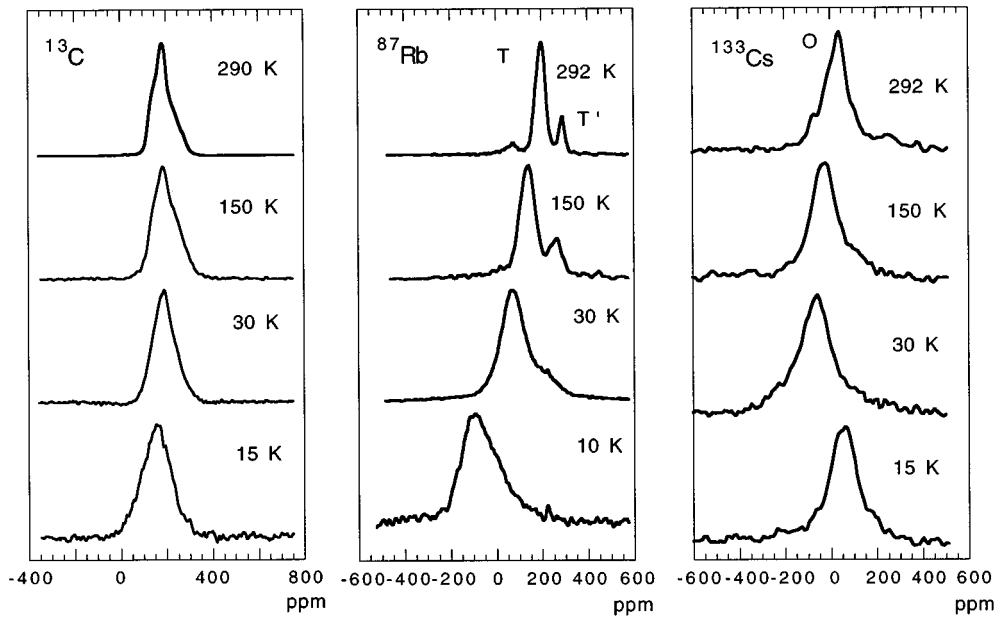


FIG. 22. $^{13}$C, $^{87}$Rb, and $^{133}$Cs spectra in $Rb_2CsC_{60}$ at indicated temperatures and an 8.8-tesla field (data of Stenger *et al.*, 1995). Note: See also Figs. 23 and 31. We cite three features of interest. (1) The $T$ and $T'$ features in the $^{87}$Rb data broaden and then heavily overlap as temperature decreases. (2) The line positions for the $^{87}$Rb $T$ and $T'$ and the $^{133}$Cs peak move to lower frequencies with decreasing temperature, by approximately the same amount; however, (3) as $T$ is lowered below $T_c$ the $^{87}$Rb frequency decreases, while the $^{133}$Cs frequency increases. This latter increase might result from a negative hyperfine coupling for $^{133}$Cs, but then its behavior in the normal state (similar to $^{87}$Rb) is difficult to understand. The contrasting behaviors of $^{87}$Rb and $^{133}$Cs in the superconducting state is used by Stenger *et al.* (1995) to extract the superconducting-state electronic-spin susceptibility.

the absence of electron-electron interactions and $\alpha\chi_0^s$ is an enhancement parameter reflecting the influence of interactions.

The interpretations given above for the three trends in alkali line positions are quite tenuous, given the possibility of substantial chemical shifts. In addition, these interpretations do not always hold up when one considers the temperature dependence of the line positions, including their behavior in the superconducting state. We have presented the interpretations here in order to guide the reader toward the kinds of analyses one might try.

### *c. Temperature dependence of the line shapes and positions*

Representative temperature dependences of the line shapes and line positions are given in Figs. 22 and 23 for a sample of $Rb_2CsC_{60}$ at 8.8 tesla.

The most important temperature dependences are observed in the $^{133}$Cs and $^{87}$Rb line positions. (In Fig. 23 we have plotted the position of the weighted average of the $T$ and $T'$ line positions—these two peaks become unresolvable at lower temperatures.) In the normal state both line positions fall to lower frequencies as temperature is lowered from 292 K to $T_c$=31 K, and in fact the decreases are very similar—a drop of 133 ppm for $^{87}$Rb and 120 ppm for (octahedral) $^{133}$Cs. From this observation alone one would conclude that the temperature de-

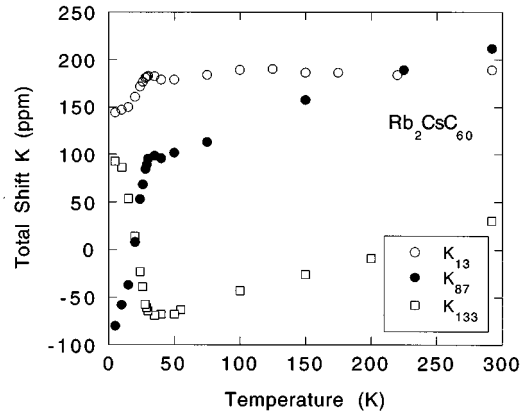


FIG. 23. Shift as a function of temperature for $^{13}$C, $^{87}$Rb, and $^{133}$Cs in $Rb_2CsC_{60}$ in an 8.8 tesla field (Stenger *et al.*, 1995). Reference compounds are the free alkali ions. See also Fig. 22 and its caption, and Fig. 31. For $^{87}$Rb the reported shift is the center of mass of the $T$ and $T'$ peaks, as shown in Fig. 22. While the $^{87}$Rb and $^{133}$Cs shifts have (perhaps by coincidence) nearly the same temperature dependence in the normal state, they behave very differently in the superconducting state, with the $^{87}$Rb frequency dropping (with decreasing temperature) and the $^{133}$Cs increasing. The increasing shift of $^{133}$Cs in the superconducting state is thought to result from a negative hyperfine coupling. The differing behavior of $^{87}$Rb and $^{133}$Cs in the superconducting state is used by Stenger *et al.* to extract the superconducting-state electronic-spin susceptibility.

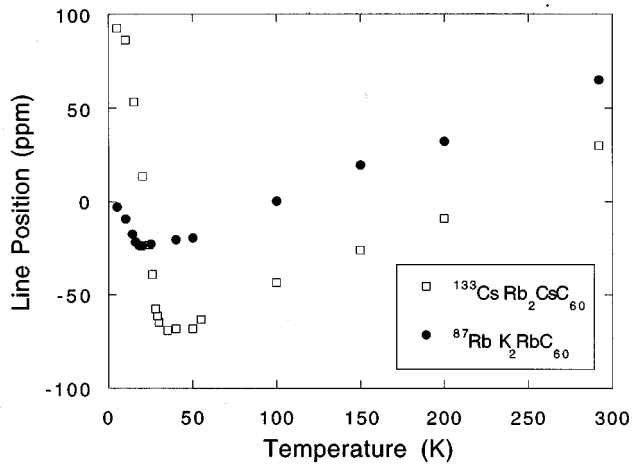


FIG. 24. Line position (of the center of mass) vs temperature for $^{87}$Rb in $K_2RbC_{60}$ and $^{133}$Cs in $Rb_2CsC_{60}$ at 8.8 tesla. In both compounds the nuclei in question are in the octahedral interstitials. As the temperature falls below $T_c$ (23 K and 31 K in zero field for $K_2RbC_{60}$ and $Rb_2CsC_{60}$, respectively) the line positions shift to a higher frequency. The shift in the superconducting state results from both the vanishing of the Knight shift and the onset of diamagnetic Meissner screening currents. Because the shift of the NMR line due to Meissner screening is always to lower frequency values, the net positive shift implies that the hyperfine couplings of the nuclei in the octahedral sites are negative.

pendence of the shift is the result of a temperature-dependent spin susceptibility. Since both nuclei drop by approximately the same amount, one would also conclude that their hyperfine couplings are similar.

The superconducting-state data, however, conflict with that simple interpretation. As $T$ is lowered from $T_c$ to 5 K, the $^{87}$Rb line position falls to lower frequency, as expected. This fall should be the net result of (1) the spin susceptibility's and the Knight shift's drop to zero as the electron spins pair up in the superconducting state; and (2) the partial shielding of the applied field by Meissner currents in the mixed state. [The superconductivity in the alkali fullerides is type II; for a review covering the magnetic properties of the superconducting state see Ramirez (1994) and Dresselhaus *et al.* (1994).] The $^{133}$Cs frequency, however, *increases* as $T$ is lowered below $T_c$. The only simple explanation is that the $^{133}$Cs must have a negative Knight shift in the normal state, resulting from a core-polarization effect (Sec. III.C.2.b). It is not possible, however, to explain the normal-state shift temperature dependences of $^{87}$Rb and $^{133}$Cs if these nuclei have hyperfine couplings of opposite signs.

Figure 24 shows the line position vs temperature of $^{87}$Rb in $K_2RbC_{60}$ and $^{133}$Cs in $Rb_2CsC_{60}$. We see that the $^{87}$Rb line position also goes to higher frequency in the superconducting state if the Rb is in the octahedral site.

### *d. Phase segregation of $C_{60}$ and $A_3C_{60}$*

In order to elucidate normal- and superconducting-state properties of $A_3C_{60}$ one might wish to produce a

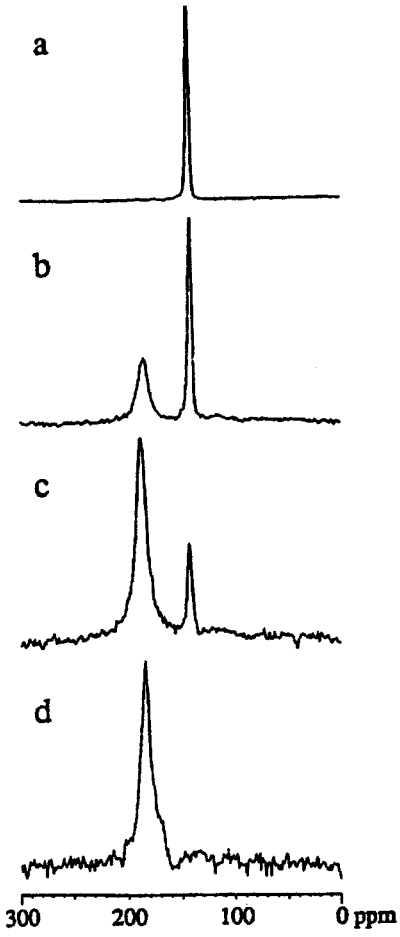


FIG. 25. $^{13}$C NMR spectra at 300 K: (a) $C_{60}$ powder; (b) $K_xC_{60}$ with nominal value $x$=1.5; (c) $K_xC_{60}$ with $x$=2.0; (d) $K_xC_{60}$ with $x$=3.1 (Tycko Dabbagh, Rosseinsky, *et al.*, 1991). If one were to produce materials with compositions ranging from $x$=0 to $x$=3, one would expect continuous variation in the NMR line position, beginning at the position corresponding to $x$=0 and ending at the $x$=3 position. However, this figure shows that, for starting compositions between 0 and 3, the NMR spectrum consists of two peaks, one at the $x$=0 position and one at the $x$=3 position. These NMR spectra clearly show that a mixture of $C_{60}$ and $A_3C_{60}$ segregates into two phases.

continuous range of dopant concentration, with dopant parameter $x$ in $A_xC_{60}$ taking on values between $x$=0 and 3. Nuclear magnetic resonance demonstrates that this is not a straightforward proposition (Tycko, Dabbagh, Rosseinsky, *et al.*, 1991). Figure 25 shows $^{13}$C line shapes of samples of starting composition $K_xC_{60}$ with $x$=0 (panel a), 1.5 (panel b), 2.0 (panel c), and 3.1 (panel d). (We take the last to be approximately $x$=3.0.) The compositions $x$=0 and $x$=3.0 are shown to have distinct, well separated $^{13}$C resonances. If one were to produce materials with compositions ranging from $x$=0 to $x$=3, one would expect continuous variation in the NMR line position, beginning at the position corresponding to $x$=0 and ending at the $x$=3 position. Instead Fig. 25 shows that, for starting compositions between 0 and 3, the

NMR spectrum consists of *two* peaks, one at the $x=0$ position and one at the $x=3$ position. The interpretation is clearly that the material is a segregated mixture of $A_3C_{60}$ and undoped $C_{60}$. To date there has been no progress on obtaining a continuous doping parameter.

### B. Dynamical properties

Nuclear magnetic resonance has uncovered unusual dynamic structural features in both pure $C_{60}$ and the alkali-doped superconductors. In the former case the combination of NMR and x-ray diffraction studies uniquely specified a novel "ratchet" phase in which molecules have orientation order from the perspective of an x-ray "snapshot," but also periodically make quick, large-angle reorientations, which show up in NMR experiments. The dynamical properties of the doped $C_{60}$ superconductors are now less well understood, yet the NMR evidence for unexpected kinds of reorientational behavior appears quite robust, coming from three independent types of experiment.

#### 1. Phase diagram for pure $C_{60}$

We first discuss the "ratchet" phase of pure $C_{60}$, which is now relatively well understood.

##### *a. Orientational ordering*

In Sec. IV.A.2 we discussed motional narrowing of the $^{13}C$ chemical-shift anisotropy powder pattern of pure solid $C_{60}$. Figure 20 demonstrates that at least partial narrowing remains at temperatures as low as 123 K. One might suspect that, due to the nearly spherical shape of the $C_{60}$ molecule, there would be small or negligible correlation of the orientations of neighboring molecules, much less long-range orientational order. In the absence of such order the $C_{60}$ system would be described as an "icosahedral glass."

Figure 20 seems to confirm that expectation—as low as 123 K, it seems that not only is there no long-range orientational order, but in fact the orientations of individual molecules are fluctuating on a rather fast time scale.

The thinking given above turns out to be correct for temperatures higher than 249 K. Heiney *et al.* (1991), however, have used x-ray powder diffraction and differential scanning calorimetry to demonstrate that below that critical temperature $C_{60}$ forms an orientationally ordered solid. The structure changes from fcc at high temperature to simple cubic, with a basis of four $C_{60}$ molecules having fixed orientations with respect to each other and with respect to the crystal lattice. A fuller description of the kind of orientational order is given in the original work of Heiney *et al.*, and in a review (Axe *et al.*, 1994).

##### *b. $^{13}C$ $T_1$ investigation of the "ratchet" and "rotator" phases*

Soon after Heiney *et al.*'s discovery of the orientational ordering transition, Tycko, Dabbagh, Fleming, *et al.* (1991) and subsequently Johnson, Yannoni, *et al.* (1992) performed NMR measurements that indicated that low-temperature $C_{60}$ (below 249 K) is in a "ratchet" phase, wherein the $C_{60}$ molecules make large, frequent orientational jumps between symmetry-equivalent states. We shall follow the treatment of Johnson *et al.*—the earlier experimental results and interpretations of Tycko *et al.* are in basic agreement.

In the "ratchet" phase the orientational jumps reshuffle the positions of the nuclei within the molecule and thereby motionally narrow the chemical-shift anisotropy powder pattern (Sec. IV.A.2) even at temperatures well below the ordering transition, 249 K. Yet a "snapshot" of the molecular orientations, as is effectively obtained through x-ray diffraction, reveals orientational order—that order is preserved in a "ratchet" orientational jump, because the molecule jumps between orientations that are equivalent.

Johnson *et al.* probe the orientational dynamics of the molecule through observation of the longitudinal relaxation time $T_1$. $T_1$ is the characteristic time for nuclear-spin populations in the two Zeeman levels (for spin-$\frac{1}{2}$ $^{13}C$) to relax to their equilibrium values, following a disturbance (such as an rf pulse that inverts the populations). In order for relaxation to occur the nuclei must see fluctuating magnetic fields oriented transverse to the static applied field $H_0$, and with spectral weight at the NMR transition frequency.

The source of these transverse fields in the pure $C_{60}$ solid is the anisotropy of the chemical-shift tensor, which is discussed in Secs. III.A.1 and IV.A.2. From Eq. (5) we see that the chemical-shift tensor $\overleftrightarrow{\sigma}$ results in an extra magnetic field $\vec{H}'$ given by

$$\vec{H}' = -\vec{\sigma}\cdot\vec{H}_0 . \tag{34}$$

From Eq. (34) we see that (1) magnetic fields applied in a direction not parallel to a principal axis will result in an extra field, which has a transverse component; (2) the magnitude of the transverse "extra" field is proportional to the applied field—thus we expect a dependence of $T_1$ upon the applied static field.

Johnson *et al.* give the relaxation time $(1/T_1)_{\mathrm{CSA}}$ from chemical-shift anisotropy (CSA) as

$$\frac{1}{T_1^{\mathrm{CSA}}} = (^{13}\gamma H_0)^2 \left(\tfrac{3}{10}\right)\sigma_{\mathrm{long}}^2\left[1+\frac{1}{3}\left(\frac{\sigma_{\mathrm{trans}}^2}{\sigma_{\mathrm{long}}^2}\right)\right]\left[\frac{\tau}{1+\omega^2\tau^2}\right], \tag{35}$$

where $^{13}\gamma$ is the $^{13}C$ gyromagnetic ratio ($2\pi\times 10.705$ MHz/tesla), $\sigma_{\mathrm{long}}$, $\sigma_{\mathrm{trans}}$ characterize the anisotropy of the chemical-shift tensor and are defined in Sec. IV.A.2.a, and $\omega$ is the NMR transition (Larmor) frequency. The reorientational correlation time $\tau$ is related to the reorientational diffusion coefficient $D$ by $\tau = 1/(6D)$. The final factor in the equation involving $\tau$ and $\omega$ reflects the necessity that the fluctuating fields have spectral weight at the Larmor frequency. A "$T_1$ minimum" occurs when $\omega\tau=1$. [There is an additional term given by Johnson *et al.* which comes from any *antisymmetric* component of $\boldsymbol{\sigma}$ (see, for example, Mehring, 1983); they estimate that it contributes ~6% to the relaxation rate. For simplicity we omit it here.] The beauty

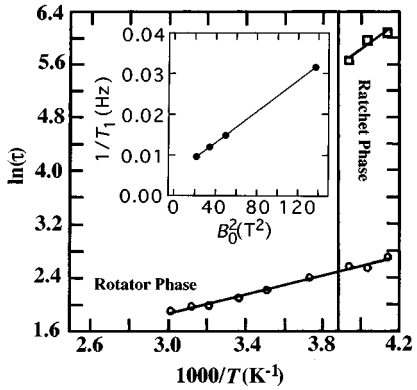


FIG. 26. Rotational correlation time $\tau$ vs temperature for $C_{60}$ in the "ratchet" and "rotator" phases, as obtained from NMR $T_1$ measurements using Eq. (35). There is a temperature window (~240–255 K) within which the "ratchet" and "rotator" phases appear to coexist, perhaps due to some sample inhomogeneity. Within that window the spin-lattice relaxation is a sum of two exponentials—one corresponding to each phase—and the two $T_1$ and $\tau$ parameters are extracted separately. In both the high-temperature "rotator" phase ($T$>249 K; $1000/T$<4) and the low-temperature "ratchet" phase, $\tau$ is fitted to Arrhenius form, $\tau=\tau_0 \exp(T_a/T)$, but with separate values of $\tau_0$ and activation temperatures $T_a$, given in Table VII. Johnson, Yannoni, *et al.* (1992) stress that the correlation times derived for the "rotator" phase are remarkably fast—approximately 5.5 ps at 300 K, which is only ~2.4 times the anticipated rotational correlation time for free $C_{60}$ molecules in the gas phase. Inset: Plot of the relaxation rate $1/T_1$ vs applied field squared $H_0^2$ for the solid $C_{60}$ (Johnson, Yannoni, *et al.*, 1992). Spin-lattice relaxation in solid $C_{60}$ results from the transverse fields produced by the chemical-shift anisotropy (CSA) of the chemical-shift tensor. Johnson *et al.* predict that the relaxation rate due to the CSA will be proportional to the square of the applied field [Eq. (35) in the text]. The above figure shows the $1/T_1$ data of Johnson *et al.* and a fit using their theory.

of Eq. (35) is that the CSA terms $\sigma_{\text{long}}$ and $\sigma_{\text{trans}}$ are known from measurements of the powder pattern line shape. Thus a measurement of $1/T_1$ directly yields the reorientational correlation time $\tau$.

Johnson *et al.* first explicitly verify a prediction of Eq. (35), that $(1/T_1)_{\text{CSA}}$ is proportional to the square of the applied field. In Fig. 26 (inset) is plotted (for $T$=283 K) $1/T_1$ vs applied field squared. (The nonzero $y$ intercept reflects a small relaxation contribution not associated with chemical-shift anistropy.)

Now, using Eq. (35), they extract $\tau$ from $T_1$ measurements. Data obtained for $\tau$ are given in Fig. 26. As shown in the figure, there is a temperature window (~240–255 K) within which the "ratchet" and "rotator" phase appear to coexist, perhaps due to some sample inhomogeneity. Within that window the spin-lattice relaxation is a sum of two exponentials—one corresponding to each phase, and the two $T_1$ parameters are extracted separately.

In both the high-temperature "rotator" phase ($T$>249 K; $1000/T$<4) and the low-temperature "ratchet" phase, $\tau$ can be fitted to Arrhenius form $\tau=\tau_0\exp(T_a/T)$, but with separate values of $\tau_0$ and activation temperatures $T_a$, given in Table VII.

Johnson *et al.* stress that the correlation times derived for the "rotator" phase are remarkably fast—approximately 5.5 ps at 300 K, which is only ~2.4 times the anticipated rotational correlation time for free $C_{60}$ molecules in a gas phase.

### 2. Reorientational dynamics in $A_3C_{60}$

The reorientational dynamics in $A_3/C_{60}$ are currently not well understood, yet there is ample NMR evidence that they confound one's expectations.

#### *a. Starting picture*

We first briefly restate and elaborate upon the widely accepted structure of $A_3C_{60}$, introduced in Sec. II.A. The $C_{60}$ molecules reside on the points of an fcc lattice, and the alkali atoms lie in the interstitial sites of tetrahedral ($T$) and octahedral ($O$) coordination. For each $C_{60}$ there are two $T$ sites and one $O$—each of these three is occupied by an alkali ion. Yet this configuration does not specify the *orientations* of the $C_{60}$ molecules.

The fcc structure was first deduced by Stephens *et al.* (1991) from x-ray diffraction data. Their depiction of one of the faces of an fcc lattice cell is given in Fig. 3. They point out that the tetrahedral interstitial site (radius ~1.1 Å) is smaller than the K ionic radius (~1.33 Å). Hence, the only way to accommodate the tetrahedrally coordinated alkali ion is to orient the $C_{60}$ molecule so that a hexagonal face is pointed along the crystal ⟨111⟩ direction. Then the alkali ion can bed down into the center of the hexagon.

It turns out that it is possible to orient a $C_{60}$ molecule so that a hexagonal face is pointed along each of the eight ⟨111⟩ directions, and in fact, there are two different ways to do so. In Fig. 3 we have shaded in the four visible ⟨111⟩ oriented hexagons for each $C_{60}$ molecule. Each shaded hexagon then would nest a tetrahedrally coordinated alkali ion (not shown). Note carefully that there are two inequivalent orientations of $C_{60}$ shown, which can be interconverted by a 90° rotation about the ⟨100⟩ direction.

Stephens *et al.* (1991) determined through x-ray diffraction that these two orientations exist in equal amounts. This situation, with equal populations for both orientations, is known as "bidirectional" structure, as opposed to "unidirectional" structure in which all molecules share the same orientation.

Barrett and Tycko (1992), Walstedt *et al.* (1993), and Yoshinari *et al.* (1993) have each presented very different kinds of NMR data which challenge this simple picture.

#### *b. Two-dimensional NMR*

Barrett and Tycko (1992) used a technique known as "2D NMR exchange spectroscopy" (see, for example, Ernst *et al.*, 1987) to probe the orientational dynamics of the $C_{60}$ molecules in $K_3C_{60}$. For the purposes of this

review it is not necessary to describe the NMR pulse sequence—we simply sketch its capabilities.

In conventional "1D NMR spectroscopy" (which is what we have been discussing in all other sections of this review), one measures the NMR absorption signal as a function of a single frequency. For example, in Sec. IV.A.2 we discussed the "chemical-shift anisotropy powder pattern." We discussed the fact that the NMR frequency for a $^{13}C$ nucleus within an atom having a $2p_z$ valence orbital (with a fixed orientation) will depend upon the orientation of magnetic field with respect to that $z$ axis.

One could imagine that perhaps the orientation of the $2p_z$ orbital for the atom would not remain fixed, but rather reorient rapidly. We saw this in Sec. IV.A.2.b when we discussed "motional narrowing" resulting from rapid reorientations of the $C_{60}$ molecule. One could also imagine an intermediate situation, in which the orientation of the molecule changed, but rather slowly compared to the width in frequency of the NMR line shape in the absence of any reorientation. In that case the NMR frequency for a typical nucleus would slowly drift around, gradually sampling the full range of shifts available to it as a function of molecular orientation.

The latter situation is well suited for investigation by 2D NMR. The 2D NMR experiment effectively does the following: At time $t=0$ it probes and "stores" the frequency of each spin. Subsequently it lets an "exchange" time $\tau_e$ elapse, and then measures the frequency of each spin at the end. One then has a data set containing NMR intensity as a function of the "before" frequency $\nu_1$ and the "after" frequency $\nu_2$.

Representative 2D data for $^{13}C$ in $K_3C_{60}$ are given in Fig. 27. We see that for short values of $\tau_e$ there is not enough time for orientational diffusion, and so the "after" frequencies ($\nu_2$) are very close to the "before" ($\nu_1$). Thus most intensity lies along the diagonal $\nu_1=\nu_2$. For longer exchange times very substantial molecular reorientation occurs, leaving 2D line shapes that are crudely circular (we shall discuss later the importance of the specifics of the 2D line shape).

Barrett and Tycko model the 2D line shapes assuming isotropic molecular reorientation and extract diffusion coefficients as a function of temperature. The reorientational correlation time $\tau$ ($=1/6D$, where $D$ is the reorientational diffusion coefficient) follows an activated temperature dependence $\tau=\tau_0 \exp(T_a/T)$, with $\tau_0=10^{(-12.4\pm1.4)}$ s and $T_a=(5300\pm700)$ K. These values are also tabulated in Table VII (Sec. IV.B.1.b), where they may be compared with analogous values for undoped $C_{60}$.

Although the correlation times for molecular reorientation are of interest, Barrett and Tycko also stress the importance of the specific shape of the 2D NMR line. As we discussed in the immediately preceding section, one expects that the tetrahedral alkali ions in $K_3C_{60}$ should do a very good job of "pinning" the orientation of the $C_{60}$ molecule. Thus one really does not expect the simple isotropic orientational diffusion that Barrett *et al.* use successfully to model their data.

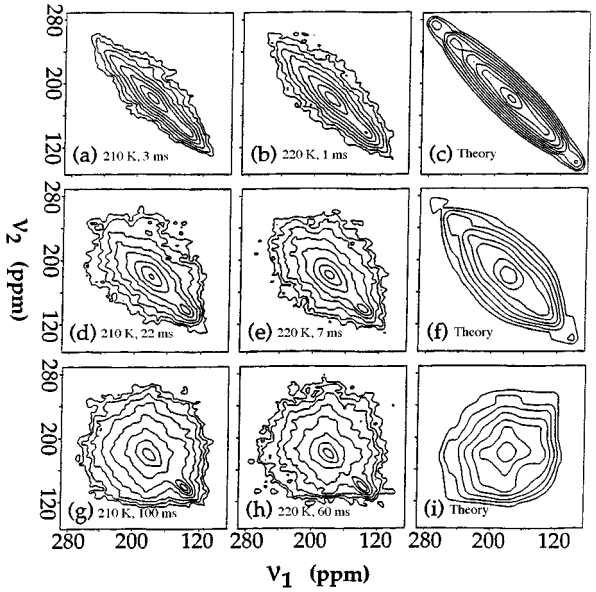


FIG. 27. 2D $^{13}C$ NMR exchange spectra of $K_3C_{60}$ for the following temperatures and exchange times $\tau_e$: (a) 210 K, 3 ms; (b) 220 K, 1 ms; (d) 210 K, 22 ms; (e) 220 K, 7 ms; (g) 210 K, 200 ms; (h) 220 K, 60 ms (Barrett and Tycko, 1992). (c), (f), and (i) are theoretical fits using the extracted values for the diffusion coefficient. The 2D NMR experiment effectively does the following: (1) At time $t=0$ the frequency of each spin ($\nu_1$) is "stored." Then an "exchange" time $\tau_e$ is allowed to elapse. Finally, after the time $\tau_e$, the frequency of each spin is measured again ($\nu_2$). One then has a data set containing NMR intensity as a function of the "before" frequency $\nu_1$ and the "after" frequency $\nu_2$. We see that for short values of $\tau_e$ there is not enough time for orientational diffusion, so that the "after" frequencies ($\nu_2$) are very close to the "before" ($\nu_1$). Thus most intensity lies along the diagonal $\nu_1=\nu_2$. For longer exchange times, very substantial molecular reorientation occurs, leaving 2D line shapes that are crudely circular. The surprising result occurs for intermediate times—there one would expect that there would be a reasonable fraction of molecules that have undergone large reorientations, as well as a fraction having undergone no reorientation at all. Then one would expect a superposition of a diagonal strip of intensity, plus a crudely circular pattern. No such superposition is detected. Barrett and Tycko conclude that smaller-angle, diffusive reorientational jumps must occur, in contrast with initial expectations that jumps would occur only between a small number of discrete orientations.

One expects, rather, the following three regimes: For short $\tau_e$ negligible reorientation will occur, producing a diagonal 2D line shape, as observed. For long $\tau_e$ all the molecules will have made several large-amplitude reorientations. Despite the discrete number (2) of orientations supposedly available to each molecule, it is likely that the 2D line shape would be hard to distinguish from one obtained from simple isotropic diffusion. The difficulty is for intermediate times. Then one expects that some reasonable fraction of the $C_{60}$'s will have made a large orientational jump, while others have not reoriented at all. The expected line shape would be a super-

TABLE VII. Arrhenius time prefactors (column 2), activation temperatures (column 3), and correlation times given at a particular temperature (column 4) for $C_{60}$ reorientation in the high-temperature "rotator" and low-temperature "ratchet" phases (from Johnson, Yannoni, *et al.*, 1992). Also given are these parameters for $K_3C_{60}$, as measured by Barrett and Tycko (1992; See Sec. IV.B.2.b) and Yoshinari *et al.* (1993; see Sec. IV.B.2.c). Yoshinari *et al.* invoke two characteristic times, $\tau_s$ (slow) and $\tau_f$ (fast), to describe an inferred anisotropic molecular reorientational motion. In column 4, $\tau$ is calculated for the indicated temperature, which is chosen to be representative of the range best probed in the respective experiments. The parameters in this table may be used to calculate temperature-dependent correlation times $\tau$ according to $\tau=\tau_0 \exp(T_a/T)$. $\tau$ is related to the orientational diffusion coefficient $D$ according to $\tau=1/(6D)$.

| Phase, research group, and technique: | $\tau_0$ (seconds) | Activation temp. $T_a$ (K) | $\tau(s)$ at specified temperature (K) |
|---|---|---|---|
| "Rotator" ($T$>249 K) Johnson, Yannoni, *et al.* (1992) ($T_1$) | $(8.1\pm1.0)\times10^{-13}$ | 695± 45 | $8.9\times10^{-12}$ (290 K) |
| "Ratchet" ($T$<249 K) Johnson, Yannoni, *et al.* (1992) ($T_1$) | $8\times10^{(-14\pm1)}$ | 2100±600 | $2.9\times10^{-9}$ (200 K) |
| $K_3C_{60}$ Barrett and Tycko (1992) (2D NMR) | $10^{(-12.4\pm1.4)}$ | 5300±700 | $3.6\times10^{-2}$ (210 K) |
| $K_3C_{60}$—"slow"; Yoshinari *et al.* (1993) ($T_2$) | $7\times10^{(-16\pm0.8)}$ | 6800±500 | $1.2\times10^{-6}$ (320 K) |
| $K_3C_{60}$—"fast"; Yoshinari *et al.* (1993) ($T_1$) | $2\times10^{(-14\pm0.7)}$ | 2600±300 | $4.8\times10^{-9}$ (210 K) |

position of a diagonal pattern with a crudely circular pattern. The experimental data do not show this. Barrett *et al.* stress that small-amplitude (less than a few tens of degrees) diffusional steps are needed to fit the data, suggesting that $C_{60}$ molecules may be oriented in many different ways, perhaps a continuum of ways, rather than in just the two discrete ways described in the previous section.

#### c. $T_1$, $T_2$ and anisotropic molecular orientational dynamics

While Barrett and Tycko infer, contrary to expectations, reorientational diffusion with a small angular "step size," Yoshinari *et al.* (1993) find indications of reorientational dynamic behavior that is even more surprising.

The 2D NMR experiments of Barrett and Tycko are particularly suited for probing slow motions—motions too slow to narrow the NMR linewidth (of the order of 10 kHz). They probe the dynamics most effectively at temperatures ~210 K, where they infer a correlation time $\tau$ of $3.6\times10^{-2}$ seconds.

Yoshinari *et al.* use NMR $T_2$ measurements to pick up the kinds of motions observed by Barrett and Tycko at substantially higher temperatures, 300–330 K, as compared to 200–220 K. The correlation times they infer ($1.2\times10^{-6}$ s at 320 K—see Table VII) map nicely onto Barrett and Tycko's observed activated behavior at lower temperature.

Yoshinari *et al.*, however, find a much more surprising feature in the behavior of $T_1$. In Sec. IV.B.1.b we discussed how the combined effects of chemical-shift anisotropy and molecular reorientations could result in a fluctuating magnetic field with a component transverse to the applied field, which could cause transitions between the nuclear Zeeman levels, thus providing a $T_1$ mechanism. Yoshinari *et al.* find that this mechanism remains operative in $K_3C_{60}$, although here one is concerned with the anisotropy of the total shift tensor rather than just the chemical shift.

Figure 28 shows the temperature dependence of the spin-lattice relaxation rate $1/T_1$ for $^{13}C$ in $K_3C_{60}$. We note two features: First, $1/T_1$ depends roughly linearly upon temperature—this is the signature of the "Korringa" relaxation mechanism from nuclear-spin interactions with conduction-electron spins (Slichter, 1990; p. 151–157). In addition, however, from ~200 to 240 K there is an additional contribution superposed upon the Korringa background. Yoshinari *et al.* show that that contribution can be attributed to the shift-anisotropy ("SA") mechanism.

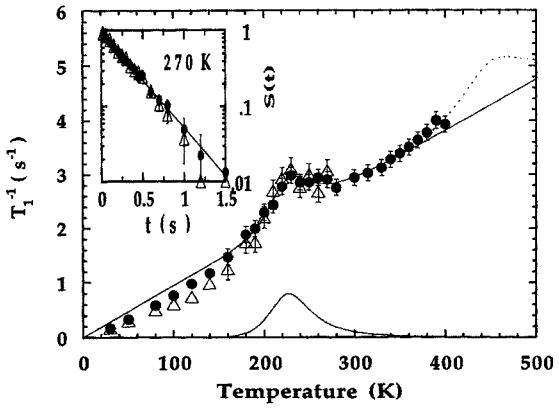


FIG. 28. Temperature dependence of the spin-lattice relaxation rate $1/T_1$ for $^{13}C$ in $K_3C_{60}$ (Yoshinari *et al.*, 1993). $1/T_1$ depends roughly linearly upon temperature, the expected Korringa behavior for relaxation through hyperfine coupling with conducting electrons. Near ~200–240 K, however, there is an additional contribution superposed upon the Korringa background which is related to molecular reorientations. From the data, a correlation time $\tau \sim 2\times10^{-9}$ s can be extracted, a time scale more than six orders of magnitude faster than the time inferred by Barrett and Tycko at the same temperature and in the same material. Thus, remarkably, two characteristic correlation times are required to understand the motional dynamics, possibly resulting from rapid reorientations about an easy axis, but much slower reorientations about a perpendicular axis. Such an anisotropic rotation is quite surprising in view of the current understanding of the structure of the material.

For a correlation time $\tau$ the SA mechanism gives a relaxation contribution

$$T_1^{-1} = 2(\gamma H_{\rm loc})^2 \frac{\tau}{1+\omega_0^2\tau^2} \tag{36}$$

(see, for example, Slichter, 1990, p. 206–215), where $H_{\rm loc}$ characterizes the shift anisotropy [see Eq. (35) for a concrete example] and $\omega_0$ is the NMR frequency (~$2\pi\times75$ MHz). Yoshinari *et al.* observe that the SA contribution to $1/T_1$ reaches a maximum (a "$T_1$ minimum") of ~0.8 $s^{-1}$ at 230 K. Because a $T_1$ minimum is observed one can infer from Eq. (36) that at that temperature $\omega_0\tau=1$. Surprisingly, then, one finds $\tau \sim 2\times10^{-9}$ s—more than six orders of magnitude faster than the time inferred by Barrett and Tycko at the same temperature and in the same material.

Using the $T_1$ minimum condition ($\omega_0\tau=1$) at 230 K, Yoshinari *et al.* infer the (presumably) constant value of $(\gamma H_{\rm loc})^2$ and then use that to extract correlation times at other temperatures. Yoshinari *et al.* fit their correlations to an activated temperature dependence $\tau=\tau_0\exp(T_a/T)$ with $\tau_0=2\times10^{(-14\pm0.7)}$ s and $T_a=(2600\pm300)$ K, as given in Table VII.

Thus, remarkably, two characteristic correlation times are required to understand the motional dynamics. Yoshinari *et al.* invoke an anisotropic model of reorientational dynamics in which the $C_{60}$ molecules execute quite rapid reorientations about an easy axis, but much slower reorientations about a perpendicular axis. Their line-shape observations also support this picture—a "narrow" component is observed superposed upon a "broad" component. The narrow component is assigned to molecules for which the applied magnetic field is oriented along the "Magic angle" (see, for example, Mehring, 1983, pp. 40–50) with respect to the easy rotation axis.

Such an anisotropic rotation is quite surprising in view of the assumed fcc structure—for that structure one expects that, from the point of view of a $C_{60}$ molecule, any "easy" axis of rotation is by symmetry equivalent to 23 others. If the molecule reoriented this rapidly, $\sim2\times10^{-9}$ s at 230 K, about *each* of these 24 axes, then the shift anisotropy would be fully motionally narrowed—but that temperature range is precisely where Barrett and Tycko perform their elegant 2D NMR experiments on the shift-anisotropy-broadened line.

Yoshinari *et al.* suggest that their results imply some kind of static distortion of the lattice which is incompatible with the high-symmetry structure inferred from x-ray diffraction by Stephens *et al.* (1991), and they speculate about a possible relationship between their findings and the $^{87}Rb$ NMR data of Walstedt *et al.* (1993), which we now discuss.

#### *d. A peculiar structural distortion in $A_3C_{60}$ and its dynamics*

We have alluded earlier (Sec. IV.A.3.b) to an unexpected feature in the $^{87}Rb$ NMR line shape of $Rb_3C_{60}$ (or more generally, alkali $C_{60}$ compounds in which the $^{87}Rb$ wholly or partially occupies a tetrahedrally coordinated interstitial site).

Assuming the structure derived from x-ray diffraction (Sec. IV.B.2.a) for $Rb_3C_{60}$, one expects two Rb in tetrahedrally coordinated interstitial sites for each $C_{60}$ and one in an octahedrally coordinated site—then one should expect *two* $^{87}Rb$ NMR peaks ($T$ and $O$) with intensity ratios 2:1.

At well above room temperature these features are clearly observed. Figure 29 (inset) shows the $^{87}Rb$ NMR line shape at 443 K. At low temperature, however [Fig. 29(a) and (b)] the "$T$" line splits into two parts, $T$ and $T'$, with relative weights 5.5 to 1. (Note that, in Sec. IV.A.3.b, Fig 21, NMR of tetrahedrally coordinated $^{133}Cs$ shows a similar $T,T'$ splitting.)

Without describing the experimental technique in detail, it suffices to say that the experiments of Walstedt *et al.* have irrefutably demonstrated several key items:

First, the $T'$ site is a kind of distorted $T$ site—not a distorted $O$ site. (This may be surprising because of the larger radius of the octahedral cavity, ~2.1 Å vs 1.1 Å.) At high temperatures $T$ and $T'$ peaks collapse to become one, while the $O$ peak remains separate. Spin-echo double-resonance ("SEDOR") experiments indicate that the distance between $T'$ and $O$ site atoms is similar to that between $T$ and $O$.

Second, the $T$ and $T'$ sites interconvert with an activated temperature dependence. The activation temperature is ~5000 K, similar to the activation temperatures for $C_{60}$ molecular reorientations (Table VII). This interconversion does not consist of the ions' jumping from

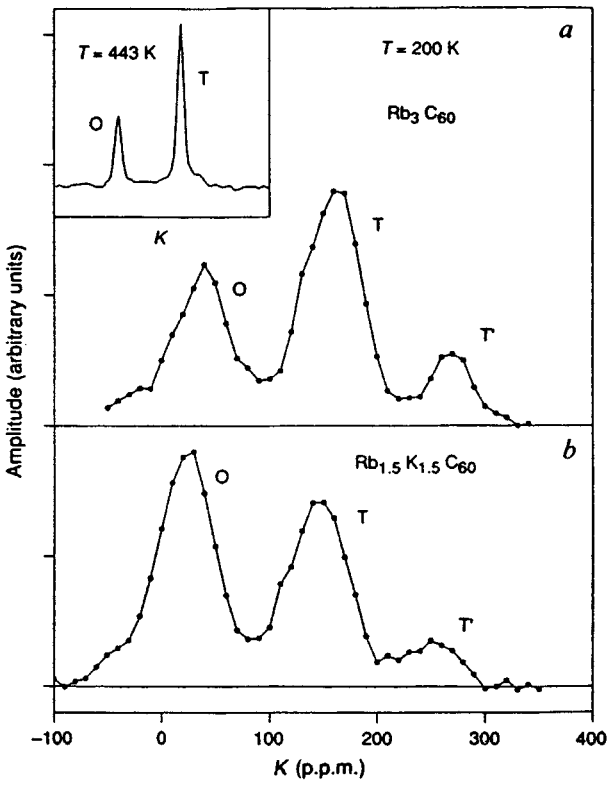


FIG. 29. $^{87}$Rb NMR spectra for powder samples at $T$=200 K and a NMR frequency of 101 MHz (Walstedt *et al.*, 1993): (a) $Rb_3C_{60}$; (b) $Rb_{1.5}K_{1.5}C_{60}$. Shifts are referred to the gyromagnetic ratio of the $Rb^+$ ion in the gas phase, $\gamma/2\pi$=13.92812 MHz/tesla. In both (a) and (b) there are three peaks in the $^{87}$Rb spectrum. The $O$ line corresponds to ions in the octahedrally coordinated sites and the $T$ and $T'$ (relative weights 5.5 to 1) lines correspond to ions in the tetrahedrally coordinated sites. The inset shows the $^{87}$Rb spectrum in $Rb_3C_{60}$ at $T$=443 K, where the $T$ and $T'$ lines collapse (motionally narrow) to form one $T$ peak. Walstedt *et al.* attribute the $T$, $T'$ splitting to a structural distortion in $Rb_3C_{60}$. The NMR of tetrahedrally coordinated $^{133}$Cs in $RbCs_2C_{60}$ shows a similar $T$, $T'$ splitting.

site to site within the structure—to do so the ions would need to pass first through the $O$ site. "Saturation transfer" experiments, however, demonstrate that that does not happen. In these experiments, for example, one initially destroys the magnetization of the $T'$ peak, then observes its intensity's being replenished at the expense of the $T$ peak. While such "give and take" is observed between $T$ and $T'$, none is observed between $T$ or $T'$ and $O$.

Walstedt *et al.* suggest several possible distortions which might account for the $T,T'$ splitting, including displacements of the alkali ions, a Jahn-Teller distortion of the $C_{60}^3$ ion, or a deviation from the expected $C_{60}$ orientational structure in which carbon hexagons face the tetrahedrally coordinated alkali ions, but as of yet there has been no success in distinguishing between these possibilities.

#### *e. Brief summary*

To summarize the current situation, a preponderance of NMR data indicates that the simple structural model given above (IV.B.2.a), an fcc lattice, with disorder entering only in the apparent random distribution of the $C_{60}$ molecular orientations between two discrete possibilities, is not adequate.

The 2D NMR work of Barrett and Tycko (1992) shows that, contrary to expectations, molecular reorientational diffusion occurs through small angular step sizes rather than through large angle jumps. Yoshinari *et al.* (1993) show that reorientation of the molecule occurs on two characteristic time scales separated by six orders of magnitude, which is only consistent with the $C_{60}$ molecule's having a very anisotropic environment. Finally, Walstedt *et al.* (1993) demonstrate that there are two kinds of "tetrahedral" Rb environments.

The nature of these experimentally detected deviations is not at all clear at present, nor is it clear whether these findings are important considerations in understanding alkali fulleride superconductivity.

## V. SUPERCONDUCTING-STATE NMR

Superconductivity in doped fullerenes is certainly one of the most exciting extensions of the discovery of the fullerene model. With transition temperatures as high as 33 K, one naturally asks whether the usual BCS mechanism of superconductivity is applicable, and, if so, what are the details? As usual, the NMR results are quite telling.

### A. Theoretical approach

In interpreting superconducting-state NMR experiments one has a hierarchy of issues—the most important being whether the experiments should be interpreted within the BCS theory of phonon-mediated pairing. The current status of this issue is discussed in Secs. II.C and II.D. To date all known superconductors are thought to involve pairing, but in some instances the pairing mechanism is thought to be nonphononic. For example, in the case of high-$T_c$ cuprate superconductors it has been proposed (Monthoux *et al.*, 1991) that antiferromagnetic spin fluctuations play the role of phonons. In such cases one can adapt the mathematical machinery of BCS and Eliashberg theory for the new mechanism, if details of the electron-"generalized phonon" coupling are known. Thus, a nonphonon mechanism has the potential to mimic a phonon mechanism, and it may be difficult to use NMR to distinguish between alternate pairing mechanisms.

In view of this difficulty we shall stick with the BCS phonon pairing model and the results of the more generalized Eliashberg theory as a starting point for thinking about NMR in the superconducting state, first attempting to discern which of the distinct phonon modes plays the predominant role in pairing within that framework, and then examining the self-consistency of such a

TABLE VIII. For calibrational purposes we list representative values of the strong-coupling parameter $T_c/\omega_{\ln}$, $T_c$, $\omega_{\ln}$, and the gap $2\Delta_0/k_BT_c$ (taken from Carbotte, 1990; p. 1068). One might pick $T_c/\omega_{\ln}>0.1$ and $2\Delta_0/k_BT_c>4$ as criteria for the label "strong coupling." (Note that the tangential, "on-ball" phonon frequencies for alkali fullerides are ~1400 $cm^{-1}$, much higher than those listed here.)

| Material | $T_c$ (K) | $T_c/\omega_{\ln}$ | λ | $\omega_{\ln}$ ($cm^{-1}$) | $2\Delta_0/k_BT_c$ |
|---|---|---|---|---|---|
| Al | 1.18 | 0.004 | 0.43 | 206 | 3.535 |
| Sn | 3.75 | 0.038 | 0.72 | 68 | 3.705 |
| Nb | 9.20 | 0.074 | 0.98 | 86 | 3.964 |
| Mo | 8.80 | 0.095 | 0.90 | 80 | 3.968 |
| Pb | 7.19 | 0.128 | 1.55 | 39 | 4.497 |
| Hg | 4.19 | 0.146 | 1.70 | 20 | 4.591 |
| Ga | 8.56 | 0.24 | 2.25 | 25 | 4.722 |
| Bi | 6.11 | 0.32 | 2.45 | 13 | 4.916 |

phonon pairing picture. As it happens, the phonon pairing picture does appear to be very plausible.

The review of Carbotte (1990) shows that a wide range of experimental data is reasonably well predicted from Eliashberg theory using a single parameter, $T_c/\omega_{\ln}$ which characterizes the degree of strong coupling. $\omega_{\ln}$ is a characteristic phonon frequency, first introduced by Allen and Dynes (1975), for the electron-phonon coupling spectrum $\alpha^2F(\omega)$. Representative values of $T_c, T_c/\omega_{\ln}, \lambda, \omega_{\ln}$, and $2\Delta_0/k_BT_c$ for conventional superconductors are given in Table VIII (from Carbotte, 1990). Recall that the Bardeen-Cooper-Schrieffer theory, derived for the limit $T_c/\omega_{\ln} \ll 1$, predicts $2\Delta_0/k_BT_c=3.52$.

For the case in which $\alpha^2F(\omega)$ is strongly peaked near a frequency $\omega_0$, $\omega_{\ln}$ is equal to $\omega_0$. Thus extracting $\omega_{\ln}$ from experimental data may provide valuable information about which phonon modes are predominant. This procedure appears promising for the case of alkali fullerides, because the five distinct phonon modes enumerated in Sec. II.C.1 [intramolecular tangential (1400 $cm^{-1}$), intramolecular radial (500 $cm^{-1}$), optical (100 $cm^{-1}$), intermolecular (40 cm), and molecular reorientational (20 $cm^{-1}$)] occur at rather well separated frequency bands.

Akis *et al.* (1991) have used the single-parameter ($T_c/\omega_{\ln}$) approach to calculate superconducting-state NMR parameters including Knight shifts and $T_1$'s providing us with the tools to extract $\omega_{\ln}$ from the NMR data. It will be found in some instances, however, that contradictory conclusions are drawn from different sets of data, leading one to speculate that a more detailed treatment of the electron-phonon coupling spectrum and other parameters might be necessary.

Before discussing the NMR data, we first provide a "roadmap" for this single-parameter theoretical approach. For each of these five phonon coupling scenarios we can calculate λ from the McMillan equation (taking $\mu^*=0$ and a known $T_c$ of ~30 K), and the temperature gap $\Delta_0$ from the following relation (Carbotte, 1990):

$$\frac{2\Delta_0}{k_BT_c}=3.53\left[1+12.5\left(\frac{T_c}{\omega_{\ln}}\right)^2\ln\left(\frac{\omega_{\ln}}{2T_c}\right)\right]. \quad (37)$$

The results are given in Table IX. Equation (37) includes the factor $3.53=2\pi/\exp(C)$, with $C$ equal to Euler's constant (0.5772,...). This constant is derived in the original Bardeen-Cooper-Schrieffer theory (1957). Equation (37), then, is a generalization to include effects of strong coupling. If tangential intramolecular phonons play a dominant pairing role in alkali fullerides, then we see from Tables VIII and IX that alkali $C_{60}$ would be a weak-coupling superconductor similar to aluminum or tin. Alternatively, optical phonons would imply a strong-coupling superconductor with $2\Delta_0/k_BT_c$ similar to that of bismuth. Lower-frequency phonons would imply a degree of strong coupling greater than has yet been seen in conventional superconductors.

Table IX shows that the superconducting energy gap $\Delta_0$ specifies which phonon modes play the predominant role in pairing. Various experimental measurements of the gap on alkali fullerides have yielded results that appear to be in conflict. Infrared reflectivity measurements (Degiorgi *et al.*, 1992) have yielded a weak-coupling gap with $2\Delta/k_BT_c$ close to 3.5, fingering the high-frequency

TABLE IX. Superconducting-state parameters $T_c/\omega$, λ, and $2\Delta/k_BT_c$, based on the assumption that the phonon modes listed in the first column play a dominant role in mediating electron pairing. The renormalized Coulomb repulsion parameter $\mu^*$ is taken to be zero.

| Phonon mode frequency ($cm^{-1}$) | $T_c/\omega$ | λ | $2\Delta/k_BT_c$ |
|---|---|---|---|
| Molecular reorientations 20 $cm^{-1}$ | 1.0 | ... | ... |
| Intermolecular vibrations 40 $cm^{-1}$ | 0.5 | ... | ... |
| Optical ($C_{60}$ alkali vibrations) 100 $cm^{-1}$ | 0.2 | 3.1 | 5.2 |
| Intramolecular radial (500 $cm^{-1}$) | 0.04 | 0.53 | 3.72 |
| Intramolecular tangential (1400 $cm^{-1}$) | 0.015 | 0.35 | 3.56 |

intramolecular phonons as the pairing glue. Scanning tunneling microscope spectroscopy (Zhang *et al.*, 1991), however, indicates $2\Delta/k_BT_c \sim 5$, suggesting the optical modes, or perhaps a more unusual mechanism. Magnetic resonance experiments, then, have the potential to address this fairly well posed question.

### B. The Knight shift: Electronic-spin susceptibility in the superconducting state

Two types of NMR experiment have been used to probe superconductivity in the fullerenes—Knight-shift, and $T_1$ measurements. We first discuss the Knight shift, which provides a way of measuring superconducting-state electronic-spin susceptibility.

#### 1. Background

The Knight shift $K^s$ (see Sec. III.A) is a fractional shift in the NMR resonance frequency,

$$\omega = -\gamma_n H(1+K^s), \tag{38}$$

which results jointly from the hyperfine interaction between the nuclear and conduction-electron spins and from conduction-electron spin (Pauli) susceptibility $\chi^s$ (Knight, 1956), given in terms of the electron-nuclear hyperfine coupling parameter ${}^{\eta}A$ by

$${}^{\eta}K^s(T) = {}^{\eta}A\,\chi^s(T). \tag{39}$$

Here $\eta$ denotes the nucleus in question (for example, $\eta = {}^{13}C$, ${}^{87}Rb$, or ${}^{133}Cs$). More generally Eq. (39) would reflect a dependence upon the orientation of the magnetic field with respect to the crystal axes of the hyperfine coupling tensor. The measurements we discuss here, however, involve a powder average over all orientations, the isotropic part of the Knight shift (Sec. III.A).

The Knight shift is important because it provides a convenient way to measure both normal-state and superconducting-state $\chi^s$. While $\chi^s(T)$ is an important and revealing quantity, containing the superconducting-state energy gap, it is also most difficult to measure directly. Especially in the superconducting state, the contribution of $\chi^s$ to the total susceptibility is very small. The intimate coupling, however, between electron and nuclear spins often makes the Knight shift quite easy to observe. While the dimensionless $\chi^s$ in metals is typically of order $10^{-6}$, the Knight shift may be of the order of $10^{-2}$.

In the normal state $\chi^s$ is temperature independent and proportional to the density of states $\rho(E_F)$ at the Fermi energy (Ashcroft and Mermin, 1976). Crudely one can understand the temperature dependence of $\chi^s$ in the following way: Filled electron states well below the Fermi level are occupied by both up and down electron spins and thus contribute nothing to the susceptibility. Only excitations, which occur within $\sim k_BT$ of $E_F$, may contribute; their number is $\approx \rho(E_F)k_BT$. With each excitation contributing a Curie susceptibility $\propto 1/T$ the total spin susceptibility is temperature independent, and the quantity $\chi^s T$ is proportional to the number of electronic excitations.

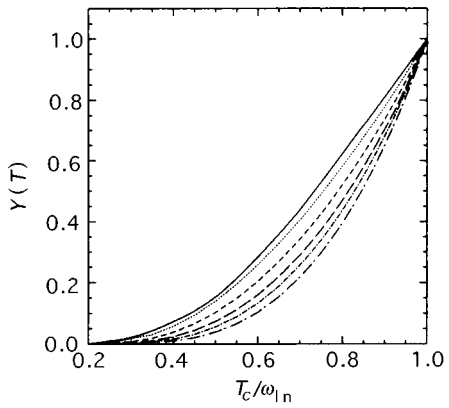


FIG. 30. Calculated Yosida functions $Y(T)$ as a function of reduced temperature $T/T_c$ for strong and weak coupling (Akis *et al.*, 1991). The solid curve is the BCS result for weak coupling. The other curves are for different values of the characteristic strong-coupling parameter $T_c/\omega_{ph}$: dotted curve, $T_c/\omega_{ph}=0.05$; short dashed curve, 0.1; long dashed curve, 0.15; short dash-dotted curve, 0.2; and long dash-dotted curve, 0.3. These curves may be compared with experimentally measured Knight-shift data (e.g., Stenger *et al.*, 1995) to extract the strong-coupling parameter.

The reasoning given above remains valid in the superconducting state, with the exception that, with the opening of an energy gap, the number of excitations freezes out, behaving at low temperature as $\exp(-\Delta/k_BT)$. The precise dependence on temperature depends on $T_c/\omega_{ln}$; the Knight shift drops more steeply to zero in strongly coupled superconductors.

The temperature dependence of $\chi^s(T)$ in the superconducting state was first derived from BCS theory by Yosida (1958; MacLaughlin; 1976); the ratio $Y(T)$ of the superconducting-state $\chi^s(T)$ to the normal-state value is given by

$$Y(T) = \int_{-\infty}^{\infty} dE \left(-\frac{\partial f}{\partial E}\right) \mathrm{Re}\left[\frac{E}{(E^2-\Delta^2)^{1/2}}\right], \tag{40}$$

where $f$ is the Fermi function and $E/(E^2-\Delta^2)^{1/2}$ is the BCS density of states. For strong coupling, the energy gap $\Delta(T)$ is complex and larger in magnitude than for weak coupling. Typical strong-coupling behavior of the function $\mathrm{Re}[E/(E^2-\Delta^2)^{1/2}]$ is illustrated by Allen and Rainer (1991). Calculated weak- and strong-coupling Yosida functions $Y(T)$ are given in Fig. 30 (Akis *et al.* 1991).

#### 2. Yosida fits of experimental data: Near the weak-coupling limit

The superconducting-state Knight shift has been measured experimentally in alkali fullerides by Stenger *et al.* (1993; 1995). The measurement is done with an applied magnetic field which is between the first and second critical fields $H_{c1}$ and $H_{c2}$; thus, while the applied field does penetrate the sample, it does not do so completely. Absent knowing the internal magnetic field, measure-

ment of the NMR frequency does not enable one to extract $K^s$, as can be seen by inspection of Eq. (38). Stenger *et al.*, using a technique reminiscent of that used by Barrett *et al.* (1990) to measure superconducting state Knight shifts in the high-$T_c$ cuprates, recognize that while the magnetic field within the sample may be reduced below the applied field due to Meissner screening currents, this reduction is the same for all nuclear species in the sample. On the other hand, the Knight shifts for different atomic species in the sample will be different, owing to their differing hyperfine couplings. Thus, by subtracting the fractional frequency shifts of two different nuclei (e.g., $^{87}$Rb and $^{133}$Cs in the material $Rb_2CsC_{60}$), one obtains a quantity proportional to $\chi^s(T)$.

Figure 31 shows the superconducting-state temperature-dependent spin susceptibility obtained for a sample of $Rb_2CsC_{60}$ by Stenger *et al.* using the technique outlined above. In Fig. 31(a) shifts are subtracted in three different ways for the nuclei $^{87}$Rb, $^{133}$Cs, and $^{13}$C, and each method yields the same result. In Fig. 31(b) the combination $^{87}K^s$-$^{133}K^s$ is shown for three different magnetic fields, demonstrating that the result is field independent.

Also shown in Fig. 31(a) and (b) are fits to Yosida functions using the strong-coupling calculations of Akis *et al.* (1991). The data are quite well fitted using the weak-coupling limit, while stronger coupling with $\omega_{ph}$=100 cm$^{-1}$, $T_c/\omega_{ph}$=0.2, and $2\Delta/k_BT_c\sim5$ clearly does not fit the data. Stenger *et al.* find a lower bound on $\omega_{ph}$ of 200 cm$^{-1}$ ($2\Delta/k_BT_c$ has an upper bound of approximately 4.2), which enables one to specify the predominance of the intramolecular phonon modes in pairing. The result, however, cannot distinguish between the high-frequency ($\sim$1400 cm$^{-1}$) tangential modes and the lower-frequency ($\sim$500 cm$^{-1}$) radial modes.

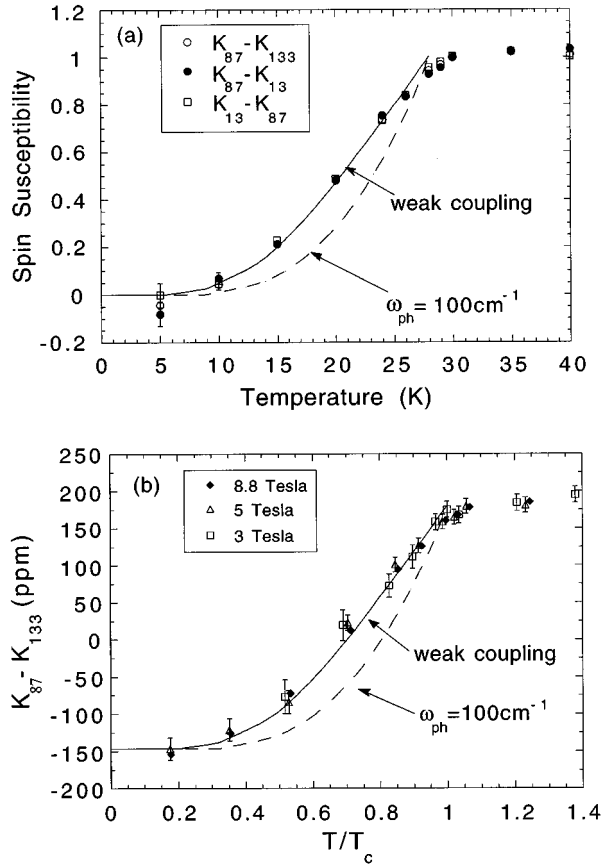


FIG. 31. NMR-derived superconducting-state spin susceptibility in $Rb_2CsC_{60}$: (a) Spin susceptibility vs $T$ of $Rb_2CsC_{60}$ at 8.8 tesla obtained by subtracting raw shift data for three pairs of different nuclei (e.g., $^{13}$C and $^{87}$Rb, or $^{87}$Rb and $^{133}$Cs), thereby eliminating effects of Meissner screening currents (Stenger *et al.*, 1995). All three pairs of nuclei give the same result (after normalization). (b) Spin susceptibility, as probed by the difference in the $^{87}$Rb and $^{133}$Cs shifts ($^{87}$K-$^{133}$K), vs $T/T_c(H)$, for $Rb_2CsC_{60}$ at several fields. The result is independent of magnetic field. Fits: Solid curve, weak-coupling BCS prediction; dashed curve, strong-coupling BCS prediction with characteristic phonon frequency 100 cm$^{-1}$. The data support the weak-coupling limit of BCS theory. The result is shown to be independent of magnetic field and independent of which pair of nuclei is used.

### 3. A few reservations on the interpretation

We present a few *caveats* on the interpretation of the Knight-shift experiment and a comparison of the apparently conventional behavior with that of high-$T_c$ superconductors.

It has been pointed out that the fits to the data in Figs. 31 and 30 do not include the effects of vertex corrections, which may change the shape of the Knight-shift curves substantially and in a way not easy to predict *a priori* (J. P. Carbotte, private communication). The importance of such effects is shown by Pickett (1982) and Mitrovic and Pickett (1987).

Additionally, even in the weak-coupling limit, the presence of Stoner enhancement of $\chi^s$ in the normal state should result in a more rapid drop in $\chi^s(T)$ as $T$ is lowered below $T_c$ (A. Leggett, private communication). Figure 32 shows how Stoner enhancement of a factor of two in the normal state modifies the shape of the Yosida curve in the weak-coupling limit.

Finally, it is interesting to compare the gradual "weak-coupling-like" drop in the Knight shift for $Rb_2CsC_{60}$ with the remarkably steep descent found for the planar Cu atoms in the high-$T_c$ cuprate $YBa_2Cu_3O_7$ (Barrett *et al.*, 1990). This comparison is given in Fig. 44 in Sec. V.E.

## C. Spin-lattice relaxation ($T_1$)

Data from superconducting state NMR spin-lattice relaxation ($T_1$) (see Sec. III.D for a review of $T_1$ in metals and superconductors) (and related muon-spin relaxation) on alkali fullerides have been a topic of interest and controversy. Tycko *et al.* (1992) first observed the apparent absence of the Hebel-Slichter coherence peak. Mechanisms for suppressing (for a review see MacLaughlin, 1976) or even eliminating the peak (Allen

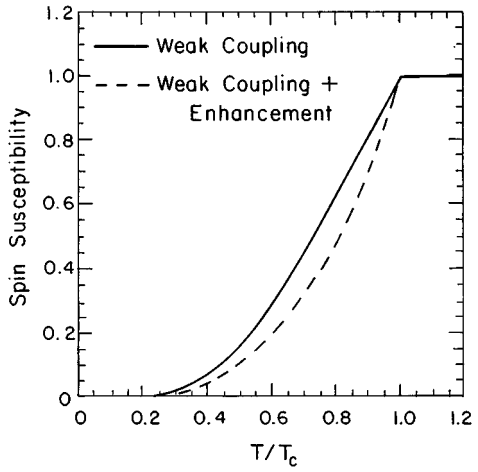


FIG. 32. Predictions for the temperature dependence of the electron-spin susceptibility in the superconducting state in the weak-coupling limit: solid curve, BCS prediction (Yosida curve); dashed curve, again, the BCS weak-coupling predictions for superconducting-state electron-spin susceptibility, but now with the assumption that the susceptibility is Stoner enhanced according to $\chi^s(T)=\chi_0^s(T)/[1-I\chi_0^s(T)]$. Here $\chi_0^s(T)$ is the unenhanced susceptibility, assumed to follow the Yosida curve, and $\chi^s(T)$ is the enhanced susceptibility, with enhancement parameter $I\chi_0^s(T)$ taken to be one half in the normal state for a factor-of-two enhancement. The inclusion of Stoner enhancement effects steepens the falloff in superconducting-state $\chi^s(T)$. It is surprising, then, that the results of Stenger *et al.* (1995) agree with the BCS Yosida weak-coupling limit quite well.

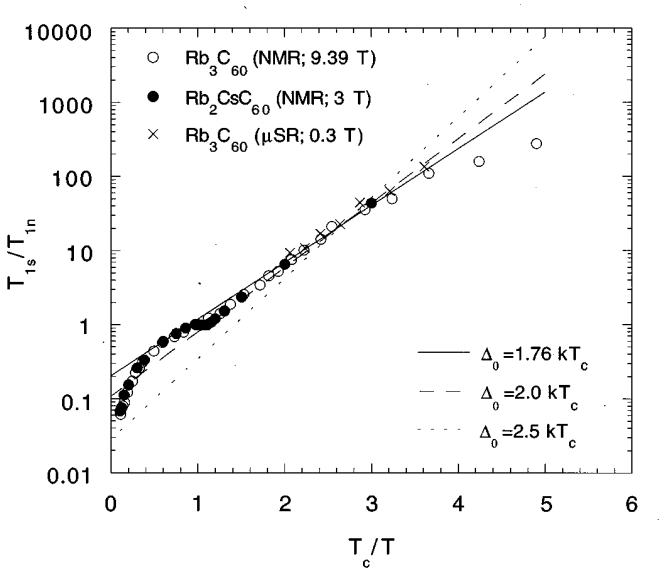


FIG. 33. Relaxation rates $T_{1s}/T_{1n}$ vs $T_c/T$ (Arrhenius plots) as measured by two different NMR groups (Tycko *et al.*, 1992; Stenger *et al.*, 1994), and through muon-spin relaxation (Kiefl *et al.*, 1993). For comparison the following Arrhenius curves are shown: solid line, $\Delta_0=1.76k_BT_c$; dashed line, $2.0k_BT_c$; and dotted line, $2.5k_BT_c$. The first value corresponds to the weak-coupling limit and the last to substantial strong coupling involving the optical phonon modes (see Table III). It is clear from this figure that only the range 1.76 to $2.0k_BT_c$ (weak-coupling limit) provides a reasonable fit. From the Arrhenius plots alone one would conclude that the $A_3C_{60}$ materials are conventional BCS superconductors.

and Rainer, 1991; Akis *et al.*, 1991a, 1991b) are known; however, the complete absence of the peak is unusual and is reminiscent of exotic systems such as heavy-fermion (Asayama *et al.*, 1988) and high-$T_c$ cuprate (Pennington and Slichter, 1990) superconductors.

The issue of the apparent absence of the Hebel-Slichter peak has been resolved by subsequent experiments (Kiefl *et al.*, 1993; Stenger *et al.*, 1994). In this section we shall review these developments as well as the less controversial issue of the low-temperature Arrhenius-law behavior of $T_1$, which probes the superconducting-state gap energy. In addition we shall compare and contrast the behaviors of alkali fullerides with those of both conventional and exotic superconductors.

### 1. The Arrhenius law: Measuring the low-temperature gap

All published magnetic resonance data are in reasonable agreement on the matter of the low-temperature gap $\Delta_0$. The expected BCS behavior is the Arrhenius form

$$\frac{1}{T_1}\propto\exp\left(\frac{-\Delta_0}{k_BT}\right), \tag{41}$$

with $\Delta_0=1.76kT_c$ in the weak-coupling limit. Figure 33 shows the temperature dependence of the low-temperature relaxation rates as measured by two different NMR groups (Tycko *et al.*, 1992; Stenger *et al.*, 1994), and through muon-spin relaxation (Kiefl *et al.*, 1993). For comparison Arrhenius curves are shown using $\Delta_0=1.76k_BT_c$; $2.0k_BT_c$; and $2.5k_BT_c$, the first value corresponding to the weak-coupling limit and the last to substantial strong coupling to the optical phonon modes (see Table IX). It is clear from the figure that only the range 1.76 to $2.0k_BT_c$ provides a reasonable fit. This conclusion is consistent with that drawn from infrared reflection data (Degiorgi *et al.*, 1992). This result taken alone would suggest a very conventional BCS superconductor.

### 2. The Hebel-Slichter peak (experimental)

The Arrhenius behavior described above was obtained quite early by Tycko *et al.* (1992). However, the same set of data also displayed an unusual feature, the absence or near absence of the Hebel-Slichter peak (Sec. III.D.3). The data of Tycko *et al.* for samples of both $K_3C_{60}$ and $Rb_3C_{60}$ are shown in Fig. 34, plotted in both linear and Arrhenius forms. The Hebel-Slichter peak would appear as an increase in $1/T_1T$ as temperature is lowered below $T_c$. What is observed instead is a monotonic dropoff.

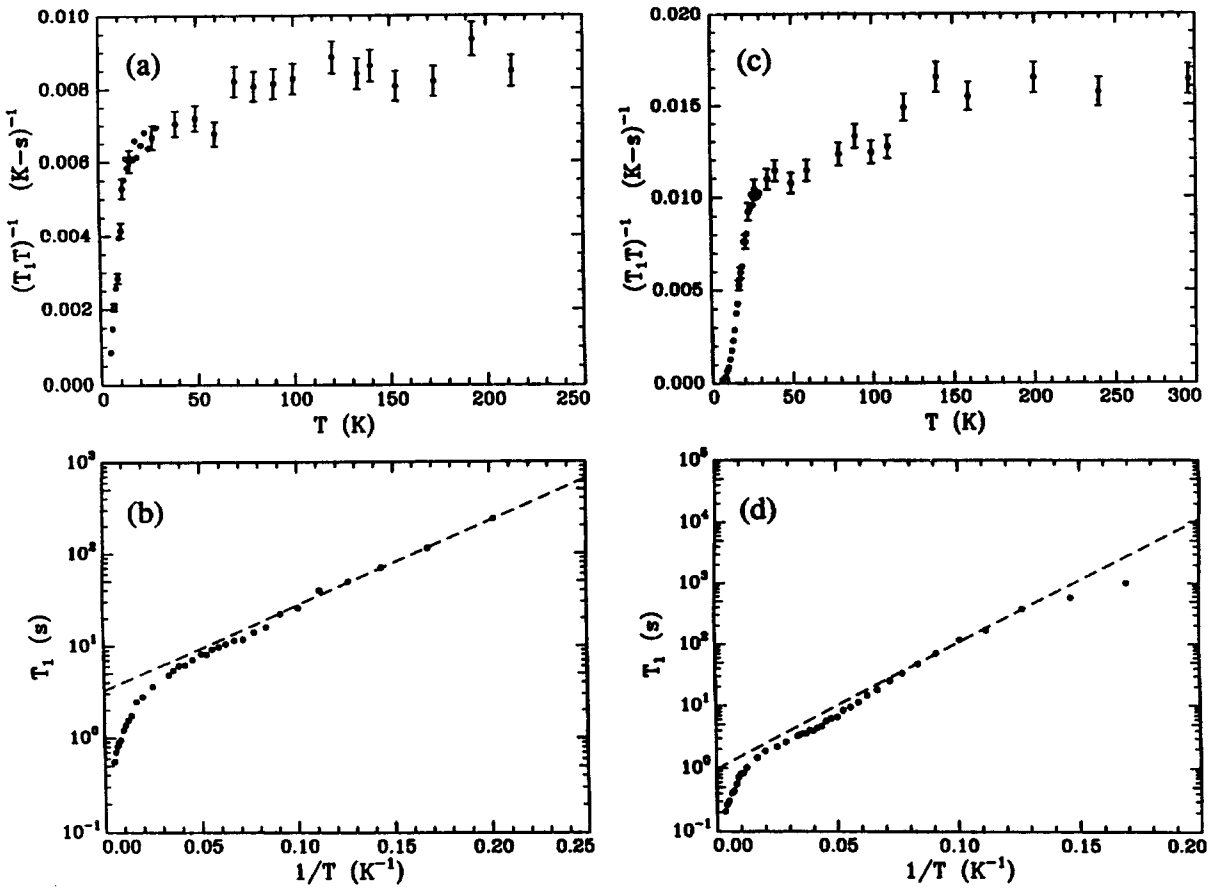


FIG. 34. Temperature dependence of the $^{13}C$ spin-lattice relaxation time $T_1$ in (a), (b) $K_3C_{60}$ and (c), (d) $Rb_3C_{60}$ plotted as follows: (a), (c), $(T_1T)^{-1}$ vs $T$; (b), (d), log $T_1$ vs $T^{-1}$, at 9.39 T (Tycko *et al.*, 1992). Error bars indicate 1 standard deviation. Dashed lines are fits of the data by Arrhenius laws (b) below 9 K and (d) from 8 to 12 K, leading to energy gaps $2\Delta^{K}\approx 42$ K and $2\Delta^{Rb}\approx 94$ K. At 9.39 T there is no indication of a Hebel-Slichter coherence peak in the $1/T_1T$ vs $T$ data [(a) and (c)] other than a suppression of $T_c$ of $\approx 3$ K below what is expected at this field. Deviation of the low-temperature $T_1$ data from Arrhenius behavior in (d) is indicative of spin diffusion between the rapidly relaxing nuclei in the normal-state vortex cores and nuclei in the bulk of the superconductor.

Subsequently muon-spin relaxation experiments (Kiefl *et al.*, 1993), performed on a sample of $Rb_3C_{60}$, displayed a Hebel-Slichter peak; the results are shown in Fig. 35. Typically the short (2.2 $\mu$s) lifetime of the muon limits its usefulness as a $T_1$ probe of conduction electrons. Kiefl *et al.*, however, found that muons in $A_3C_{60}$ are located inside the $C_{60}$ cage, and trap electrons to form endohedral muonium ($\mu^+e^-$) atoms in which there exist strong electron-muon hyperfine couplings, resulting in normal-state $T_1$ values on the order of 0.1 $\mu$s. Kiefl *et al.* found that their data could be fitted using a gap value $2\Delta_0/k_BT_c=3.6$ and a phenomenological gap broadening parameter near $T_c$ of approximately 5–8 Kelvin, or 0.2–0.3$T_c$ (for $T_c=29.2$ K).

The 1.5 tesla applied field in the muon-spin relaxation experiment was substantially lower than the value of 9.39 tesla used by Tycko *et al.* in their NMR measurements; at the time the strength of the magnetic field was not known to be an important parameter. Stenger *et al.* (1994), however, soon showed that a coherence peak is present in NMR experiments as well, but that the peak is strongly suppressed by magnetic fields larger than a few tesla. Shown in Fig. 36 is the ratio $R_s/R_n$ of superconducting to normal-state relaxation rates for $Rb_2CsC_{60}$ ($T_c=31$ K for zero applied field). The figure

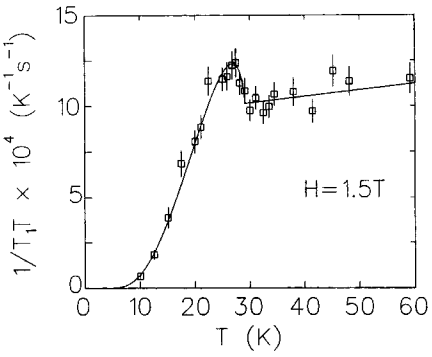


FIG. 35. Muon-spin relaxation ($\mu$SR) measurement of $(T_1T)^{-1}$ of $Rb_3C_{60}$ in a magnetic field of 1.5 tesla (Kiefl *et al.*, 1993). The solid line is a fit to the theory of Hebel and Slichter, with a broadened density of states. The Hebel-Slichter peak, seen just below $T_c$, is present in the muon-spin relaxation data, in contrast to early NMR data taken at high magnetic field.

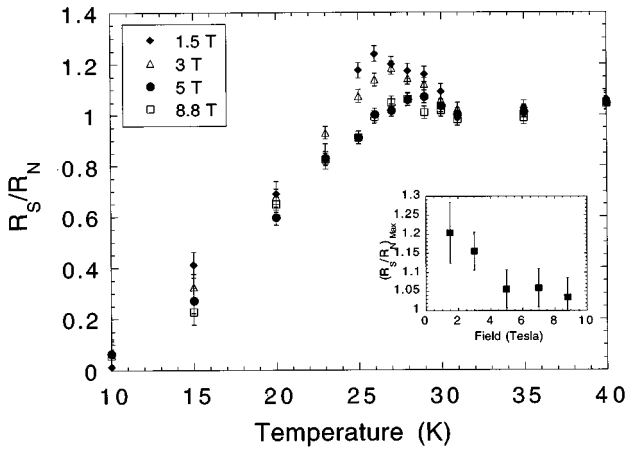


FIG. 36. $^{13}C$ $R_s/R_n$ vs $T$ of $Rb_2CsC_{60}$ for several magnetic fields (Stenger *et al.*, 1995). Inset: Maximum of $R_s/R_n$ vs applied field. The data demonstrate that the Hebel-Slichter peak (appearing as a bump just below $T_c$), which was not observed in early, high-field NMR experiments, is easily suppressed by the application of large magnetic fields, but is present at lower fields, in agreement with muon-spin relaxation data.

shows that, while the Hebel-Slichter peak is only faintly observable for high fields (greater than ~5 tesla), it is clearly observable for fields of 3 tesla and 1.5 tesla. In fact, the low-field NMR data of Stenger *et al.* on $Rb_2CsC_{60}$ are quite similar to the 1.5 tesla muon-spin relaxation data on $Rb_3C_{60}$, as is shown in Fig. 37.

### 3. Interpretations using Eliashberg theory

The results of the single-parameter approach to superconducting-state $T_1$ measurements are shown in Fig. 38 (Akis and Carbotte, 1991). In addition, Fig. 39

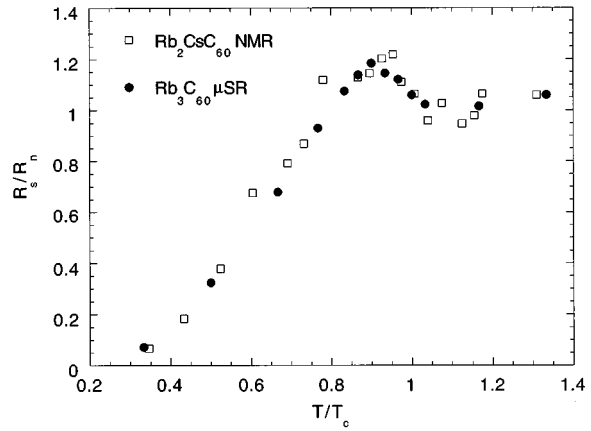


FIG. 37. $R_s/R_n$, the ratio of the superconducting spin-lattice relaxation rate $R_s$ (or superconducting-state $1/T_1$) to the normal-state rate $R_n$, vs $T/T_c$, for the alkali fullerides. Data are for $Rb_2CsC_{60}$ at 3 tesla from $^{13}C$ NMR (Stenger *et al.*, 1995) and for $Rb_3C_{60}$ at a field of 1.5 tesla using the muon-spin relaxation technique (Kiefl *et al.*, 1993). The figure demonstrates that NMR and muon-spin relaxation yield results that are in agreement for low applied magnetic fields.

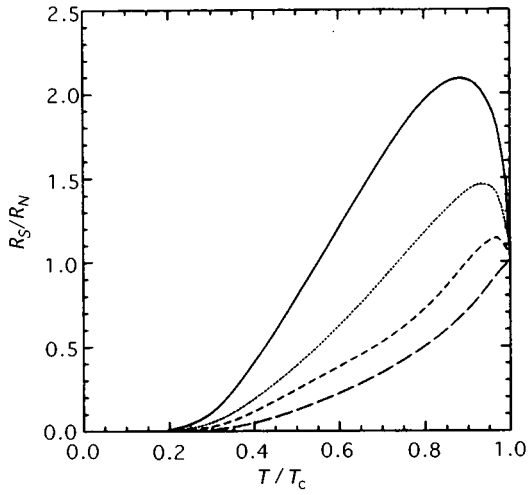


FIG. 38. Single-parameter calculation of the normalized NMR relaxation rates $R_s/R_n$ as a function of reduced temperature $T/T_c$ for four values of the strong-coupling index $T_c/\omega_{ph}$: solid curve, $T_c/\omega_{ph}$=0.1; dotted curve, 0.15; short dashed curve, 0.2; and long dashed curve, 0.3 (Akis *et al.*, 1991). From these results of Akis *et al.* it is clear that the Hebel-Slichter peak may be completely absent even within the framework of the BCS theory, if very strong coupling is present. Pb, often considered to be a strong-coupling superconductor, has a strong-coupling index $T_c/\omega_{ph}$ of only 0.13, while the weak-coupling superconductor Al has $T_c/\omega_{ph}$=0.004. A strong-coupling index of ~0.3 is, however, realized in Bi (Carbotte, 1990).

gives the maximum value of $R_s/R_n$, which is reached below $T_c$ as a function of the parameter $T_c/\omega_{ln}$. The latter figure reveals that the Hebel-Slichter peak completely vanishes for $T_c/\omega_{ln}$ greater than approximately 0.3. The experimental observation of a peak then implies very clearly that $\omega_{ln}$>70 $cm^{-1}$.

In fact, the size of the observed maximum in $R_s/R_n$ of ~1.2 implies $T_c/\omega_{ln}$~0.18. This alone would clearly indicate the optical phonon modes, with $\omega_{ln}$~100 $cm^{-1}$. For

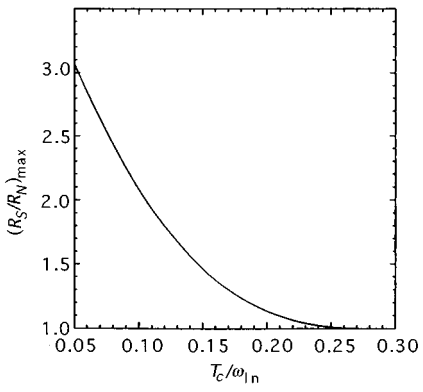


FIG. 39. The calculated maximum in the normalized relaxation rate $R_s/R_n$ as a function of the coupling parameter $T_c/\omega_{ph}$ (Akis and Carbotte, 1991). As the coupling strength is increased the maximum in $R_s/R_n$ falls rapidly to zero. The range exhibited by conventional superconductors is from 0.0 to 0.3.

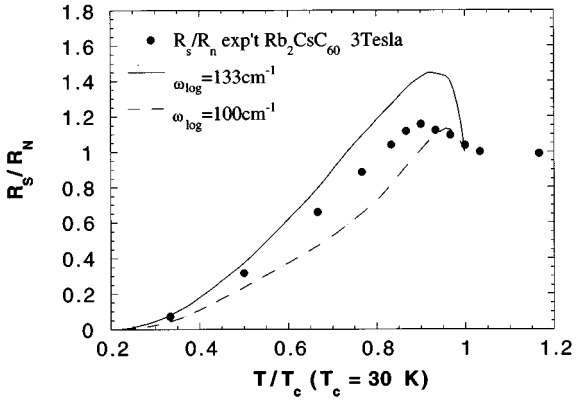


FIG. 40. Experimental $R_s/R_n$ (ratio of superconducting to normal-state relaxation rates) vs $T/T_c$ for $Rb_2CsC_{60}$ at 3 tesla (Stenger *et al.*, 1995), together with Eliashberg theory calculations of Akis and Carbotte (1991) for two values of effective phonon frequency $\omega_{\ln}$ 100 and 133 $cm^{-1}$ (the characteristic frequency of phonons mediating pairing). The data lie in between the two theoretical curves, suggesting that $\omega_{\ln}$ is not far from 100 $cm^{-1}$, which would indicate strong coupling. In the text, however, arguments are given to suggest that the inferred frequency should be considered as only a lower limit for the phonon frequency.

illustration, Fig. 40 shows the experimental $R_s/R_n$, together with the one-parameter calculations of Akis and Carbotte for $\omega_{\ln}\sim 100$ and 130 $cm^{-1}$. The data lie between the curves, suggesting that $\omega_{\ln}$ is in the vicinity of 100 $cm^{-1}$. In fact, this number should be considered as a robust lower limit on $\omega_{\ln}$, as additional mechanisms can only reduce the height of the Hebel-Slichter peak (see below).

Several factors make it likely that the true $\omega_{\ln}$ is larger than 100 $cm^{-1}$. First, one should remember that the low-temperature $T_1$ data follow an Arrhenius law with $2\Delta_0/k_BT_c$ of ~3.5 to 4. This finding is inconsistent with $\omega_{\ln}$=100 $cm^{-1}$, which would imply a gap $2\Delta_0/k_BT_c$ of approximately 5 (see Table IX). Second, the Knight-shift measurements described above provide a seemingly conservative lower limit on $\omega_{\ln}$ of 200 $cm^{-1}$. Finally, other mechanisms of peak suppression may be present.

### 4. Other mechanisms of Hebel-Slichter peak suppression

Other mechanisms of Hebel-Slichter peak suppression, apart from strong coupling, are well known (MacLaughlin, 1976).

#### *a. Gap anisotropy and inhomogeneity*

Clem (1966) has treated the effects of energy-gap anisotropy; anisotropy in the energy gap broadens the singularity in the BCS density of states and thus reduces the Hebel-Slichter peak. This mechanism seems unlikely here, first because the degree of anisotropy required would be quite large, comparable in fact to the gap itself (see Akis *et al.*, 1991). Second, one expects alkali fullerides to be in the "dirty limit" (see, for example, Dresselhaus, Dresselhaus, and Saito, 1994; p. 525–530), in which any gap anisotropy would be averaged away by rapid elastic scattering.

Any substantial gap inhomogeneity (of unspecified origin) in the parameter $\Delta_0$, or an effective spread in $T_c$ within the sample, can also broaden the Hebel-Slichter peak. Such a mechanism would require, however, roughly a 20% spread in $T_c$ and/or $\Delta_0$ in order to explain the observed behavior.

#### *b. Mechanisms associated with applied magnetic fields*

Finally, we enumerate three mechanisms associated with the application of magnetic fields, leaving the possibility that fields lower than 1.5 tesla may be necessary for observation of the intrinsic Hebel-Slichter peak. We consider the mixed state, with $(H_{c1}<H_{\text{applied}}<H_{c2})$.

First, magnetic fields add a perturbation that has opposite signs for the two one-electron states making up a Cooper pair. This leads to "pair breaking"—a finite lifetime for Cooper pairs (see DeGennes, 1989; Chapter 8). This lifetime mechanism also leads to broadening of the effective energy gap. In the dirty limit the gap, and the NMR $T_1$, are local properties, taking on different values depending upon position relative to the vortex cores. Cyrot (1966) has calculated the effect upon $T_1$, which can be applied only for $H_{\text{applied}}$ near $H_{c2}$,

$$\left.\frac{d(R_s/R_n)}{dT}\right|_{T=T_c(H)} = \frac{ec}{\sigma}\,\frac{(dH_{c2}/dT)}{\beta_A(2\kappa_2{}^2-1)}\,\frac{1}{k_BT_c}\,g(t), \tag{42}$$

where $\sigma$ is the electrical conductivity, $\beta_A$ is a coefficient of order 1, $\kappa$ is the Landau-Ginsberg parameter, and $t=T_c(H)/T_c$, where $T_c(H)$ is the suppressed value of $T_c$ in the applied field $H$. $g(t)$ is computed numerically by Cyrot and is given as follows: $g(t)$ diverges as $t$ approaches one, vanishes at $t$=0.6, and is given by –0.18 for $x$=0. For $t$ approximately 0.8 to 0.95, the region of interest, $g$ is of order one. The main features of the above prediction have been verified in conventional superconductors by Masuda and Okubo (1969); their data are shown in Fig. 41. For the case of alkali fullerides, estimates of the quantity $d(R_s/R_n)/dT$ using Eq. (2) are typically at least an order of magnitude larger than observed by Stenger *et al.*, although there are considerable uncertainties in the formula input parameters and in the experimentally measured slope. The expression assumes that no other broadening mechanisms are present.

Stenger and Pennington (unpublished) have used a cruder model to explain the Hebel-Slichter peak suppression. The model was introduced by Goldberg and Weger (1968) for conventional type-II superconductors to describe relaxation rates for $T\ll T_c$.

Stenger *et al.* take an area of $\pi\xi^2$ at the vortex core to consist of normal metal and to relax at the normal-metal (Korringa) rate; the fraction $f_n$ of normal sample is then given by $f_n=H/2\pi H_{c2}(T)$. $f_n$ approaches one at temperatures near $T_c(H)$. The remainder of the material of fractional area $1-f_n$ is assumed to relax at the intrinsic (possibly strong-coupling) superconducting-state rate.

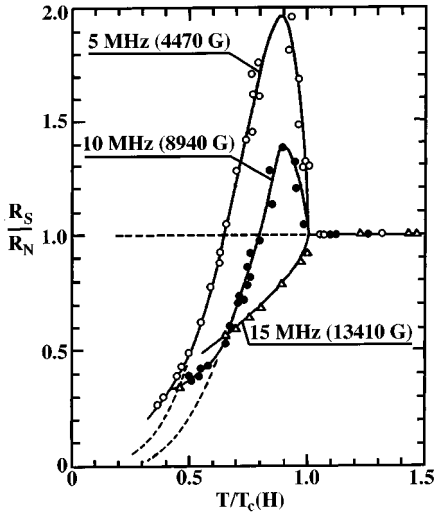


FIG. 41. $R_s/R_n$ using $^{51}$V NMR on superconducting $V_3Sn$ at magnetic fields of 4.5, 8.9, and 13.4 kG, showing suppression of the Hebel-Slichter peak by large applied fields (Masuda and Okubo, 1969). The second critical field for this material at zero temperature is 16 kG. The data show that for large enough applied fields the Hebel-Slichter (HS) peak is completely eliminated. The data also confirm theoretical predictions of Cyrot (1966), predicting a complete Hebel-Slichter peak suppression at magnetic fields large enough to suppress $T_c$ by 40%. In this instance that occurs near 11 kG. From these results one would not expect the Hebel-Slichter peak to vanish in the alkali fullerides until fields reached several tens of tesla. Note, however, that the intrinsic, zero-field peak in the alkali fullerides is much smaller than it is in $V_3Sn$, and thus not much suppression is required to reduce to peak to a size too small to be detected.

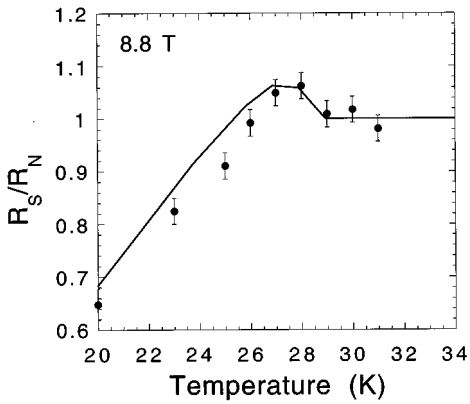


FIG. 42. $^{13}$C $R_s/R_n$ (the ratio of the superconducting to the normal-state relaxation rate) for $Rb_2CsC_{60}$ in a field of 8.8 tesla (Stenger *et al.*, 1995). The points with error bars are the experimental data. The solid curve is a prediction obtained as follows: the total relaxation rate is assumed to be equal to a weighted average of the intrinsic, zero-field relaxation rate $R_s|_{\rm int}$ and the normal-state rate $R_n$. The weighted average is written $R_s=(1-f_n)R_s|_{\rm int}+f_nR_n$, where $f_n$ is the fraction of the sample volume within the vortex cores. The fraction $f_n$ is estimated as $f_n=H/2\pi H_{c2}(T)$, with $H_{c2}(T)=\phi_0/2\pi\xi^2$, $\phi_0$ equal to the flux quantum, and $\xi$ the coherence length. $H_{c2}$ is taken to be 50 tesla at low temperature, and the BCS temperature dependence is assumed. The intrinsic rate $R_s|_{\rm int}$ is first obtained by applying the methodology to data taken at 3 tesla, where the Hebel-Slichter peak is more pronounced. That intrinsic rate is then used in the weighted average to predict $R_s/R_n$ at 8.8 tesla. The fact that the prediction yields a very small Hebel-Slichter peak, in agreement with the data, demonstrates that field suppression of the peak should not be considered as unexpected.

They estimate that the experimentally derived relaxation rate should be close to a weighted average of the normal rate $R_n$ and the intrinsic rate $R_s|_{\rm int}$.

$$R_s/R_n|_{\rm expt}=f_n+(1-f_n)R_s/R_n|_{\rm int}. \tag{43}$$

Stenger *et al.* use an estimate of 50 tesla for $H_{c2}(T=0)$ and take a BCS temperature dependence of $H_{c2}(T)$ to extract $R_s|_{\rm int}$ from their low-field (3 tesla) data, making the correction for the rather small but nonzero $f_n$ at these fields. Then they utilize the extracted $R_s|_{\rm int}$ and the same values of $H_{c2}(T)$ to calculate the high-field (8.8 tesla) result. Results, shown in Fig. 42, demonstrate that this approach can be used to explain the extent of Hebel-Slichter peak suppression. How can this model be consistent with the results of Cyrot? The resolution of this paradox is as follows: Cyrot predicts that the Hebel-Slichter peak will be completely eliminated only for fields that suppress $T_c$ by some 40% or more. The Cyrot model, however, assumes that the intrinsic (zero-field limit) Hebel-Slichter peak is quite large. For the case of the alkali fullerides, however, the intrinsic peak is not very large. Thus when a large fraction of the sample (that within the vortex cores) relaxes at the normal-state rate, it is quite easy for any vestiges of a feeble Hebel-Slichter peak to be obscured in the scatter of the experimental data.

Finally, we present one other field suppression mechanism, which has not appeared in the literature and which was suggested to us by K. E. O'Hara (unpublished). The source of the Hebel-Slichter peak is a singularity in the BCS density of states at the gap edge. As discussed in Sec. III.D.3, the BCS expression for $R_s/R_n$ is

$$R_s/R_n=\frac{2}{k_BT}\int_\Delta^\infty dE_i f(E_i)[1-f(E_i)] \times\left(1+\frac{\Delta^2}{E_iE_f}\right)\frac{N_{\rm BCS}(E_i)N_{\rm BCS}(E_f)}{N_{\rm norm}^2}. \tag{44}$$

The usual argument is that, because $E_i$ and $E_f$ differ by only the very small nuclear Zeeman energy, one can take $N_{\rm BCS}(E_i)N_{\rm BCS}(E_f)$ equal to $N_{\rm BCS}^2$. This procedure is surely valid for experiments done at low or zero field, as in the original Hebel-Slichter experiment. However, the situation is different for type-II superconductors, where often $T_1$ is measured in the presence of a large applied field. Most $T_1$ hyperfine terms require that, in order to flip the nuclear spin, the electron spin must be flipped as well. Thus the initial and final states appearing in Eq. (44) differ in the electron-spin orientation.

Figure 43 illustrates the effect. It can be seen that the gap edges for up spins and down spins differ in energy

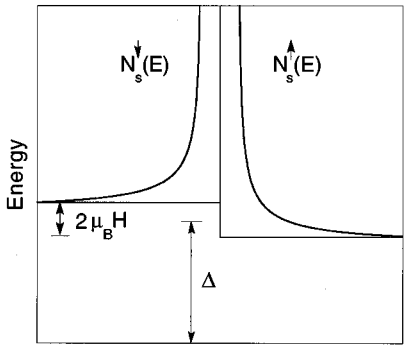


FIG. 43. BCS density of states in an applied magnetic field $H$. The effect of the magnetic field on the electron density of states is to shift the zero-point energy by $+\mu_B H$ and $-\mu_B H$ for electrons in spin-down and spin-up states, respectively. For applied magnetic fields of 10 tesla, this splitting corresponds to 13.4 K, comparable to or even larger than the BCS temperature-dependent energy gap. This provides an effective broadening of the singularity in the density of states and should result in a reduction of the Hebel-Slichter coherence peak.

by $2\mu_B H$, where $\mu_B$ is the Bohr magneton. For applied magnetic fields of 10 tesla this splitting corresponds to 13.4 K, comparable to or even larger than the temperature-dependent BCS energy gap. This provides an "effective" broadening of the singularity and should result in a substantial suppression of the Hebel-Slichter peak.

### D. Summary of superconducting-state NMR results

The NMR Knight-shift data yield an apparently simple result. They are consistent with the weak-coupling limit of BCS theory, which would specify the intramolecular phonon modes as the pairing agent—probably the high-frequency intramolecular phonons above 1000 $cm^{-1}$, but certainly above 200 $cm^{-1}$. This interpretation is clear if we neglect some of the reservations on the interpretation discussed in Sec. V.B.3.

Spin-lattice relaxation ($1/T_1$) results are more ambiguous. The low-temperature superconducting-state relaxation rate follows an Arrhenius law and suggests a low-temperature energy gap consistent with the weak-coupling limit. The data near $T_c$, however, show a Hebel-Slichter peak that is, though clearly present at low magnetic fields, strongly suppressed, consistent with a degree of strong coupling similar to that of Hg, Ga, or Bi.

Mazin *et al.* (1993) have analyzed early high-field NMR data (*sans* Hebel-Slichter peak) together with tunneling data suggesting strong coupling (Zhang *et al.*, 1991) using Eliashberg theory and incorporating *two* peaks in $\alpha^2F(\omega)$—one high-frequency peak at ~1000 $cm^{-1}$ representing intramolecular vibrations and a very-low-frequency peak characterizing the molecular reorientations. J. P. Carbotte (private communication) has suggested to the authors that such an approach might permit one to have both a strongly suppressed Hebel-Slichter peak and a low-temperature gap close to the weak-coupling limit value.

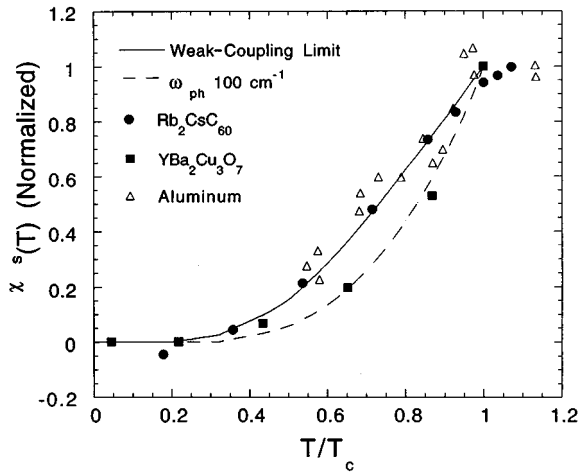


FIG. 44. Normalized superconducting-state spin susceptibility $\chi^s(T)$ as measured by the Knight shift for the conventional superconductor Al (Fine *et al.*, 1969), for $Rb_2CsC_{60}$ (Stenger *et al.*, 1995) and for the high-$T_c$ ($T_c$=93 K) cuprate superconductor $YBa_2Cu_3O_7$ (Barrett *et al.*, 1990). Also shown is a weak-coupling limit Yosida curve (solid line) and the strong-coupling fit for $\omega_{ph}$=100 $cm^{-1}$ (Akis *et al.*, 1991). The $C_{60}$ superconductor behaves quite conventionally, while the $YBa_2Cu_3O_7$ shows a much steeper falloff of $\chi^s(T)$ as $T$ drops below $T_c$.

The authors believe that a calculation demonstrating this possibility would be an important confirmation that the BCS framework can provide a consistent description of the full range of experimental data.

### E. Phenomenological comparison with other classes of superconductors

Finally, we compare NMR results on $C_{60}$ superconductors with those on other classes, including conventional and high-$T_c$ cuprate superconductors, with a minimum of commentary.

Figure 44 shows the normalized superconducting-state spin susceptibility $\chi^s(T)$ as measured by the Knight shift for the conventional superconductor Al (Fine *et al.*, 1969), for $Rb_2CsC_{60}$ (Stenger *et al.*, 1995), and for the high-$T_c$ ($T_c$=93 K) cuprate superconductor $YBA_2Cu_3O_7$ (Barrett *et al.*, 1990). Also shown is a weak-coupling-limit Yosida curve. The $C_{60}$ superconductor behaves quite conventionally, while the $YBa_2Cu_3O_7$ shows a much steeper falloff on $\chi^s(T)$ as $T$ drops below $T_c$. If we were to assume that $YBa_2Cu_3O_7$ were an $s$-wave, phonon-mediated pairing superconductor, we would find that the strong-coupling parameter required would be near 0.3.

Ratios of superconducting to normal-state relaxation rates $R_s/R_n$ for the same materials (Al: Masuda and Redfield, 1962; $Rb_2CsC_{60}$: Stenger *et al.*, 1995; $YBa_2Cu_3O_7$: Imai *et al.*, 1988) are given in Fig. 45. It can

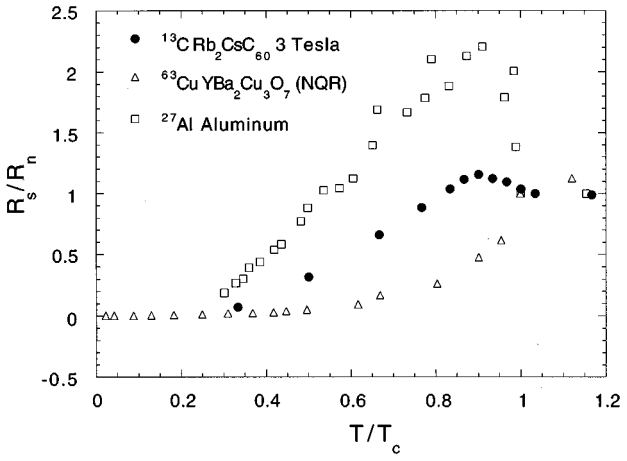


FIG. 45. Ratios of the superconducting to normal-state relaxation rates $R_s/R_n$ for aluminum (Masuda and Redfield, 1962), $Rb_2CsC_{60}$ (Stenger *et al.*, 1995), and $YBa_2Cu_3O_7$ (Imai *et al.*, 1988). Although the Hebel-Slichter peak in $Rb_2CsC_{60}$ is much less pronounced than in the conventional superconductor aluminum, its suppression is not at all comparable to that of $YBa_2Cu_3O_7$.

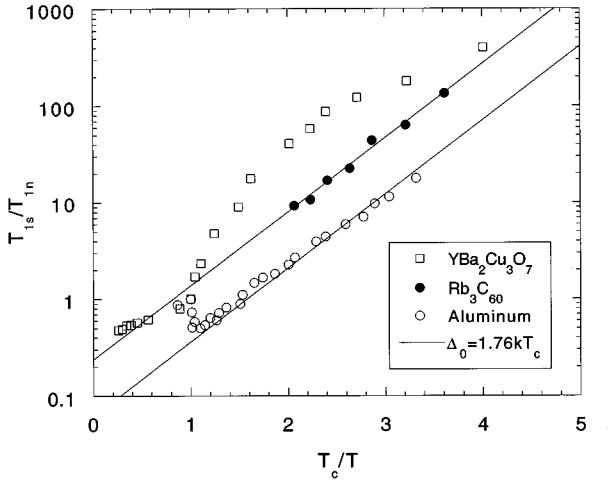


FIG. 46. Arrhenius plots ($T_{1s}/T_{1n}$ vs reduced temperature $T_c/T$) for aluminum (Masuda and Redfield, 1962), $Rb_3C_{60}$ (Kiefl *et al.*, 1993), and $YBa_2Cu_3O_7$ (Imai *et al.*, 1988). Also shown is the BCS weak-coupling prediction (solid line). For temperatures well below $T_c$ both the Al and the $Rb_3C_{60}$ $T_{1s}/T_{1n}$ data follow the Arrhenius law for weak coupling. In contrast, the $YBa_2Cu_3O_7$ data do not follow the Arrhenius dependence over any extended temperature range. Thelen *et al.* (1993) ascribe this unusual temperature dependence to $d$-wave pairing and strong coupling to antiferromagnetic fluctuations rather than phonons.

be seen that, while the Hebel-Slichter peak of $Rb_2CsC_{60}$ is less pronounced than that of Al, its suppression is not at all comparable to that of $YBa_2Cu_3O_7$. For example, at $T/T_c$=0.95, $R_s/R_n$ is approximately 2.0 and 1.1 for Al and $Rb_2CsC_{60}$, but it is 0.6 for $YBa_2Cu_3O_7$.

The sharply contrasting behavior of the high-$T_c$ material can also be observed in an Arrhenius plot of the same classes of materials, shown in Fig. 46 (Al: Masuda and Redfield, 1962; $Rb_3C_{60}$: Kiefl *et al.*, 1993; $YBa_2Cu_3O_7$: Imai *et al.*, 1988). Also given in Fig. 46 is a straight line representing Arrhenius-law behavior with $\Delta=1.76k_BT_c$. For temperatures well below $T_c$, both Al and $Rb_3C_{60}$ follow the Arrhenius law rather well, even taking on the appropriate slope within experimental error. In contrast, the $YBa_2Cu_3O_7$ data do not follow the Arrhenius dependence over any extended temperature range. Thelen *et al.* (1993) ascribe this unusual temperature dependence to $d$-wave pairing and strong coupling to antiferromagnetic fluctuations rather than phonons.

Thus, taking a phenomenological approach, the alkali fullerides do not appear particularly unusual, but the high-$T_c$ cuprates continue to stand out.

## VI. INFERENCES FROM NORMAL-STATE NMR OF $A_3C_{60}$

Thus far, we have looked at NMR as a probe of structure and of superconductivity. We have certainly received some unusual and unexpected information about the structure and orientational dynamics of the $C_{60}$ molecules, while at the same time confirming some of the coarse features of the conventional view. Similarly, superconducting-state NMR appears, in the opinion of the authors, to be consistent with a BCS picture, while more work is needed to reconcile all of the available data fully. Finally, we turn to normal-state NMR data, especially the spin-lattice relaxation $1/T_1$ and Knight shifts. We ask what can be learned about (1) normal-state electronic structure, and (2) superconductivity, specifically relationships between electronic densities of states and $T_c$'s, as in the McMillan equation.

### A. Inferences about normal-state electronic structure

The story of high-$T_c$ cuprate superconductors illustrates the difficulty involved in predicting the electronic properties of many materials, especially when electron correlations are likely to play a role. Band theory predicts that the parent compound $La_2CuO_4$ is a conductor, yet it turns out to be an antiferromagnetic Mott insulator. One must wonder if such effects of strong correlation could be in operation for fullerene superconductors as well. Indeed there exist both theoretical and experimental suggestions that this is the case, discussed in Sec. II and especially Sec. II.D. If strong correlations were present, one would expect that they would appear as anomalies in NMR experiments, as they certainly have in the case of the cuprates (Slichter, 1994). With this in mind we now survey experimental NMR results, looking for any signs of strong correlations. As it turns out, the body of available data does not require it.

Numerous investigators have contributed on this issue (Tycko, Dabbagh, Rosseinsky, *et al.*, 1992; Wong *et al.*, 1992; Antropov *et al.*, 1993; Holczer, 1993; Holczer *et al.*, 1993; Mehring, 1993; Quirion *et al.*, 1993; Tycko, Dabbagh, Murphy *et al.*, 1993; Yannoni *et al.*, 1993; Zimmer *et al.*, 1993a, 1993b; Kerkoud *et al.*, 1994; Maniwa *et al.*,

1994; Shastry *et al.*, 1994; Stenger *et al.*, 1995) and inevitably we do not cite specific contributions in all cases. Rather we present a more personal overview which benefits from the insights gained from the accumulated work. Some of what follows is our own reconstruction and analysis of our data and that of others, and appears for the first time in this review.

We shall inquire about the presence or absence of four different effects, which historically have indicated strong coupling—here we list them in order from least to most theory-dependent.

(1) Differing behavior of the NMR spin-lattice relaxation rates for nuclei situated at differing positions within the unit cell (as occurs, for example, for $^{17}O$ and $^{63}Cu$ in the cuprates).

(2) Unusual temperature dependence of the spin-lattice relaxation rates, deviating from the Korringa law $1/T_1 \propto T$.

(3) Substantial enhancement or reduction of $1/T_1T$ from the value predicted by the Korringa relation using the experimentally derived Knight shift.

(4) Substantial enhancement or reduction of $1/T_1T$ from the value calculated from band theory density-of-states estimates, and hyperfine coupling estimates. We find that the apparent anomalies of the type described above can in all cases be reasonably understood without having to resort to a strong-correlation argument.

### 1. $1/T_1T$ behaviors for different nuclei

In Sec. III.D.2 we discuss the relationship between spin-lattice relaxation and $\chi''(\vec{q},\omega)$, the imaginary part of the wave vector and frequency-dependent electronic-spin susceptibility. In terms of $\chi''(\vec{q},\omega)$, $1/T_1$ is given by

$$\frac{1}{T_1} = \frac{4k_BT}{\hbar} \sum_{\substack{\vec{q}, \\ \alpha=xx,yy}} \left( \frac{A_\alpha(\vec{q})}{\gamma_e\hbar} \right)^2 \frac{\chi''(\vec{q},\omega)}{\hbar\omega},$$

where $A_\alpha(\vec{q})$ is a spin-wave vector-dependent hyperfine coupling. In the usual case $A_\alpha(\vec{q})$ is $\vec{q}$ independent. However, in the case of high-$T_c$ cuprates, the $\vec{q}$ dependence of the hyperfine coupling plays an important role. Because the planar $^{17}O$ in these materials is located halfway between two Cu moments, its hyperfine coupling to antiferromagnetic fluctuations vanishes, while the $^{63}Cu$ coupling is nonzero. The temperature dependence of the strong antiferromagnetic fluctuations and correlations leads to very different relaxation behavior of $^{63}Cu$ and $^{17}O$. Figure 47 shows the $1/T_1T$ data for $^{63}Cu$ and $^{17}O$ in $YBa_2Cu_3O_{6.63}$ of Takigawa (1992).

Strong magnetic correlations might be expected to result in a similar, analogous difference between the spin-lattice relaxation behaviors of $^{13}C$ and the alkali-metal nuclei. Without a specific model of the correlations one cannot predict the extent of the difference. The data, however, show none of the effects observed in the cuprates. Figure 48 shows $1/T_1T$ vs $T$ for $^{87}Rb$, $^{133}Cs$, and $^{13}C$ in $Rb_2CsC_{60}$. In sharp contrast to the high-$T_c$ cuprates, the temperature dependence of $1/T_1T$ in the alkali fullerides is independent of location within the unit cell, providing some kind of upper limit on effects of strong correlations.

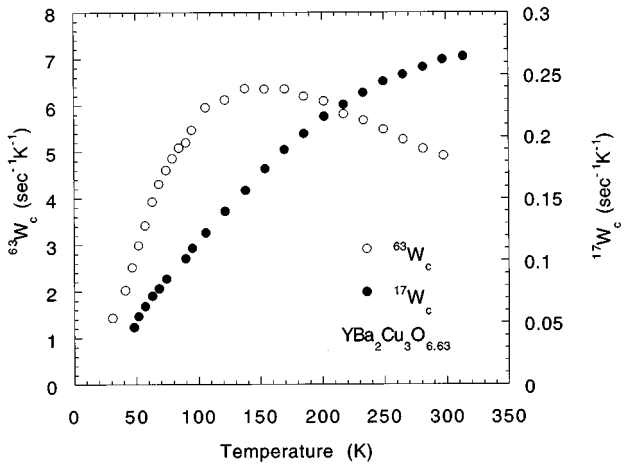


FIG. 47. The contrasting spin-lattice relaxation behaviors of $^{17}O$ and $^{63}Cu$ spin-lattice relaxation rates for the high-$T_c$ cuprate superconductor $YBa_2Cu_3O_{6.63}$. The quantity $W$ plotted in the figure is equal to $1/T_1T$. Neither nucleus even remotely obeys the Korringa relation, $W$=const. Furthermore, the behaviors of the two nuclei contrast sharply with each other, even though they are located less than two angstroms apart in the unit cell. This behavior is in contrast to that of the various nuclei in the alkali fullerides. The temperature dependences of their relaxation rates are very similar, and none deviate strongly from the Korringa relation, especially after thermal expansion of the lattice is taken into account. This kind of comparison (between fullerenes and high-$T_c$ cuprates) gives evidence that strong correlations are not present in the fullerene superconductors, at least not to the extent observed in the cuprates.

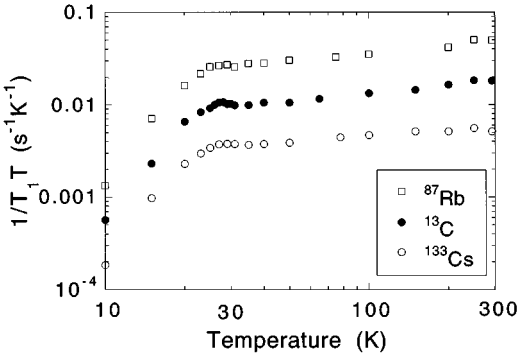


FIG. 48. Temperature-dependent spin-lattice relaxation ($1/T_1T$) of $^{87}Rb$, $^{13}C$, and $^{133}Cs$ in $Rb_2CsC_{60}$ ($T_c$=31 K) taken at an applied field of 8.8 tesla (Stenger *et al.*, 1994). Uncertainty is estimated at ±5%. The temperature dependence for all three nuclei is the same. This is in sharp contrast to the behavior in the high-$T_c$ cuprate superconductors, where the NMR behavior of the $^{17}O$ and $^{63}Cu$ are quite different, suggesting the importance of antiferromagnetic fluctuations in those materials.

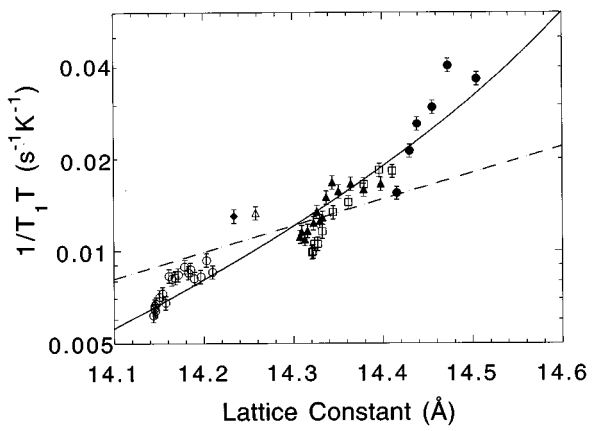


FIG. 49. $(1/T_1T)$ for $^{13}C$ vs lattice parameter $a$ for $A_3C_{60}$ compounds with temperature and dopant ion as implicit parameters (Stenger *et al.*, 1995). Materials: ○, $K_3C_{60}$ (between $T_c$ and room temperature, from Tycko *et al.* 1992); ▲, $Rb_3C_{60}$ (between $T_c$ and room temperature, from Tycko *et al.*, 1992); ♦, $RbK_2C_{60}$ (292 K), (Stenger *et al.*, 1995); △, $Rb_2KC_{60}$ (292 K) (Stenger *et al.* 1995); □, $Rb_2CsC_{60}$ (between $T_c$ and room temperature, from Stenger *et al.*, 1995); ●, $RbCs_2C_{60}$ (between $T_c$ and room temperature, from Stenger *et al.*, 1995). Fits: dashed curve, "Band theory" fit to $1/T_1T \propto \rho^2 \propto \exp(2a/\sqrt{2}d)$ with $d$ estimated from LDA and Huckel calculations; solid curve, fit to $1/T_1T$ proportional to the enhanced density of states squared, with enhancement parameters taken from specific-heat, spin susceptibility, $T_c$, and isotope-effect data of Ramirez, Rosseinsky, *et al.* (1992). The data demonstrate that $1/T_1T$ in the alkali fulleride superconductors is at least nearly a universal function of lattice constant, with temperature and dopant ion acting as implicit parameters. The good fit of the solid curve also demonstrates that the density-of-states parameters obtained from other independent experiments can be used successfully to understand the lattice-constant dependence of $1/T_1T$. These same parameters also provide a rather complete picture of superconductivity in the weak-coupling limit of BCS theory (see text, and Stenger *et al.*, 1995).

### 2. Temperature dependence of $1/T_1T$

Section III.D.1 describes the Korringa relation for metals with noninteracting electrons, which specifies the relation $1/T_1T$=const in the normal state. Deviations from this relation indicate the effects of electron correlations; they are clearly present in Fig. 47 for the high-$T_c$ cuprates. Indeed, the data for the alkali fullerides shown in Fig. 48 also reveal a temperature-dependent $1/T_1T$ in the normal state—it is found that $1/T_1T$ rises by about 80% as the temperature is increased from $T_c$=31 K to room temperature (Stenger *et al.*, 1995). Tycko, Dabbagh, Rosseinsky, *et al.* (1992) first reported a temperature-dependent $1/T_1T$ and suggested the possibility that the thermal expansion of the lattice might result in a decrease in overlap between the wave functions of adjacent molecules, an increase in the electronic density of states, and a resulting increase in $1/T_1T$. Data in Fig. 49 from Stenger *et al.* (1995) support this picture.

Figure 49 shows the $^{13}C$ $1/T_1T$ vs the lattice parameter $a$ for both a range of temperatures and a range of alkali intercalant ionic radii. Both temperature and intercalant are implicit variables. The significance of the result is that $1/T_1T$ is nearly a universal function of lattice parameter—nearly independent of temperature after thermal expansion is taken into account. Thus $C_{60}$ compounds very nearly follow the Korringa law—another null result in our search for signs of strong correlations.

### 3. Hyperfine mechanisms and understanding the magnitude of $1/T_1T$

We now consider the magnitude of $1/T_1T$, Tycko *et al.* (1992) and Wong *et al.* (1992) first considered the Fermi contact interaction (Sec. III.A.2) hyperfine mechanism as the source of spin-lattice relaxation (Sec. III.D.1), using the following expression:

$$1/T_1T = \tfrac{64}{9}\,\pi^3\hbar^3\gamma_e^2\gamma_n^2[\langle|\psi(0)|^2\rangle_{E_F}]^2\rho^2(E_F),$$

where $\rho(E_F)$ is the density of states at the Fermi level and $\langle|\psi(0)|^2\rangle_{E_F}$ is the average over the Fermi surface of the square magnitude of the Bloch wave function evaluated at the site of the nucleus. Using theoretical estimates of $\langle|\psi(0)|^2\rangle_{E_F}$ and the measured $T_1T$=100 K s at $T_c$ for $Rb_3C_{60}$ and 165 K s for $K_3C_{60}$, Tycko *et al.* estimated densities of states as 22 states/(eV spin molecule) for $Rb_3C_{60}$ and 17 states/(eV spin molecule) for $K_3C_{60}$. This was somewhat larger than theoretical estimates based on the local-density approximation (Sec. II.B.2), which are typically ~9 states/(eV spin molecule) for $K_3C_{60}$, but not at all far from values inferred from spin susceptibility by Wong *et al.* and Ramirez, Rosseinsky, *et al.* (1992). It is now accepted, however, that this agreement was fortuitous. Tycko *et al.* noted that their value for hyperfine coupling resulted in a $^{13}C$ Knight shift of ~200 ppm, much larger than experiment, and that there was a possibility that a dipolar hyperfine coupling mechanism (Sec. III.D.1) might play a role in spin-lattice relaxation as well.

Antropov *et al.* (1993) then proposed that the dipolar mechanism dominates spin-lattice relaxation. They performed local-density approximation calculations to find hyperfine couplings and densities of states directly, and showed that measured values of $1/T_1T$ were not unreasonable, and in fact consistent with bare density-of-states values of 7.2 and 8.1 states/(eV spin molecule) for $K_3C_{60}$ and $Rb_3C_{60}$, respectively. The work of Antropov *et al.* was an important demonstration that strong-correlation effects are not required to understand $1/T_1T$ for $^{13}C$.

### 4. Comparison of $1/T_1T$ and the Knight shift from the Korringa relation

One important prediction of Antropov *et al.* was that, given the dipolar relaxation mechanism, $^{13}C$ spin-lattice relaxation should be anisotropic—dependent on the orientation of the magnetic field with respect to the $2p_{z'}$ orbital at the atomic site of the $^{13}C$, where $z'$ is directed radially from the center of the buckyball sphere. Of

course, in powder samples, the magnetic field will take on all possible orientations with respect to the $z'$ axes with equal probability per unit solid angle. Nevertheless Pennington *et al.* (1995) have found a way to extract the anisotropy of $T_1$ and thus to test the dipolar relaxation proposal of Antropov *et al.* and, in fact, to test the Korringa relation.

The dipolar relaxation and shift mechanism is discussed briefly in Sec. III.D.1, but here we discuss it in more detail. Figure 50 provides a schematic explanation for the effects of anisotropy which occur for the dipolar hyperfine mechanism. For this mechanism alone, the anisotropic shift tensor is given in terms of the angle $\theta$ between the direction $z$ of the applied field and the direction $z'$ of the carbon $2p$ orbital. In terms of the angle $\theta$, the anisotropic Knight shift is given by

$$K(\theta)=\frac{2}{5}\left\langle\frac{1}{r^3}\right\rangle\chi^s(3\cos^2\theta-1). \tag{45}$$

The analogous expression for spin-lattice relaxation is

$$(T_1T)^{-1}=\tfrac{1}{3}(2+3\sin^2\theta)\times\left\langle\frac{\pi}{2}\right\rangle k_B\hbar^3\gamma_e^2\gamma_n^2\left[\frac{4}{5}\left\langle\frac{1}{r^3}\right\rangle\rho(\varepsilon_F)\right]^2. \tag{46}$$

From Eqs. (45) and (46) it is clear that $1/T_1T$ and $K$ for a line shape are correlated—that is, intensity at the high-frequency end of the line shape is predicted to relax at a rate 2.5 times that of the intensity at the low-frequency end.

To test this prediction, Pennington *et al.* (1995) measured $T_1$ as a function of frequency for a fixed applied field, for $Rb_2CsC_{60}$. Figure 51 shows these results for $T$=80 K. From the figure it is clear that although there is substantial anisotropy, it is not as large as 2.5 to 1. The relaxation rate at the low-frequency end (with $2p_{z'}$ orbitals oriented perpendicular to the applied field) has a fast relaxation rate of 1.17 $s^{-1}$, while the intensity at the high frequencies relaxes at the rate 0.75 $s^{-1}$, giving a ratio of 1.56 (and a powder average rate of 1.03 $s^{-1}$).

Pennington *et al.* proposed that in addition to the dipolar relaxation mechanism of Antropov *et al.* there is an incoherent, isotropic mechanism associated with the isotropic hyperfine couplings ($A_{\rm iso}$, $B$, and $B'$) discussed in Sec. III.B.2. It is important to note that the shift contribution of these mechanisms may partially cancel, yet the relaxation contributions may in fact add. The measured anisotropy of 1.56 implies an isotropic rate contribution of 0.49 $s^{-1}$, and the powder-averaged anisotropic dipolar rate is then 0.54 $s^{-1}$. Using this rate and the Korringa relation for dipolar shifts and relaxation [Eq. (27) in Sec. III.D.1], Pennington *et al.* calculated an anisotropic shift tensor of (–97,–97,194) ppm. This tensor was then added to the anisotropic part of the $C_{60}$ shift tensor (77,43,–118) ppm, along with the measured isotropic shift. The resulting powder pattern line shape is compared with the experimental line shape in Fig. 52. The overall width of the theoretical powder pattern is in reasonable agreement with experiment. Note, however, that the experimental data do not contain the sharp features of the calculated pattern. Pennington *et al.* found that by taking the calculated pattern and convoluting it with a square function of width ±50 ppm, a very reason-

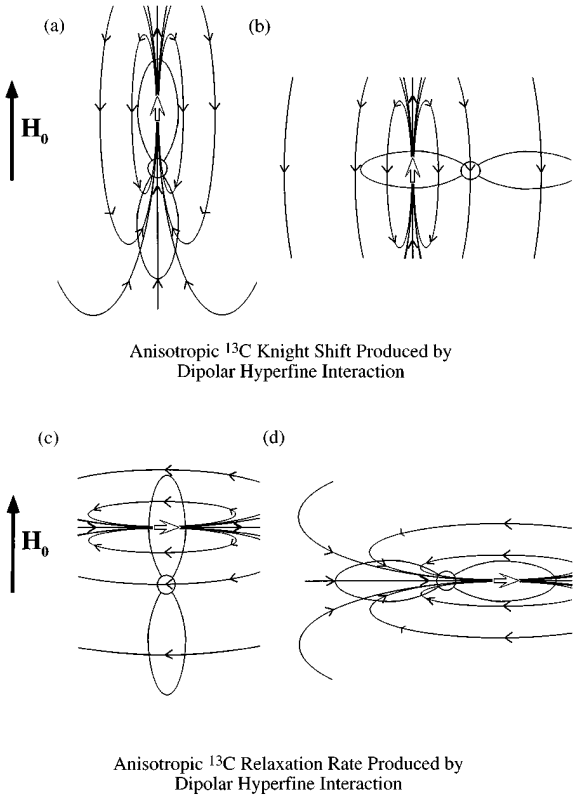


FIG. 50. This figure explains the expected anisotropy in the Knight shift and $T_1$ associated with the nuclear-electron dipole-dipole hyperfine coupling mechanism. Panels (a) and (b) address the Knight shift. In panel (a) we consider a situation in which the applied magnetic field is oriented parallel to the $p_z$ orbital of the carbon atom. The electron magnetic moment on average will have a polarization parallel to the field. Its magnetic dipole moment then produces a field that, at the site of the nucleus, is parallel to the applied field and positive. In panel (b), however, the applied field is perpendicular to the $p_z$ orbital. The electron polarization is again parallel to the applied field; however, now the dipolar field that it produces at the site of the nucleus is opposite the direction of the applied field, resulting in a negative Knight shift, half as large in magnitude as the shift for the parallel case. Panels (c) and (d) address the spin-lattice relaxation mechanism ($1/T_1$) and its anisotropy. Spin-lattice relaxation is sensitive to fluctuations of the electron spin, which produce fluctuation field components transverse to the applied field. In panel (c) is shown a carbon atom with the applied field parallel to the $p_z$ orbital. In order to produce a magnetic field at the site of the nucleus that is perpendicular to the applied field, the electron spin must also point perpendicular. In panel (d), the magnetic field is now perpendicular to the $p_z$ orbital. If the electron spin is oriented transverse to the applied field, then the magnetic field it produces at the site of the nucleus is now twice as big as the field in case (c). This difference results in an anisotropic spin-lattice relaxation, meaning that the relaxation rate depends upon the direction of the applied field with respect to the $p_z$ orbital of the carbon under investigation. Of course, in powder samples, all orientations will occur, and relaxation then has a broad range of exponential rates.

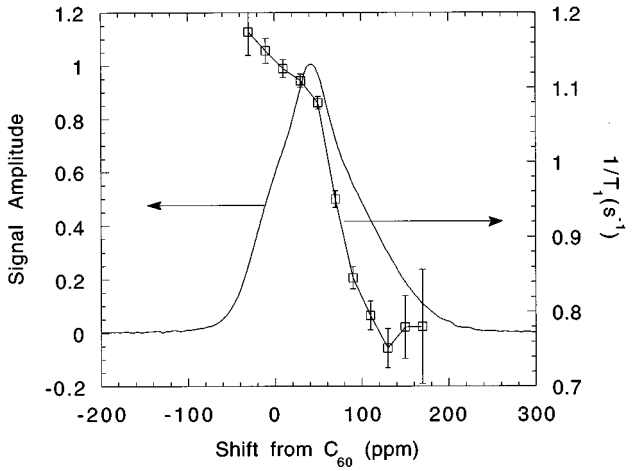


FIG. 51. $^{13}C$ NMR line shape of a powder sample of $Rb_2CsC_{60}$ taken at temperature 80 K in a 9-tesla field (Pennington *et al.*, 1995). Also shown is the spin-lattice relaxation rate $1/T_1$ measured separately at different frequencies within the line shape. Spin-lattice relaxation rates at the low-frequency range are found to be approximately 1.56 times as fast as rates at the high range. This ratio can be compared with the predicted anisotropy of 2.5 to 1 for the electron-nuclear dipolar interaction. Pennington *et al.* conclude that there is an additional isotropic relaxation mechanism. They infer the magnitude of both the isotropic and the anisotropic parts, and compare the magnitude of the anisotropic part with the measured linewidths using a Korringa relation. These results are shown in Fig. 52.

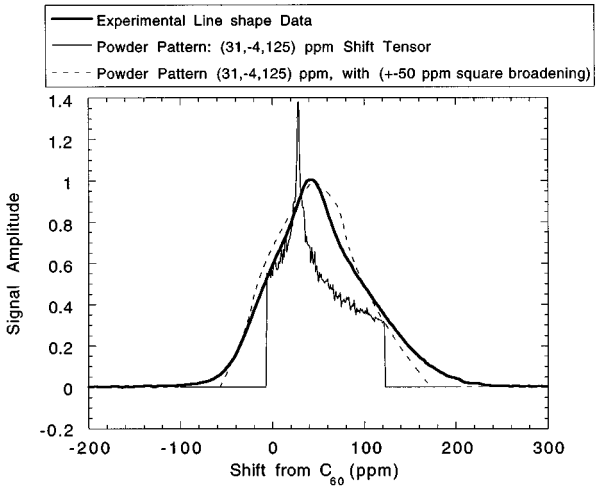


FIG. 52. Experimental and theoretical $^{13}C$ lineshapes. Pennington *et al.* (1995) propose that in addition to the dipolar relaxation mechanism there is an incoherent isotropic mechanism, associated with the isotropic hyperfine couplings. Using the relaxation-rate contribution of the dipolar mechanism only and the appropriate Korringa relation, they calculate an anisotropic Knight-shift tensor of (–97,–97,194) ppm. This tensor is then added to the anisotropic part of the $C_{60}$ shift tensor (77,43,–118) ppm, along with the measured isotropic shift, to obtain a shift tensor (31,–4,125) ppm. The resulting powder pattern line shape is compared with the experimental line shape in this figure. The overall width of the theoretical powder pattern is in reasonable agreement with experiment. Note, however, that the experimental data do not contain the sharp features of the calculated pattern. It is found that by taking the calculated pattern and convoluting it with a square function of width ±50 ppm, a very reasonable match to the experimental data is obtained; this broadened theoretical powder pattern is also shown (dashed line).

able match to the experimental data could be obtained; this broadened pattern is also given in Fig. 52.

It is unlikely that the analysis of Pennington *et al.* is correct in every detail. Nevertheless, their arguments demonstrate two important facts. First, the dipolar hyperfine mechanism of spin-lattice relaxation proposed by Antropov *et al.* does contribute a substantial fraction of the total $^{13}C$ spin-lattice relaxation, though certainly not all of it. Second, the Korringa mechanism predicts a $^{13}C$ powder pattern width in very reasonable agreement with experiment—hence it is not necessary to invoke effects of strong correlation, leading to an enhancement or suppression of spin-lattice relaxation relative to the Knight shift.

#### 5. Summary of implications regarding electronic structure

The search for effects of strong correlations in the NMR data has not been productive. In contrast to photoemission data and to certain theoretical notions (Sec. II.D.1), neither the NMR Knight shift nor spin-lattice relaxation requires effects of strong correlations. This must be regarded as a fairly impressive null result, as the statement covers a wide range of data—comparisons of different nuclei within the unit cell, analysis of the temperature dependence and magnitude of $1/T_1T$, and even the Korringa relationship between spin-lattice relaxation and Knight shift.

### B. Inferences about superconductivity

Within the BCS framework of fullerene superconductivity, the identity of the phonons that predominate in pairing is a key issue. The question may be addressed using the McMillan equation (Sec. II.C.2):

$$k_B T_c = \frac{\hbar \omega_{\rm ph}}{1.2} \exp\left[\frac{-1.04(1+\lambda_{\rm ph})}{\lambda_{\rm ph}-\mu^*(1+0.62\lambda_{\rm ph})}\right] \tag{47}$$

Here $\lambda_{\rm ph}$ is the electron-phonon coupling parameter and is proportional to the electronic density of states at the Fermi energy $\rho(E_F)$. If one can determine $\lambda_{\rm ph}$ or, equivalently, $\rho(E_F)$ for fullerene compounds with different $T_c$'s, then one can extract $\omega_{\rm ph}$, which is assumed to be approximately the same for all.

Normal-state NMR spin-lattice relaxation should be useful, since $1/T_1T$ is also proportional to $\rho^2(E_F)$, and hence $(1/T_1T)^{1/2}=c\lambda_{\rm ph}$, where $c$ is a constant. Normal-state NMR data, then, can be used to extract the phonon frequency dominant in superconductivity.

The complicating factor of the approach given above is that $\lambda_{\rm ph}$ in the McMillan equation actually involves the bare density of states $\rho_0(E_F)$, while in contrast $1/T_1T$ is proportional to the enhanced density of states $\rho_e^2(E_F)$

which governs the static spin susceptibility. In a simple model (Moriya, 1963) these quantities are related as follows:

$$\rho_e = \frac{\rho_0}{1 - I\rho_0}, \tag{48}$$

and the product $I\rho_0$, is known as the "Stoner enhancement parameter." It is important to note a feature of Eq. (48)—that, as $\rho_0$ increases, $\rho_e$ also increases, but the enhancement factor in the denominator makes the variation in $\rho_e$ more dramatic, especially if $I\rho_0$ becomes comparable to one.

NMR quantities such as the Knight shift and $T_1$ are interpreted within the framework of Stoner enhancement (with the effects of a short electron mean free path included) by Shastry and Abrahams (1994). They also find that there are corrections to the relationship $1/T_1T \propto \rho_e^2$ and the Korringa relation $1/T_1T \propto K^2$, both of which we neglect here.

Tycko *et al.* (1992) first exploited these relationships to extract information about the phonon frequency $\omega_{ph}$ assuming no Stoner enhancement. They found the ratio $R$ of $Rb_3C_{60}$ ($T_c$=29 K) spin-lattice relaxation to that of $K_3C_{60}$ ($T_c$=18 K) to be in the range $1.28<R<1.40$. Using reasonable values of $\mu^*$, they found, using the McMillan equation, a phonon frequency of $\omega_{ph} \approx 200$ cm$^{-1}$, a frequency substantially lower than the intramolecular "tangential" modes ($\sim$1400 cm$^{-1}$), and in a range between the "radial" intramolecular modes ($\sim$500 cm$^{-1}$) and the "optical" intermolecular modes. Tycko *et al.* emphasize, however, that the analysis does neglect Stoner enhancement.

Maniwa *et al.* (1994) used a similar analysis with a wider range of alkali intercalants, compounds ranging from $Na_2RbC_{60}$ to $Cs_2RbC_{60}$, so as to vary $T_c$ from 3.5 to 33 K. Figure 53 shows Maniwa *et al.*'s measured $(1/T_1T)^{1/2} = c\lambda_{ph}$ vs $T_c$. Taking a range of reasonable values of $\mu^*$, Maniwa *et al.* fit the experimental data to find best values of $c$ and $\omega_{ph}$. These fits, shown in Fig. 54, yield $\omega_{ph} \approx 500$ cm$^{-1}$, consistent with radial, intramolecular modes. Maniwa *et al.* as well, though, noted that the effective density of states determining $(1/T_1T)^{1/2}$ might in fact be Stoner enhanced. From analysis of the magnitude of $1/T_1T$ they estimated an upper limit on the Stoner parameter $I$. Using this upper limit the inferred $\omega_{ph}$ is $\sim$1700 cm$^{-1}$.

Stenger *et al.* (1995) concluded that Stoner enhancement is indeed necessary to understand the lattice-constant dependence of $1/T_1T$, which was first addressed in Sec. VI.A.2. Moreover, the Stoner enhancement required to understand NMR is consistent with the weak-coupling model developed by Ramirez, Rosseinsky, *et al.* (1992), which explains the observed isotope effect, specific-heat jump, spin susceptibility, and variation of $T_c$ with lattice parameter. Figure 49 in Sec. VI.A.2 shows $1/T_1T$ vs lattice constant $a$ with both temperature and alkali dopant as implicit parameters. Also shown are two fits to the data. The dashed curve, which does not fit the data well, is obtained as follows: $1/T_1T$ is taken to be proportional to the unenhanced squared density of states $\rho_0^2(E_F)$, where the lattice-constant dependence of $\rho_0$ is taken as $\rho_0 \propto \exp(a/d)$ and $d$ is taken as 1.00 Å, a value that lies in the middle range of band theory estimates. For example, this value of $d$ predicts that the ratio of the density of states for $Rb_3C_{60}$ to that of $K_3C_{60}$ is 1.22, while band theory estimates for this ratio, as in Table II of Sec. II.B.2, range from 1.14 to 1.27. The fact that this approach does not match the data suggests that a Stoner enhancement is necessary. As it happens, this conclusion turns out to be required if one

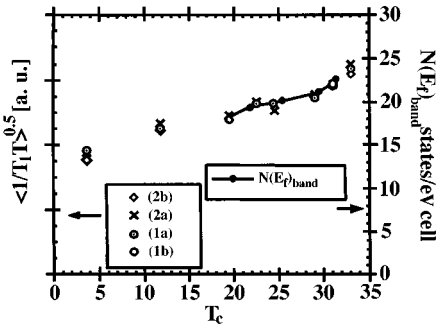


FIG. 53. $(1/T_1T)^{1/2}$ vs $T_c$ for alkali fulleride superconductors with a range of alkali intercalant sizes, densities of states, and $T_c$'s (Maniwa *et al.*, 1994). The various symbols on the graph represent different assumptions about hyperfine couplings, which we neglect in our discussion. Figure 54 and its caption describes the conclusions drawn from this work.

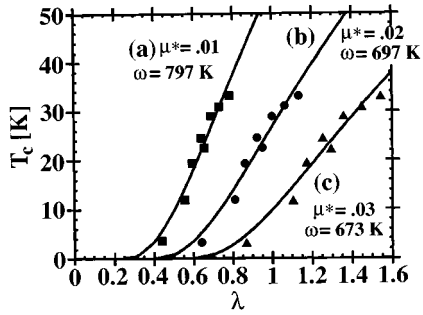


FIG. 54. Best values of $c$, $\lambda_{ph}$, and $\omega_{ph}$. Maniwa *et al.* (1994) have measured the room-temperature spin-lattice relaxation rate $1/T_1T$ for alkali-doped $C_{60}$ compounds ranging from those with the smallest dopant and smallest density of states, such as $Na_2RbC_{60}$, to those with large dopants and the highest density of states, such as $Cs_2RbC_{60}$. For that range, $T_c$ varies from 3.5 to 33 K. The previous figure, Fig. 53, shows $(1/T_1T)^{1/2}$ vs. $T_c$. $1/T_1T$, however, is expected to be proportional to the electron-phonon coupling parameter $\lambda_{ph}$; $(1/T_1T)^{1/2} = c\lambda_{ph}$. In this figure Maniwa *et al.* assume a reasonable range of values of $\mu^*$, and then fit the experimental data to find best values of $c$, $\lambda_{ph}$, and $\omega_{ph}$. The fits yield $\omega_{ph} \approx 500$ cm$^{-1}$ and $\lambda_{ph}$ ranging from 0.4 to 1.4, depending on the material and the assumed value of $\mu^*$. Maniwa *et al.* note, though, that the effective density of states determining $(1/T_1T)^{1/2}$ may in fact be Stoner enhanced and thus not so simply related to $\lambda_{ph}$. Analysis of the magnitude of $1/T_1T$ gives an upper limit on the Stoner enhancement. Taking that upper limit results in a substantially higher frequency of $\omega_{ph} \sim 1700$ cm$^{-1}$, which is the weak-coupling limit.

wishes to postulate a weak-coupling scenario involving the high-frequency 1400 $cm^{-1}$ tangential intramolecular phonons as the pairing agent.

The solid curve in Fig. 49 gives const $\times\rho_e^2$ vs $a$, where the parameters $d$ and the Stoner parameter I used to calculate $\rho_e^2$ are the same values used by Ramirez, Rosseinsky, *et al.* (1992) to understand simultaneously their spin susceptibility, isotope effect, and specific-heat jump data on both $K_3C_{60}$ and $Rb_3C_{60}$ near the weak-coupling limit, with $\omega_{ph}\approx$1400 $cm^{-1}$. For $K_3C_{60}$, $I\rho_0$ is found to be $\sim$0.5, and thus $\rho_e$ is found to be enhanced by a factor of approximately 2. As noted by Maniwa *et al.* (1994), such an enhancement is not unusual and is similar to the enhancements for the simplest metals (Narath and Weaver, 1968). The solid curve provides a quite reasonable fit to the lattice-constant dependence of $1/T_1T$. This result demonstrates that the lattice-constant (or, equivalently, alkali dopant) dependence of the NMR $1/T_1T$ in the normal state is consistent with weak coupling, and indeed may require it.

### C. Summary of inferences regarding normal-state NMR data

Normal-state NMR data on alkali fullerides has been a very difficult subject of investigation, and in fact most of the conclusions drawn from the earliest data have since been modified by a consensus of investigators. Two factors have led to the difficulty in interpretation: First, there are several different sources of $^{13}C$ hyperfine couplings whose relative contributions have not been easy to predict. Second, the effects of electron-electron interactions obscure the relationship between $1/T_1$ and the bare density of states, and thus interpreting NMR and $T_c$'s using the McMillan equation has been confusing. It appears that both of these difficulties have now been recognized, if not completely understood. Currently there are no NMR data that require unusual strong-correlation effects for the normal state. Regarding the superconducting state, the normal-state NMR data give compelling evidence for a lower bound on dominant phonon frequencies of approximately 500 $cm^{-1}$, which assuredly fingers some kind of intramolecular mode. The data in fact seem more consistent with the tangential intramolecular phonons near 1400 $cm^{-1}$. This conclusion also agrees well with superconducting-state NMR data.

## VII. CONCLUDING REMARKS

The puzzle of superconductivity in the fullerenes has not yet been fully assembled. Nonetheless it is surprising the extent to which experimental results, including prominently those from NMR, which initially appeared very unusual, as did those of the high-$T_c$ cuprate superconductors, have now yielded to prosaic explanations, in sharp contrast to high $T_c$. Early anomalous features included the "absent-without-leave" Hebel-Slichter peak, but in fact this fugitive was only hiding nearby under a too-large magnetic field. The intrinsic superconducting-state $T_1$ behavior is not too far out of the ordinary. The superconducting-state spin susceptibility as probed by the Knight shift is almost too ordinary. Although these pieces of data have not been completely reconciled with a detailed theory, most likely they could be.

The normal-state NMR data also once seemed very unusual, perhaps implying strong-correlation effects, but they now seem to be much better understood. Initial expectations that the doped fullerenes might have effects of strong correlation may not be disproven, but they are not required to understand current data. As we show in Sec. III, however, the $^{13}C$ and alkali-metal Knight shifts and hyperfine couplings are perhaps one to two orders of magnitude smaller than predicted and in some cases even have the wrong sign. These anomalies may be clues to important required modifications of the Fermi-surface wave functions. Most, if not all, of the unusual temperature dependence of $T_1$ can be explained in terms of the known thermal expansion of the lattice and a degree of Stoner enhancement similar to the alkali metals. The $T_1$'s of $^{13}C$ and the alkali nuclei have the same temperature dependence, and the Korringa relation between $T_1$ and the Knight shift appears to hold. The variation of $1/T_1T$ for samples with different alkali dopant can be interpreted within the McMillan equation; the crudest model indicates that the phonon mode dominant in superconductivity is assuredly intramolecular, and a more detailed inspection suggests that it is a higher-frequency ($\sim$1400 $cm^{-1}$), tangential, intramolecular mode, a conclusion quite consistent with superconducting-state data.

The least well understood topic that we have encountered is the structure. The usual picture of the structure of doped materials, described in Sec. II.A, calls for "merohedral" disorder. Each $C_{60}$ molecule is thought to have available two discrete orientational possibilities, which are populated randomly and in a ratio of 1 to 1. Two-dimensional NMR spectroscopy indicates that a more continuous range of orientations occurs. $^{87}Rb$ NMR displays an unexpected extra peak, reflecting some unknown distortion, which Walstedt speculates may be an orientational traveling or standing wave, analogous to a charge-density wave. At appropriate temperatures $^{13}CT_1$ measurements suggest a single "easy axis" of rotation for individual $C_{60}$ molecules, which is also inconsistent with the conventional picture of the structure. It is not clear at present to what extent these structural peculiarities are related to superconductivity.

NMR investigations of orientational dynamics in undoped $C_{60}$ reveal separate "ratchet" and "rotor" phases at moderate and high temperatures, respectively. The transition does not appear in NMR line-shape measurements, since the line is motionally narrowed in both phases. Thus it was initially detected by x-ray diffraction. The "ratchet" phase, however, was initially thought to be a frozen state with no reorientations. NMR $T_1$ measurements, however, specified that in the "ratchet" phase the molecules make discrete "jumps" on time scales fast compared to the NMR linewidth, but

in between these jumps the molecules are static on the much faster x-ray time scales. This beautiful work emphasizes the complementarity of NMR with other techniques.

The NMR technique has once again proven to be a valuable weapon for the analytical arsenal. It has provided a picture of a relatively simple metal (though made up of a lattice of weakly overlapping, sixty-atom, beautifully symmetric molecules) with a combination of electronic structural and electron-phonon parameters that lead to superconductivity at temperatures among the highest for the BCS mechanism. The objections to this picture, discussed in Sec. II.D, though mostly not derived from experiment, are nevertheless formidable. Notably they include the very large phonon frequencies involved relative to the electron bandwidths. It remains to be seen whether these objections can be resolved theoretically in a way that is consistent with the accumulating weight of experiment.

## ACKNOWLEDGMENTS

We have benefitted greatly from discussions with numerous colleagues, including G. Clark, D. L. Cox, T. R. Lemberger, D. E. MacLaughlin, C. P. Slichter, R. Tycko, and R. E. Walstedt. We especially acknowledge R. P. Ziebarth, who has unfailingly provided us with generous daily doses of insight, aid, and encouragement, and whose research group, including especially but not exclusively, D. R. Buffinger and S. M. Lee, has collaborated with us on wide-ranging investigations of fullerene compounds. We have also benefitted in particular from both generous experimental and theoretical assistance from C. H. Recchia. This work was supported by a National Young Investigator award from the National Science Foundation, Division of Materials Research, Contract No. NSF DMR9357600.

## REFERENCES

Abragam, A., 1961, *The Principles of Nuclear Magnetism* (Clarendon, Oxford).

Akis, R., and J. P. Carbotte, 1991a, "Damping Effects on NMR in Superconductors," Solid State Commun. **78**, 393.

Akis, R., C. Jiang, and J. P. Carbotte, 1991b, "Quasiparticle Damping, Anisotropy, and Fermi Liquid Corrections to NMR in Superconductors," Physica C **176**, 485.

Akitt, J. W., 1987, "The Alkali and Alkaline Earth Metals," in *Multinuclear NMR*, edited by Joan Mason (Plenum, New York), p. 189.

Allen, K. M., W. I. F. David, J. M. Fox, R. M. Ibberson, and M. J. Rosseinsky, 1995, "Molecular Structure of the Fulleride Anions in Superconducting $K_3C_{60}$ and Insulating $K_6C_{60}$ Determined by Powder Neutron Diffraction," Chem. Mater. **7**, 764.

Allen, P. B., and R. C. Dynes, 1975, "Transition Temperature of Strong-Coupled Superconductors Reanalyzed," Phys. Rev. B **12**, 905.

Allen, Phillip B., and Dierk Rainer, 1991, "Phonon Suppression of Coherence Peak in Nuclear Spin Relaxation Rate of Superconductors," Nature **349**, 396.

Antropov, V. P., I. I. Mazin, O. K. Andersen, A. I. Liechtenstein, and O. Jepsen, 1993, "Dominance of the Spin-Dipolar NMR Relaxation Mechanism in Fullerene Superconductors," Phys. Rev. B **47**, 12 373.

Asayama, K., Y. Kitaoka, and Y. Kohori, 1988, "NMR Study of Heavy Fermion Materials," J. Magn. Magn. Mater. **76**,**77**, 449.

Ashcroft, N. W., and N. D. Mermin, 1976, *Solid State Physics* (Holt, Rinehart, and Winston, New York).

Axe, J. D., S. C. Moss, and D. A. Neumann, 1994 "Structure and Dynamics of Crystalline $C_{60}$," in *Solid State Properties of Fullerenes and Fullerene-Based Materials*, Solid State Physics Vol. 48, edited by H. Ehrenreich and Frans Spaepen (Academic, Boston), pp. 149–224.

Bardeen, J., L. N. Cooper, and J. R. Schrieffer, 1957, "Theory of Superconductivity," Phys. Rev. **108**, 1175.

Barrett, S. E., D. J. Durand, C. H. Pennington, C. P. Slichter, T. A. Friedmann, J. P. Rice, and D. M. Ginsberg, 1990, "$^{63}$Cu Knight Shifts in the Superconducting State of $YBa_2Cu_3O_{7-\delta}$ ($T_c$=90 K)," Phys. Rev. B **41**, 6283.

Barrett, S. E., and R. Tycko, 1992, "Molecular Orientational Dynamics in $K_3C_{60}$ Probed by Two-Dimensional Nuclear Magnetic Resonance," Phys. Rev. Lett. **69**, 3754.

Beckmann, A., K. D. Boklen, and D. Elke, 1974, "Precision Measurements of the Nuclear Magnetic Dipole Moments of $^6$Li, $^7$Li, $^{23}$Na, $^{39}$K, and $^{41}$K," Z. Phys. **270**, 173.

Benning, P. J., F. Stepniak, D. M. Poirier, J. L. Martins, J. H. Weaver, L. P. F. Chibante, and R. E. Smalley, 1993, "Electronic Properties of $K$-doped $C_{60}$ (111): Photoemission and Electron Correlation," Phys. Rev. B **47**, 13 843.

Bernier, P., F. Rachdi, M. Ribet, J. Reichenbach, L. Firlej, J. M. Lambert, A. Zahab, Z. Belahmer, and R. Aznar, 1993, "NMR Studies of Fullerene $C_{60}$-Based Compounds," in *Electronic Properties of Fullerenes*, edited by H. Kuzmany, J. Fink, M. Mehring, and S. Roth (Springer, Berlin/Heidelberg), pp. 348–353.

Bloembergen, N., and P. P. Sorokin, 1958, "Nuclear Magnetic Resonance in the Cesium Halides," Phys. Rev. **110**, 865.

Breitmaier, Eberhard, and Gerhard Bauer, 1984, *$^{13}$C NMR Spectroscopy: A Working Manual With Exercises* (Harwood Academic, London).

Bulut, N., and D. J. Scalapino, 1992, "Analysis of NMR Data in the Superconducting State of $YBa_2Cu_3O_7$," Phys. Rev. Lett. **68**, 706.

Carbotte, J. P., 1990, "Properties of Boson-Exchange Superconductors," Rev. Mod. Phys. **62**, 1027.

Carver, G. P., 1970, "Nuclear Magnetic Resonance in Cesium-Graphite Intercalation Compounds," Phys. Rev. B **2**, 2284.

Chakravarty, Sudip, Martin P. Gelfand, and Steven Kivelson, 1991, "Electronic Correlation Effects and Superconductivity in Doped Fullerenes," Science **254**, 970.

Chakravarty, Sudip, Sergei Khlebnikov, and Steven Kivelson, 1992, "Comment on 'Electron-Phonon Coupling and Superconductivity in Alkali-Intercalated $C_{60}$ Solid'," Phys. Rev. Lett. **69**, 212.

Clem, John R., 1966, "Effects of Energy Gap Anisotropy in Pure Superconductors," Ann. Physics (N.Y.) **40**, 268.

Clementi, E., and D. L. Raimondi, 1963, "Atomic Screening Constants and SCF Functions," J. Chem. Phys. **38**, 2686.

Cooper, Leon, 1973, "Microscopic Quantum Interference in the Theory of Superconductivity," Phys. Today **26**(8), 31.

Cornad, J., H. Estrade, P. Lauginie, H. Fuzellier, G. Furdin, R. Vasse, 1980, "Graphite Lamellar Compounds $^{13}C$ NMR Studies," Physica B **99**, 521.

Cyrot, Michel, 1966, "Relaxation Spin-Reseau dans les Alliages Suprconducteurs Sales en Champ Fort," J. Phys. (Paris) **27**, 283.

de Gennes, P. G., 1989, *Superconductivity of Metals and Alloys* (Addison Wesley, Reading, MA).

Degiorgi, L., P. Wachter, G. Gruner, S.-M. Huang, J. Wiley, and R. B. Kaner, 1992, "Optical Response of the Superconducting State of $K_3C_{60}$ and $Rb_3C_{60}$," Phys. Rev. Lett. **69**, 2987.

Deverell, C., 1968, "Nuclear Magnetic Resonance Studies of Electrolyte Solutions," in *Progress in NMR Spectroscopy, Vol. 4*, edited by J. W. Emsley, J. Feeney, and L. H. Sutcliffe (Pergamon, Oxford), p. 235.

DiSalvo, F. J., S. A. Safran, R. C. Haddon, J. V. Waszczak, J. E. Fischer, 1979, "Large Anisotropy and Stage Dependence of the Magnetic Susceptibility of Alkali-Graphite Intercalation Compounds," Phys. Rev. B **20**, 4883.

Dresselhaus, M. S., and G. Dresselhaus, 1981, "Intercalation Compounds of Graphite," Adv. Phys. **30**, 139.

Dresselhaus, M. S., G. Dresselhaus, and R. Saito, 1994, "Superconducting Properties of Fullerenes," in *Physical Properties of High Temperature Superconductors, Vol. IV*, edited by D. M. Ginsberg (World Scientific, Singapore), pp. 471–564.

Ernst, R. R., G. Bodenhausen, and A. Wokaun, 1987, *Principles of Nuclear Magnetic Resonance in One and Two Dimensions* (Oxford, New York).

Erwin, S. E., and W. E. Pickett, 1992, "Theoretical Fermi Surface Properties and Superconducting Parameters for $K_3C_{60}$," Science **254**, 842.

Fessenden, Richard W., 1967, "Electron Spin Resonance Spectra of Some Isotopically Substituted Hydrocarbon Radicals," J. Phys. Chem. **71**, 74.

Fibich, M., 1965, "Phonon Effects on Nuclear Spin Relaxation in Superconductors," Phys. Rev. Lett. **14**, 561.

Fine, H. L., M. Lipsicas, and M. Strongin, 1969, "Vanishing Knight Shift in Superconducting Aluminum Films," Phys. Lett. A **29**, 366.

Fleming, R. M., A. P. Ramirez, M. J. Rosseinsky, D. W. Murphy, R. C. Haddon, S. M. Zahurak, and A. V. Makhija, 1991, "Relation of Structure and Superconducting Transition Temperatures in $A_3C_{60}$," Nature **352**, 787.

Friedberg, R., T. D. Lee, and H. C. Ren, 1992, "Parity doublets and the pairing mechanism in $C_{60}$," Phys. Rev. B **46**, 14 150.

Geilikman, B. T., and V. Z. Kresin, 1972, "About the Connection Between the Transition Temperature and the Energy Gap for Superconductors with Strong Coupling," Phys. Lett. A **40**, 123.

Gelfand, M. P., 1993

Gelfand, M. P., 1994, "Alkali Fullerides: Theoretical Perspectives, Progress, and Problems," Superconductivity Review **1**, 103.

Gelfand, Martin P., and Jian Ping Lu, 1992, "Orientational Disorder and Electronic States in $C_{60}$ and $A_3C_{60}$ where $A$ is an Alkali Metal," Phys. Rev. Lett. **68**, 1050.

Goldberg, I. B., and M. Weger, 1968, "Spin Lattice Relaxation Processes in Type II Superconductors," J. Phys. Soc. Jpn. **24**, 1279.

Haddon, R. C., 1988, "$\pi$-Electrons in Three Dimensions," Acc. Chem. Res. **21**, 243.

Haddon, R. C., 1992, "Electronic Structure, Conductivity, and Superconductivity of Alkali Metal Doped $C_{60}$," Acc. Chem. Res. **25**, 127.

Haddon, R. C., L. E. Brus, and Krishnan Raghavachari, 1986, "Electronic Structure and Bonding in Icosahedral $C_{60}$," Chem. Phys. Lett. **125**, 459.

Haddon, R. C., L. F. Schneemeyer, J. V. Waszczak, S. H. Glarum, R. Tycko, G. Dabbagh, A. R. Kortan, A. J. Muller, A. M. Mujsce, M. J. Rosseinsky, S. M. Zahurak, A. V. Makhija, F. A. Thiel, K. Raghavachari, E. Cockayne, and V. Elser, 1991, "Experimental and Theoretical Determination of the Magnetic Susceptibility of $C_{60}$ and $C_{70}$," Nature **350**, 46.

Hanye, G. S., Clark W. White, William M. Hughes, and H. G. Robinson, 1968, "Determination of $g_I/g_J$ of $^{133}Cs$ and $g_J(^{133}Cs)/g_J(^{87}Rb)$ for Free Cs and Rb Atoms," Bull. Am. Phys. Soc. **13**, 20.

Hawkins, Joel M., Stefan Loren, Axel Meyer, and Rudi Nunlist, 1991, "2D Nuclear Magnetic Resonance Analysis of Osmylated $C_{60}$," J. Am. Chem. Soc. **113**, 7770.

Hawkins, Joel M., Axel Meyer, Timothy Lewis, Stefan Loren, and Frederick J. Hollander, 1991, "Crystal Structure of Osmylated $C_{60}$: Confirmation of the Soccer Ball Framework," Science **252**, 312.

Hebard, Arthur F., 1992, "Superconductivity in Doped Fullerenes," Phys. Today **45** (11), 26.

Hebel, L. C., and C. P. Slichter, 1959, "Nuclear Spin Relaxation in Normal and Superconducting Aluminum," Phys. Rev. **113**, 1504.

Heiney, Paul A., John E. Fischer, Andrew R. McGhie, William J. Romanow, Arnold M. Denenstein, John P. McCauley Jr., and Amos B. Smith III, 1991, "Orientational Ordering Transition in Solid $C_{60}$," Phys. Rev. Lett. **66**, 2911.

Holczer, K., 1993, "$^{13}C$ Nuclear Relaxation in the Normal State of the $K_3C_{60}$ Superconductor," in *Electronic Properties of Fullerenes*, edited by H. Kuzmany, J. Fink, M. Mehring, and S. Roth (Springer, Berlin/Heidelberg), pp. 323–329.

Holczer, K., O. Klein, H. Alloul, Y. Yoshinar, F. Hippert, S.-M. Huang, R. B. Kaner, and R. L. Whetten, 1993, "Non-Korringa $^{13}C$ Nuclear Relaxation in the Normal State of the $K_3C_{60}$ Superconductor," Europhys. Lett. **23**, 63.

Huang, M.-Z., Y.-N. Xu, and W. Y. Ching, 1992, "Electronic Structures of $K_3C_{60}$, $RbK_2C_{60}$, $Rb_2KC_{60}$, $Rb_3C_{60}$, $Rb_2CsC_{60}$, and $Cs_3C_{60}$ Crystals," Phys. Rev. B **46**, 6572.

Ikenberry, Dennis, and T. P. Das, 1965a, "Nuclear Magnetic Shielding in Alkali Halide Crystals," Phys. Rev. **138**, 822A.

Ikenberry, Dennis, and T. P. Das, 1965b, "Nuclear Magnetic Shielding of Alkali Ions in Crystals and Dilute Aqueous Solutions," J. Chem. Phys. **43**, 2199.

Ikenberry, Dennis, and T. P. Das, 1966, "Chemical Shift Calculations in Alkali Halides," J. Chem. Phys. **45**, 1361.

Imai, T., T. Shimizu, H. Yasuoka, Y. Ueda, and K. Kosuge, 1988, "Anomalous Temperature Dependence of Cu Nuclear Spin-Lattice Relaxation in $YBa_2Cu_3O_{6.91}$," J. Phys. Soc. Jpn. **57**, 2280.

Ishiguro, T., and K. Yamaji, 1989, *Organic Superconductors* (Springer, New York).

Jannossy, A., O. Chauvet, S. Pekker, J. R. Cooper, and L. Forro, 1993, "Conduction Electron Spin Resonance in $Rb_3C_{60}$," Phys. Rev. Lett. **71**, 1091.

Johnson, Robert D., Donald S. Bethune, and Constantino S. Yannoni, 1992, "Fullerene Structure and Dynamics: A Magnetic Resonance Potpourri," Acc. Chem. Res. **25**, 169.

Johnson, Robert D., Constantino S. Yannoni, Harry C. Dorn, Jesse R. Salem, and Donald S. Bethune, 1992, "$C_{60}$ Rotation in the Solid State: Dynamics of a Faceted Spherical Top," Science **255**, 1235.

Kälber, T., G. Zimmer, and M. Mehring, 1995a, "Phase separation and phase transitions in $KC_{60}$: A $^{13}C$ NMR study," Phys. Rev. B **51**, 16 471.

Kälber, T., G. Zimmer, and M. Mehring, 1995b, "Evidence for $sp^3$ Carbons in $Rb_1C_{60}$ from $^{13}C$ MAS NMR," Z. Phys. B **97**, 1.

Karplus, Martin, 1959, "Interpretation of Electron Spin Resonance Spectrum of the Methyl Radical," J. Chem. Phys. **30**, 15.

Karplus, Martin, and George K. Fraenkel, 1961, "Theoretical Interpretation of Carbon-13 Hyperfine Interactions in Electron Spin Resonance Spectra," J. Chem. Phys. **35**, 1312.

Kerkoud, R., P. Auban-Senzier, D. Jérome, J. M. Lambert, A. Zahab, and P. Bernier, 1994, "$^{13}C$ Knight Shift of the Doped Fullerene $K_3C_{60}$," Europhys. Lett. **25**, 379.

Kiefl, R. F., W. A. MacFarlane, K. H. Chow, S. Dunsiger, T. L. Duty, T. M. S. Johnston, J. W. Schneider, J. Sonier, L. Brard, R. M. Strongin, J. E. Fischer, and A. B. Smith III, 1993, "Coherence Peak and Superconducting Energy Gap in $Rb_3C_{60}$ Observed by Muon Spin Relaxation," Phys. Rev. Lett. **70**, 3987.

Knight, W. D., 1956, "Nuclear Magnetic Resonance in Metals," in *Solid State Physics*, Vol. II, edited by F. Seitz and D. Turnbull (Academic, New York), p. 93.

Kondo, J., and J. Yamashita, 1959, "Nuclear Quadrupolar Relaxation in Ionic Crystals," J. Phys. Chem. Solids **10**, 245.

Korringa, J., 1950, "Nuclear Magnetic Relaxation and Resonance Line Shift in Metals," Physica **16**, 601.

Kroto, H. W., J. R. Heath, S. C. O'Brien, R. F. Curl, and R. E. Smalley, 1985, "$C_{60}$: Buckminsterfullerene," Nature **318**, 162.

Lammert, P. E., D. S. Rokshar, S. Chakravarty, S. Kivelson, and M. I. Salkola, 1995, "Metallic Screening and Correlation Effects in Superconducting Fullerenes," Phys. Rev. Lett. **74**, 996.

Landau, L. D., and E. M. Lifshitz, 1977, *Quantum Mechanics (Non Relativistic Theory)*, (Pergamon, Oxford), p. 251.

Lieber, C. M., and C.-C. Chen, 1994, "Preparation of Fullerenes and Fullerene Based Materials," in *Solid State Properties of Fullerenes and Fullerene-Based Materials*, *Solid State Physics Vol. 48*, edited by H. Ehrenreich and Frans Spaepen (Academic, Boston), pp. 109–149.

Lieber, C. M., and Z. Zhang, 1994, "Physical Properties of Metal Doped Fullerene Superconductors," in *Solid State Properties of Fullerenes and Fullerene-Based Materials*, *Solid State Physics Vol. 48*, edited by H. Ehrenreich and Frans Spaepen (Academic, Boston), pp. 349–384.

Lindman, Bjorn, and Sture Forsen, 1978, "The Alkali Metals," in *NMR and the Periodic Table*, edited by Robin K. Harris and Brian E. Mann (Academic, New York), pp. 129–139.

Lof, R. W., M. A. van Veenendaal, B. Koopmans, H. T. Jonkman, and G. A. Sawatzky, 1992, "Band Gap, Excitons, and Coulomb Interaction in Solid $C_{60}$," Phys. Rev. Lett. **68**, 3924.

MacLaughlin, D. E., 1976, "Magnetic Resonance in the Superconducting State," in *Solid State Physics Vol. ?*, edited by H. Ehrenreich, F. Seitz, and D. Turnbull (Academic, New York), pp. 1–69.

Mahan, Bruce H., 1975, *University Chemistry* (Addison-Wesley, Reading, MA), third ed.

Maniwa, Y., K. Mizoguchi, K. Kume, K. Tanigaki, T. W. Ebbeson, S. Saito, J. Mizuki, J. S. Tsai, and Y. Kubo, 1992, "$^{133}Cs$ NMR in $C_{60}$ Superconductors: $Cs_xRb_{3-x}C_{60}$ ($x$=1,2)," Solid State Commun. **82**, 783.

Maniwa, Y., T. Saito, A. Ohi, K. Mizoguchi, K. Kume, K. Kikuchi, I. Ikemoto, S. Suzuki, Y. Achiba, M. Kosaka, K. Tanigaki, and T. Ebbeson, 1994, "Electronic States and Superconductivity in Alkali Intercalated Fullerides: $^{13}C$ NMR Study in $Na_2RbC_{60}$, $Na_2CsC_{60}$, $K_3C_{60}$, $K_2RbC_{60}$, $K_2CsC_{60}$, $KRbCsC_{60}$, $Rb_2CsC_{60}$, and $RbCs_2C_{60}$," J. Phys Soc. Jpn. **63**, 1139.

Martindale, J. A., S. E. Barrett, K. E. O'Hara, S. M. DeSoto, C. P. Slichter, T. A. Friedmann, and D. M. Ginsberg, 1992, "Anisotropy and Magnetic Field Dependence of the Planar Copper NMR Spin-Lattice Relaxation Rate in the Superconducting State of $YBa_2Cu_3O_7$," Phys. Rev. Lett. **68**, 702.

Martindale, J. A., S. E. Barrett, K. E. O'Hara, C. P. Slichter, W. C. Lee, and D. M. Ginsberg, 1993, "Magnetic Field Dependence of Planar Copper and Oxygen Spin-Lattice Relaxation Rates in the Superconducting State of $YBa_2Cu_3O_7$," Phys. Rev. B **47**, 9155.

Martins, Jose Luis, and N. Troullier, 1992, "Structure and Electronic Properties of $K_nC_{60}$," Phys. Rev. B **46**, 1766.

Masuda, Y., and N. Okubo, 1969, "Nuclear Spin-Lattice Relaxation in the Superconducting Mixed State," J. Phys. Soc. Jpn. **26**, 309.

Masuda, Y., and A. G. Redfield, 1962, "Nuclear Spin-Lattice Relaxation in Superconducting Aluminum," Phys. Rev. **125**, 159.

Mazin, I. I., G. V. Dolgov, A. Golubov, S. V. Shulga, 1993, "Strong-Coupling Effects in Alkali-Metal-Doped $C_{60}$," Phys. Rev. B **47**, 538.

McMillan, W. L., 1968, "Transition Temperature of Strong-Coupled Superconductors," Phys. Rev. **167**, 331.

McMillan, W. L., and J. M. Rowell, 1969, "Tunneling and Strong-Coupling Superconductivity," in Superconductivity, Vol. 1, edited by R. D. Parks (Marcel Dekker, New York), pp. 561–613.

Mehring, Michael, 1983, High Resolution NMR in Solids, 2nd ed. (Springer, Berlin).

Mehring, Michael, 1993, "Is the $^{13}C$ Nuclear Spin-Lattice Relaxation in $A_3C_{60}$ ($A$=Rb, K) Unconventional?," in *Electronic Properties of Fullerenes*, edited by H. Kuzmany, J. Fink, M. Mehring, and S. Roth (Springer, Berlin/Heidelberg), pp. 330–333.

Mehring, M., F. Rachdi, and G. Zimmer, 1994, "Analysis of the $^{13}C$ Knight shift and spin-lattice relaxation in $A_3C_{60}$ ($A$ =Rb, or K)," Philos. Mag. B **70**, 787.

Mila, F., and T. M. Rice, 1989, "Analysis of Magnetic Resonance Experiments in $YBa_2Cu_3O_7$," Physica C **157**, 561.

Millis, A. J., Hartmut Monien, and David Pines, 1990, "Phenomenological Model of Nuclear Relaxation in the Normal State of $YBa_2Cu_3O_7$," Phys. Rev. B **42**, 167.

Mitrovic, B., and W. Pickett, 1987, "Effect of the Electron-Phonon Interaction on the Spin Susceptibility in A15 Compounds," Phys. Rev. B **35**, 3415.

Mizutani, U., M. Suganuma, and T. Kondow, 1981, "The Electronic Structure of Donor- and Acceptor-Type Intercalation Compounds by Means of Low Temperature Specific Heats and $^{13}C$ Nuclear Magnetic Resonance," in *Physics of Intercalation Compounds*, edited by L. Pietronero and E. Tosatti (Springer, New York), pp. 280–286,

Monthoux, P., A. V. Balatsky, and D. Pines, 1991, "Toward a Theory of High-Temperature Superconductivity in the Antiferromagnetically Correlated Cuprate Oxides," Phys. Rev. Lett. **67**, 3448.

Morel, P., and P. W. Anderson, 1962, "Calculation of the Superconducting State Parameters with Retarded Electron-Phonon Interaction," Phys. Rev. **125**, 1263.

Moriya, T., 1956a, "Nuclear Magnetic Relaxation in Antiferromagnetics," Prog. Theor. Phys. **16**, 23.

Moriya, T., 1956b, "Nuclear Magnetic Relaxation in Antiferromagnetics II," Prog. Theor. Phys. **16**, 641.

Moriya, T., 1963, "The Effect of Electron-Electron Interaction on the Nuclear Spin Relaxation in Metals," J. Phys. Soc. Jpn. **18**, 516.

Moriya, T., 1977, "Recent Developments in the Theory of Spin Fluctuations in Itinerant Electron Magnets," Physica B **86-88**, 356.

Morrison, Robert T., and Robert N. Boyd, 1973, *Organic Chemistry* (Allyn and Bacon, Boston).

Morse, R. W., H. V. Bohm, 1957, "Superconducting Energy Gap from Ultrasonic Attenuation Measurements," Phys. Rev. **108**, 1094.

Murphy, D. W., M. J. Rosseinsky, R. M. Flemming, R. Tycko, A. P. Ramirez, R. C. Haddon, T. Siegrist, G. Dabbagh, J. C. Tully, and R. E. Walstedt, 1992, "Synthesis and Characterization of Alkali Metal Fullerides: $A_3C_{60}$," J. Phys. Chem. Solids **53**, 1321.

Nakamura, Y. O., Y. Yokoya, N. Matsuda, and Y. Shiina, 1993, "Important Role of Intermolecular Vibrational Modes in the Superconductivity in Alkali Metal Doped Fullerenes," Solid State Commun. **86**, 627.

Narath, Albert, and H. T. Weaver, 1968, "Effects of Electron-Electron Interactions on Nuclear Spin Lattice Relaxation Rates and Knight Shifts in Alkali and Noble Metals," Phys. Rev. **175**, 373.

Noer, R. J., and W. D. Knight, 1964, "Nuclear Magnetic Resonance and Relaxation in Superconducting Vanadium," Rev. Mod. Phys. **36**, 177.

Novikov, D. L., V. A. Gubanov, and A. J. Freeman, 1992, "Electronic Structure, Electron-Phonon Interaction, and Superconductivity in $K_3C_{60}$, $Rb_3C_{60}$, and $Cs_3C_{60}$," Physica C **191**, 399.

Oshiyama, A., S. Saito, N. Hamada, and Y. Miyamoto, 1992, "Electronic Structure of $C_{60}$ Fullerides and Related Materials," J. Phys. Chem. Solids **53**, 1457.

Pasquarello, Alfredo, Michael Schluter, and R. C. Haddon, 1992, "Ring Currents in Icosahedral $C_{60}$," Science **257**, 1660.

Pennington, C. H., and C. P. Slichter, 1990, "Nuclear Resonance Studies of $YBa_2Cu_3O_{7-\delta}$," in *Physical Properties of High Temperature Superconductors, Vol. II*, edited by D. M. Ginsberg (World Scientific, Singapore), pp. 269–367.

Pennington, C. H., V. A. Stenger, C. Hahm, K. Gorny, C. H. Recchia, D. R. Buffinger, and R. P. Ziebarth, 1995, "$^{13}$NMR hyperfine couplings, $T_1$ anisotropy, and Korringa relations in $Rb_2CsC_{60}$: Search for effects of strong correlation," Phys. Rev. B **53**, R2967.

Pickett, W., 1982, "Generalization of the Theory of the Electron-Phonon Interaction: Thermodynamic Formulation of the Superconducting- and Normal-State Properties," Phys. Rev. B **26**, 1186.

Pickett, Warren E., 1994, "Electrons and Phonons in $C_{60}$-Based Materials," in *Solid State Properties of Fullerenes and Fullerene-Based Materials*, *Solid State Physics Vol. 48*, edited by H. Ehrenreich and Frans Spaepen (Academic, Boston), pp. 226–347.

Quirion, G., C. Bourbonnais, E. Barthel, P. Auban, P. Wzietek, and D. Jerome, 1993, "NMR Spectroscopy in $K_3C_{60}$ as a Function of Temperature and Pressure," Synthetic Metals **55-57**, 3154.

Quirion, G., C. Bourbonnais, R. Kerkoud, E. Barthel, P. Auban, D. Jerome, J. M. Lambert, A. Zahab, P. Bernier, C. Fabre, and A. Rassat, 1993, "NMR Investigation of $K_3C_{60}$ Under Pressure," in *Electronic Properties of Fullerenes*, edited by H. Kuzmany, J. Fink, M. Mehring, and S. Roth (Springer, Berlin/Heidelberg), pp. 334–338.

Rachdi, F., C. Goze, J. Reichenbach, J. Lukyanchuk, N. Kirova, G. Zimmer, M. Mehring, and P. Molinié, 1995, "Alkali Intercalated $C_{60}$: NMR and Magnetic Susceptibility Studies," Acta Phys. Pol. A **87**, 861.

Radzig, A. A., and B. M. Smirnov, 1985, *Reference Data on Atoms, Molecules, and Ions*, Springer Series in Chemical Physics (Springer, Berlin), pp. 101–116.

Ramirez, Arthur P., 1994, "$C_{60}$ and its Superconductivity," Superconductivity Review **1**, 1.

Ramirez, A. P., A. R. Kortan, M. J. Rosseinsky, S. J. Duclos, A. M. Mujsce, R. C. Haddon, D. W. Murphy, A. V. Makhija, S. M. Zahurak, and K. B. Lyons, 1992a, "Isotope Effect in Superconducting $Rb_3C_{60}$," Phys. Rev. Lett. **68**, 1058.

Ramirez, A. P., M. J. Rosseinsky, D. W. Murphy, and R. C. Haddon, 1992b, "Specific Heat Jump at $T_c$ and Normal-State Magnetic Susceptibility of $A_3C_{60}$," Phys. Rev. Lett. **69**, 1687.

Redfield, A. G., 1959, "Nuclear Spin Relaxation Time in Superconducting Aluminum," Phys. Rev. Lett. **3**, 85.

Redfield, A. G., and A. G. Anderson, 1959, "Nuclear Spin-Lattice Relaxation in Metals," Phys. Rev. **116**, 583.

Roth, G., K. Luders, P. Pfluger, H.-J. Guntherodt, 1981, "$^7$Li and $^{133}$Cs NMR Parameters in $C_6Li$ and $C_8Cs$ Intercalated Oriented Graphites," Solid State Commun. **39**, 423.

Ruoff, R. S., D. Beach, J. Cuomo, T. McGuire, R. L. Whetten, and F. Diederich, 1991, "Confirmation of a Vanishingly Small Ring-Current Magnetic Susceptibility of Icosoahedral $C_{60}$," J. Phys. Chem. **95**, 3457.

Saito, S., and A. Oshiyama, 1991, "Cohesive Mechanism and Energy Levels of Solid $C_{60}$," Phys. Rev. Lett. **66**, 2637.

Sasaki, S., A. Matsuda, and C. W. Chu, 1994, "Fermi-Liquid Behavior and BCS $s$-Wave Pairing of $K_3C_{60}$ Observed by $^{13}$C-NMR", J. Phys. Soc. Jpn. **63**, 1670.

Satpathy, S., 1986, "Electronic Structure of the Truncated Icosahedral $C_{60}$ Cluster," Chem. Phys. Lett. **130**, 545.

Satpathy, S., V. P. Antropov, O. K. Anderson, O. Jepsen, O. Gunnarsson, and A. I. Lichtenstein, 1992, "Conduction-Band Structure of Alkali-Metal-Doped $C_{60}$," Phys. Rev. B **46**, 1773.

Scalapino, D. J., 1969, "The Electron-Phonon Interaction and Strong-Coupled Superconductors," in *Superconductivity* Vol. 1, edited by R. D. Parks (Dekker, New York), pp. 449–560.

Schrader, D. M., and M. Karplus, 1964 "Orbital Following in the Methyl Radical," J. Chem. Phys. **40**, 1593.

Schrieffer, J. R., 1988, *Theory of Superconductivity*, Fourth Printing (Addison-Wesley, Redwood City, California).

Shastry, B. Sriram, and Elihu Abrahams, 1994, "What Does the Korringa Ratio Measure?" Phys. Rev. Lett. **72**, 1933.

Shore, Susan E., 1986, "Nuclear Magnetic Resonance Study of the Bonding of Carbon Monoxide to Palladium and Platinum Surfaces," Ph.D. thesis (University of Illinois at Urbana-Champaign).

Slichter, C. P., 1990, *Principles of Magnetic Resonance* (Springer, New York), 3rd edition.

Slichter, C. P., 1994, "Experimental Evidence for Spin Fluctuations in High Temperature Superconductors," in *Strongly Correlated Electron Materials*, edited by Kevin S. Bedell, Ziqiang Wang, David E. Meltzer, Alexander V. Balatsky, and Elihu Abrahams (Addison Wesley, Reading, MA).

Solomons, T. W. Graham, *Fundamentals of Organic Chemistry* (Wiley, New York), 3rd Ed.

Stenger, V. A., C. H. Pennington, D. R. Buffinger, and R. P. Ziebarth, 1995, "Nuclear Magnetic Resonance of $A_3C_{60}$ Superconductors," Phys. Rev. Lett. **74**, 1649.

Stenger, V. A., C. Recchia, C. H. Pennington, D. R. Buffinger, and R. P. Ziebarth, 1994, "NMR Studies of Alkali $C_{60}$ Superconductors," J. Superconductivity **7**, 931.

Stenger, V. A., C. Recchia, J. Vance, C. H. Pennington, D. R. Buffinger, and R. P. Ziebarth, 1993, "NMR Measurement of Superconducting-State Spin Susceptibility in Alkali Fullerides," Phys. Rev. B **48**, 9942.

Stephens, Peter W., Laszlo Mihaly, Peter L. Lee, Robert L. Whetten, Shiou-Mei Huang, Richard Kaner, François Deiderich, and Karoly Holczer, 1991, "Structure of Single Phase Superconducting $K_3C_{60}$," Nature **351**, 632.

Takigawa, M., 1992, "$^{63}$Cu and $^{17}$O NMR Studies on the Magnetic and Superconducting Properties of $YBa_2Cu_3O_{7-y}$," Appl. Magn. Reson. **3**, 495.

Tanigaki, K., I. Hirosawa, T. W. Ebbesen, J. Mizuki, Y. Shimakawa, Y. Kubo, J. S. Tsai, and S. Kuroshima, 1992, "Superconductivity in Sodium- and Lithium-Containing Alkali-Metal Fullerides," Nature **356**, 419.

Taylor, Roger, J. P. Hare, A. K. Abdul-Sada, and H. W. Kroto, 1990, "Isolation, Separation and Characterization of the Fullerenes $C_{60}$ and $C_{70}$: The Third Form of Carbon," J. Chem. Soc., Chemical Communications **20**, 1423.

Teslic, S., T. Egami, and J. E. Fischer, 1995, "Short-range antiferromagnetic orientational correlations in $Rb_3C_{60}$," Phys. Rev. B **51**, 5973.

Thelen, D., D. Pines, and J. P. Lu, 1993, "Evidence for $d(x^2-y^2)$ Pairing from Nuclear Magnetic Resonance Experiments in the Superconducting State of $YBa_2Cu_3O_7$," Phys. Rev. B **47**, 9151.

Tinkham, Michael, 1980, *Introduction to Superconductivity* (Robert E. Krieger Publishing, Malabar, Florida).

Tycko, R., G. Dabbagh, R. M. Fleming, R. C. Haddon, A. V. Makhija, and S. M. Zahurak, 1991, "Molecular Dynamics and the Phase Transition in Solid $C_{60}$," Phys. Rev. Lett. **67**, 1886.

Tycko, R., G. Dabbagh, D. W. Murphy, Q. Zhu, and J. E. Fischer, 1993, "Electronic Properties and Phase Transitions of $RbC_{60}$ and $CsC_{60}$: Investigation by NMR Spectroscopy," Phys. Rev. B **48**, 9097.

Tycko, R., G. Dabbagh, M. J. Rosseinsky, D. W. Murphy, R. M. Fleming, A. P. Ramirez, and J. C. Tully, 1991, "$^{13}$C NMR Spectroscopy of $K_xC_{60}$: Phase Separation, Molecular Dynamics, and Metallic Properties," Science **253**, 884.

Tycko, R., G. Dabbagh, M. J. Rosseinsky, D. W. Murphy, A. P. Ramirez, and R. M. Fleming, 1992, "Electronic Properties of Normal and Superconducting Alkali Fullerides Probed by $^{13}$C Nuclear Magnetic Resonance," Phys. Rev. Lett. **68**, 1912.

Tycko, R., R. C. Haddon, G. Dabbagh, S. H. Glarum, D. C. Douglass, and A. M. Mujsce, 1991, "Solid-State Magnetic Resonance Spectroscopy of Fullerenes," J. Phys. Chem. **95**, 518.

Ueda, K., and T. Moriya, 1975, "Nuclear Magnetic Relaxation in Weakly Antiferromagnetic Metals," J. Phys. Soc. Jpn. **38**, 32.

Varma, C. M., J. Zaanen, and K. Raghavachari, 1991, "Superconductivity in the Fullerenes," Science **254**, 989.

Veeman, W. S., 1984, "Carbon-13 Chemical Shift Anisotropy," in *Progress in Nuclear Magnetic Resonance Spectroscopy, Vol. 16* (Pergamon, Oxford), pp. 1–108.

Volhardt, D., and P. Wölfle, 1989, *Superfluid $^3$He* (A. Hilger, London).

Walstedt, R. E., D. W. Murphy, and M. Rosseinsky, 1993, "Structural Distortion in $Rb_3C_{60}$ Revealed by $^{87}$Rb NMR," Nature **362**, 611.

Watson, R. E., and A. J. Freeman, 1961, "Origin of Effective Fields in Magnetic Materials," Phys. Rev. **123**, 2027.

Weaver, J. H., and D. M. Poirier, 1994, in *Solid State Properties of Fullerenes and Fullerene-Based Materials*, *Solid State Physics Vol. 48*, edited by H. Ehrenreich and Frans Spaepen (Academic, Boston), pp. 1–108.

Wehrli, F. W., and T. Wirthlin, 1976, *Interpretation of Carbon-13 NMR Spectra* (Heyden and Son, London), p. 57.

Weigert, Frank J., and John D. Roberts, 1972, "Nuclear Magnetic Resonance Spectroscopy: Carbon-Carbon Coupling," J. Am. Chem. Soc. **94**, 6021.

Weil, J. A., J. R. Bolton, and J. E. Wertz, 1994, *Electron Paramagnetic Resonance: Elementary Theory and Practical Applications* (Wiley Interscience, New York), pp. 534–536.

White, C. W., W. M. Hughes, G. S. Hayne, and H. G. Robinson, 1968, "Determination of $g$-Factor Ratios for Free $^{85}$Rb and $^{87}$Rb Atoms," Phys. Rev. **174**, 23.

White, R. M., 1983, *Quantum Theory of Magnetism* (Springer, New York), 2nd Ed.

Wong, W. H., M. E. Hanson, W. G. Clark, G. Grüner, J. D. Thompson, R. L. Whetten, S.-M. Huang, R. B. Kaner, F. Diederich, P. Petit, J.-J. André, and K. Holczer, 1992, "Normal State Magnetic Properties of $K_3C_{60}$," Europhys. Lett. **18**, 79.

Yannoni, C. S., P. P. Bernier, D. S. Bethune, G. Meijer, and J. R. Salem, 1991, "NMR Determination of the Bond Lengths in $C_{60}$," J. Am. Chem. Soc. **113**, 3190.

Yannoni, C. S., R. D. Johnson, G. Meijer, D. S. Bethune, and J. R. Salem, 1991, "$^{13}$C NMR Study of the $C_{60}$ Cluster in the Solid State: Molecular Motion and Carbon Chemical Shift Anisotropy," J. Phys. Chem. **95**, 9.

Yannoni, C. S., H. R. Wendt, M. S. de Vries, R. L. Siemens, J. R. Salem, J. Lyerla, R. D. Johnson, M. Hoinkis, M. S. Crowder, C. A. Brown, and D. S. Bethune, 1993, "Characterization of Fullerenes and Doped Fullerenes," Synthetic Metals **59**, 279.

Yildirim, T., J. E. Fischer, R. Dinnebier, P. W. Stephens, and C. L. Lin, 1995, "Fullerene Superconductors and Orientational Order: $T_c$ vs Lattice Constant in $Na_2Rb_xCs_{1-x}C_{60}$," Solid State Commun. **93**, 269.

Yoshinari, Y., H. Alloul, G. Kriza, and K. Holczer, 1993, "Molecular Dynamics in $K_3C_{60}$: A $^{13}$C NMR Study," Phys. Rev. Lett. **71**, 2413.

Yosida, K., 1958, "Paramagnetic Susceptibility in Superconductors," Phys. Rev. **110**, 769.

Zhang, Z., C.-C. Chen, S. P. Kelty, H. Dai, and C. M. Lieber, 1991, "The Superconducting Energy Gap of $Rb_3C_{60}$," Nature **353**, 333.

Zhou, Otto, G. B. M. Vaughan, Q. Zhu, J. E. Fischer, P. A. Heiney, N. Counstel, J. B. McCauley, Jr., and A. B. Smith III,

1992, "Compressibility of $M_3C_{60}$ Fullerene Superconductors: Relation Between $T_c$ and Lattice Constant," Science **255**, 833.

Ziebarth, R., S.-M. Lee, V. A. Stenger, and C. Pennington, 1995, "Synthesis and NMR Characterization of New $C_{60}^{3-}$ Salts by Ion Exchange," in *Recent Advances in the Chemistry and Physics of Fullerenes and Related Materials: Volume 2*, edited by K. M. Kadish and R. S. Ruoff (The Electrochemical Society; Pennington, NJ).

Zimmer, G., M. Helmle, M. Mehring, F. Rachdi, J. Reichenbach, L. Firlej, and P. Bernier, 1993a, "NMR on Alkali Doped $C_{60}$," in *Electronic Properties of Fullerenes*, edited by H. Kuzmany, J. Fink, M. Mehring, and S. Roth (Springer, Berlin/Heidelberg), pp. 339–343.

Zimmer, G., M. Helmle, M. Mehring, F. Rachdi, J. Reichenbach, L. Firlej, and P. Bernier, 1993b, "Analysis of $^{87}$Rb and $^{13}$C Hyperfine Interaction in $Rb_3C_{60}$," Europhys. Lett. **24**, 59.

Zimmer, G., M. Helmle, M. Mehring, and F. Rachdi, 1994, "Lattice Dynamics and $^{13}$C Paramagnetic Shift in $K_4C_{60}$," Europhys. Lett. **27**, 543.

Zimmer, G., M. Mehring, C. Goze, and F. Rachdi, 1995, "Rotational dynamics of $C_{60}^{4-}$ and electronic excitation in $Rb_4C_{60}$," Phys. Rev. B **52**, 13 300.